PUBLIKACIJE ELEKTROTEHNIČKOG FAKULTETA UNIVERZITETA U BEOGRADU
PUBLICATIONS DE LA FACULTÉ D'ÉLECTROTECHNIQUE DE L'UNIVERSITÉ À BELGRADE

SERIJA: MATEMATIKA I FIZIKA — SÉRIE: MATHÉMATIQUES ET PHYSIQUE

№ 354 — № 356 (1971)

355. SOME OPTICAL PROPERTIES OF LEAD-TIN-CHALCOGENIDE ALLOYS

Pantelija M. Nikolić

ABSTRACT. The thesis describes an investigation into the properties of alloys formed between certain IV - VI semiconducting compounds namely: PbTe-SnTe, PbTe-SnSe, PbSe-SnTe, PbSe-SnSe, PbTe-SnS, PbTe-SnS (lead-tin-chalcogenides) and PbTe-Ge Te, PbTe-GeSe, PbTe-GeS, PbSe-GeTe, PbSe-GeSe, PbSe-GeS (lead-germanium chalcogenides). The interest in these alloys is that they extend the range of properties of the IV - VI semiconductors and it is shown in the thesis that certain of the alloys are promising as potential photodetectors or emitters in the range 4—15 μm and even beyond. The thesis describes the methods used for preparing specimens and the techniques used to investigate the range of solid solution, structure, lattice parameters and grain size of the alloys as well as their optical properties which give information on the band structure of the alloys which is perhaps the principal interest in this work.

The thesis starts with a general review of the properties of semiconducting alloys and in particular describes theoretical work which justifies the use of band theory in these disordered structures. We have then described in some detail what is known of the band structure of the particular compounds from which the alloys studied in this work have been made since it is the changes in these structures with alloying that we have investigated. The methods of preparing the compounds and the alloys in both bulk and film shape have been described in some detail. Special attention has been given to the preparation of the single crystal film specimens used for optical work and the thesis describes the effect of different substrates on the structure of the films and their optical properties. The measurements made on the alloys included X-ray diffraction and electron microscopy for investigations of structure etc. and measurements of reflectivity and transmission covering the range from the infra-red to the ultra-violet using various monochromators and spectrophotometers.

We have measured for the first time the range of solid solution of GeSe, GeS and SnS in PbTe and also found, by annealing the samples closer to their melting points, that solid solution of GeSe and GeS in PbSe and SnSe in PbSe extends

further than the values previously reported in the literature. At the beginning of the work, we showed that the fundamental energy gaps of the lead-tin chalcogenide alloys all decrease with concentration of tin chalcogenide and that all these gaps increase with temperature. Some of these results have since been confirmed by other workers. We have also found that the energy gaps of most of the lead-germanium chalcogenides increase with concentration of germanium chalcogenide and decrease with temperature.

The energy band structure of GeTe proposed by TSU et al. (1968) to explain their data is not consistent with our data on PbTe-GeTe alloys and we have suggested a new structure consistent with both sets of data.

Reflectivity measurements have been made on a number of alloy film specimens and from these the optical dielectric constant, optical conductivity, plasma wavelength and carrier relaxation time for each specimen have been calculated using a computer fitting procedure.

Finally, optical investigations have been made on certain compounds — GeSe, SnSe, SnTe — of which rather little appears to be known. We have seen in the transmission data higher optical transitions in addition to the fundamental energy gap. Our reflectivity data on these compounds confirm earlier measurements or are consistent with values extrapolated from alloys.

1. ALLOY SEMICONDUCTORS

Semiconducting alloys are of practical interest because they extend the range of available semiconducting materials. If two semiconducting compounds with the same or even with different structures are alloyed, semiconductors with energy gaps intermediate between those of the starting components are normally produced. The first alloy system to have been investigated was GeSi. The initial work was by STÖHR and KLEMM (1939) who found complete solid solubility throughout the whole composition range. A great deal of work has now been carried out on these alloys particularly since 1954 (HERMAN et al. 1957, IOFFE and REGEL 1960 and WOOLLEY 1964): the physical properties of the pure constituents are very well known, and this is of course of help in interpreting the alloy data. Furthermore homogeneous single crystal specimens of any composition can easily be prepared (JOHNSON and CHRISTIAN 1954, and BRAUNSTEIN et al. 1958).

By an alloy we normally mean a random structure. When ordering occurs the element of randomness disappears, and a periodic crystal potential is found. This ordered alloy might well be called a compound in which case one could say that the only true alloys of solid substitutional solutions are those which are disordered. Defect semiconductors are similar in many respects to alloys, the random arrangement of atoms and vacancies replacing the random arrangement of the two kinds of atom.

A fundamental problem in semiconducting alloys is the problem of the applicability of band theory to the structure where the periodic crystal potential is affected by large random perturbation. In this chapter we shall present a short review of the virtual crystal model. It follows in this model that bands and forbidden gaps exist in semiconducting alloys but that the band edges are less well defined than in ordered materials.

1.1. Band structure of semiconducting alloys

The band theory of solids is practically a one electron theory in which an electron moves in a regular crystal with a lattice periodicity. When a substitutional solid solution of two semiconducting elements is considered the sites occupied by different type of atoms can either be randomly distributed as in a disordered alloy or regularly distributed as in an ordered compound. PARMENTER (1955) proposed that a band picture similar to that of the compounds is retained by their alloys, so that the properties of alloys could be explained by similar parameters to those of the compounds from which they are formed. He followed the approach of the "virtual crystal" approximation used by NORDHEIM and MUTO for three dimensional alloys. The NORDHEIM virtual crystal model of an alloy assumed that the potential acting on an electron moving through the disordered alloy formed by a random configuration of atoms can be separated into a periodic and an aperiodic component

$$V_{alloy}(\vec{r}) = V_{periodic}(\vec{r}) + V_{aperiodic}(\vec{r}) \tag{1}$$

where the periodic part is the average alloy potential taken over all possible random arrangements of atoms in the alloy. The aperiodic potential is a measure of the deviation of $V_{\text{alloy}}(\vec{r})$ from the average $V_{\text{periodic}}(\vec{r})$. The periodic potential function defines the virtual crystal of the alloy and the effect of disorder is represented by the aperiodic potential function. We can now write the one electron SCHRÖDINGER equation for a configuration of atoms in an alloy

$$\left[-\frac{\hbar^2}{2m}\nabla^2 + V(\vec{r})\right]\psi(\vec{r}) = E\psi(r) \tag{2}$$

where V, ψ and E depend on the positions of the N atoms in the alloy. PARMENTER (1955) assumed that the crystal potential V can be expressed as a spatial sum of atomiclike potentials.

$$V(\vec{r}) = \sum_n V_{sn}(\vec{r} - \vec{R}_n) \tag{3}$$

where R_n is the position of the n^{th} lattice site: the index s denotes the type of atom on the n^{th} lattice and $V_s(\vec{r})$ is an atomic like potential associated with an atom of type s.

In order to use perturbation theory, an unperturbed potential $V_0(\vec{r})$ is first chosen and assumed to have the periodicity of the lattice associated with the alloy, i.e.

$$V_0(\vec{r}) = \sum_n V_0(\vec{r} - \vec{R}_n). \tag{4}$$

The perturbing potential is then:

$$V'(\vec{r}) = \sum_n V'_{sn}(\vec{r} - \vec{R}_n) \tag{5}$$

where

$$V_s'(\vec{r}) = V_s(\vec{r}) - V_0(\vec{r}). \tag{6}$$

The HAMILTONian can therefore be written as

$$H(\vec{r}) = H_0(\vec{r}) + V'(\vec{r}) \tag{7}$$

where

$$H_0(\vec{r}) = -\frac{\hbar^2}{2m}\nabla^2 + V_0(\vec{r}). \tag{8}$$

V_0 and H_0 depend on the composition of the alloy because the lattice constant is a function of composition. For this situation the unperturbed wave functions are the eigenfunctions of the HAMILTONian H_0 describing the periodic potential. Using nondegenerate perturbation theory PARMENTER continued to label the perturbed wave function with the index k which is now of course only a pseudo-quantum number.

If we restrict our attention to electrons with energies in the neighbourhood of an extremum of a nondegenerate allowed energy band $E_0(k)$ (SLATER, 1949) one can write another equation equivalent to (2)

$$\left[-\frac{\hbar^2}{2m}\nabla W_0 \nabla + V'(\vec{r})\right]\psi(\vec{r}) = E\psi(\vec{r}) \tag{9}$$

where the energy E is the same in both equations, W_0 is the reciprocal effective mass tensor and V' is only a slowly varying function of positions on an atomic scale. Here ψ can be taken as the conventional wave function for a particle with reciprocal effective mass W_0 moving in a potential V'. In this notation the electron is actually in a potential $V_0 + V'$.

With all these assumptions the problem is much simplified and unperturbed SCHRÖDINGER equation can be written as follows:

$$-\nabla W_0 \nabla \psi_0(\vec{k}, \vec{r}) = E_0(k)\,\psi_0(\vec{k}, \vec{r}) \tag{10}$$

which has the simple solution of a normalized plane wave:

$$\psi(\vec{k}, \vec{r}) = (N\Omega)^{-\frac{1}{2}} e^{i\vec{k}\vec{r}} \tag{11}$$

where Ω is the volume per lattice site in the alloy, N is the number of atoms in the alloy and k is any one of the series of k vectors which satisfy the periodic boundary conditions. The eigenvalues of this equation are quadratic functions of the components of k i. e.

$$E_0(\vec{k}) = \vec{k} W_0 \vec{k}. \tag{12}$$

It can be further shown that one can obtain the perturbed eigenvalues associated with equation (9) by using non-degenerate perturbation theory carried out to all orders of the perturbation i. e. an exact solution. Thus

$$E(\vec{k}) = \sum_n E_n(\vec{k}) \tag{13}$$

where $E_n(k)$ is the contribution of the n^{th} order perturbation theory. It can also be shown that for $n \geqslant 1$, E_n can be expressed as a power series expansion over the

fraction f_c of lattice sites occupied by atoms of type s associated with the various impurity atoms added i.e.

$$E_n(\vec{k}) = \sum_s f_s \varepsilon_{sn}(\vec{k}) + \sum_{s,t} f_s f_t \tau_{stn}(\vec{k}) + \text{higher} \tag{14}$$

order terms in the various f_s's ...

Finally one can show that the dependence upon k of the energies calculated for all orders of perturbation theory are qualitatively similar to those calculated to only second order.

As an example of this we consider the case of a binary alloy. This can be treated using the expression for the energy calculated either exactly or to second order. In both cases one obtains the same expression for the energy $E(k)$. This is written in terms of a parameter ε proportional to the $E(\vec{k})$ (PARMENTER, 1955, 1956).

$$\varepsilon(\vec{k}) = (2k/a)^2 - \varepsilon_0 [1 + (2\vec{k}/a)^2]^{-1} \tag{15}$$

where

$$\varepsilon(\vec{k}) = (2/a)^2 E(\vec{k}), \qquad \varepsilon_0 = (8\pi/a^5 \Omega) \sum_s f_s A_s^2, \qquad \eta = (2\pi)^2 (2/a)^3 n. \tag{16}$$

From these the density of states $(d\eta/d\varepsilon)$ can be calculated and this is shown in Figure 1.1. as a function of ε for various values of ε_0. It can be seen that at large values of ε_0 a low energy tail appears indicating that the band edges are moved into the forbidden bands. At very low values of ε_0 however the result is qualitatively similar to that produced by thermal vibrations on the energy levels of a perfect crystal (FAN 1951).

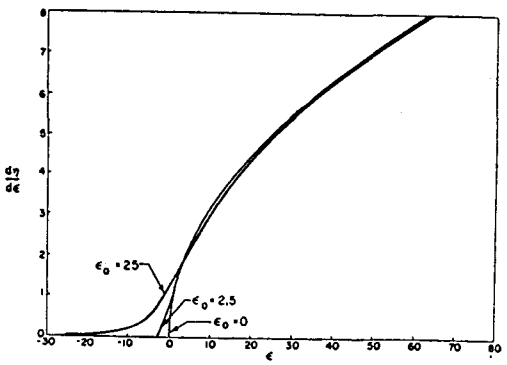

Figure 1.1. Density of states $(d\eta/d\varepsilon)$ versus ε for various values of ε_0

We have seen that perturbation theory can provide a bridge between the cases of ordered and disordered crystals in such a way that a BRILLOUIN zone scheme and energy bands can be associated with the periodic virtual crystal potential function. Provided that second order perturbation theory is adequate our knowledge of the zones and energy bands in perfect crystals may be applied to disordered alloys taking into account the broadening of the band edges. Hence one can use in disordered alloys a quantum number k to label the quantum states and hence to determine such parameters as the effective mass the density of states etc. One must always bear in mind however that the wave vector k is not the "right" quantum number.

As we discussed earlier alloying causes the band edges to be displaced into the forbidden regions and this results in curvature of the band extrema. This is expected to be manifest in low effective masses, high carrier mobilities and low density of states in the region of the band extrema. In practice the electron mobilities are observed to decrease with alloying because of the additional scattering associated with the disorder.

1.2. Previous work on the optical properties of some semiconducting alloys

The first optical measurements made on Ge-Si alloys were of infra-red transmission by JOHNSON and CHRISTIAN (1954). They showed that there was a marked change in slope of the variation of the energy gap, E_g, with concentration at approximately 10% Si. Further measurements of optical transmission were made by BRAUNSTEIN et al. (1958) who also reported an abrupt change of slope in the variation of E_g although in their work this was at about 15% Si. This change in slope can be explained from a knowledge of the band structure of the two semiconducting elements (HERMAN, 1954). In Figure 1.2. it can be seen that there are three types of conduction band minima in pure Ge. When Si atoms are substituted for Ge atoms, these minima increase in energy. It is found that the increase in the minima at

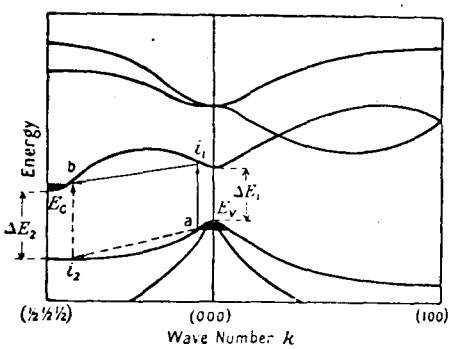

Figure 1.2. Schematic diagram of energy band in Ge along [111] and [100] axes in k space.

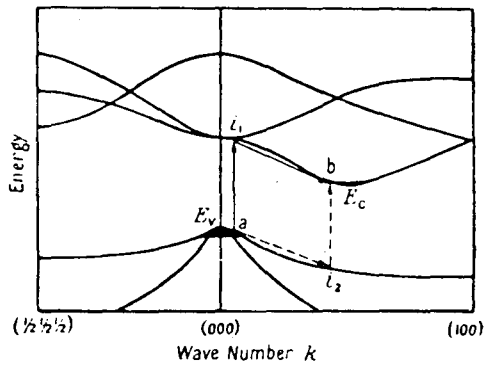

Figure 1.3. Diagram of the energy bands Si in k space.

k = [111] is the most rapid, because in pure Si this minimum is very much higher in energy than the others (Figure 1.3.) Between 0 and 15% Si the lowest minimum is still that at [111] as in pure germanium. Hence the linear change of E_g with Si content in this region is attributed to the rapid movement of this minimum. At 15% Si, the [111] minimum rises above the [100] minimum so that there is a change in the band structure. The [100] minimum remains the lowest at all higher Si concentrations, so that alloys with more than 15% Si have the band structure of pure silicon. This changeover in the conduction band minima was confirmed by GLICKSMAN (1956). In the range of composition between 10 and 17% Si he observed a sharp decrease in the mobility. The variation calculated on the assumption that the mobility is limited by interband transitions is in good agreement with the measured variation indicating that there are indeed two degenerate conduction bands throughout this composition range. The reflectivity data of the Ge-Si alloys (TAUC and ABRAHAM 1961 and PHILLIPS 1962) together with our knowledge of the detailed band structure of pure Ge and Si, confirms the movement of the bands on alloying.

A great deal of work has been also carried out on III—V alloys. A review of their preparation and crystallographic properties has been given by WOOLLEY (1962) and their physical properties have been extensively examined in a series of papers by WOOLLEY and his collaborators (WOOLLEY et al. (1961), WOOLLEY (1964) etc.). One of the most interesting properties of the alloys is the change in the room temperature energy gap that was observed in the InSb-InAs alloy system.

E_g was found to decrease if either of the compounds was dissolved into the other (WOOLLEY and WARNER 1964). The nearest behaviour to this in other systems occurs in the InSb-GaSb system in which E_g lies on a curve rising from InSb to GaSb (WOOLLEY et al. 1959), which is concave when looked at from above.

In the last five years several reports on the optical properties of alloy systems prepared by thermal evaporation have appeared. For example POTTER and KRETSCHMAR (1964) reported measurements of optical transmission from 1 to 6 microns for the InSb-InAs system made on specimens prepared by the so-called four temperature method. The optical and electrical properties of single crystal films of PbSe-SnSe alloys deposited on single crystal KCl substrates have been measured by STRAUSS (1967) and a similar technique has been used for obtaining single crystal films of some other IV—VI alloys (e.g. PbSe-PbTe alloys (BIS and ZEMEL, 1966) and PbTe-SnTe alloys (BYLANDER, 1966) etc.).

2. IV—VI SEMICONDUCTING COMPOUNDS

2.1. Introduction

A considerable amount of data has now been published on the properties of IV—VI compounds and, in the last few years, this has mostly been on single crystal material which is now fairly easy to obtain. In this section we shall review some of the work on these compounds together with recent theoretical ideas on their band structure. There is a large number of semiconducting compounds in this group and the discussion will be restricted to those on which work is reported later in this thesis, in particular optical work on film specimens since in general this work proved to be more informative than optical work on bulk specimens. These compounds are: PbTe, SnTe and GeTe and to a somewhat lesser extent, GeSe and SnSe.

2.2. PbTe

Lead telluride is one of the lead chalcogenide group of compounds which are all polar semiconductors. Their structure is that of sodium chloride in which each atom is octahedrally coordinated to six atoms of the other element. The principal characteristics of lead telluride are its very small optical energy gap, its high mobility and its rather high dielectric constant.

SCANLON (1959) has reported values of 0.32 and 0.29 eV for the direct and indirect optical transitions for PbTe. These values, which are those generally quoted in the literature, were obtained from transmission measurements through bulk samples.

There are also earlier transmission measurements (GIBSON 1950 and 1952) made on both film and bulk samples. In more recent work (CARDONA and GREENAWAY, 1964) measurements of both transmission and reflectivity were made on very thin films of lead salts deposited epitaxially. Using the KRAMERS-KRONIG relationship they calculated both the real and imaginary parts of the dielectric constant for all the lead chalcogenide compounds. By comparing the positions of the reflectivity peaks of the lead salts they observed that the energy of all six transitions decreased monotonically with increase of lattice parameter. Furthermore this was not found to be true in compounds in which lead is substituted for by an atom of smaller

atomic number such as Ge and Sn. The absorption coefficients for PbTe and the other compounds were either computed from reflectivity data or determined directly from transmission measurements. Both methods gave results which were in good agreement with each other.

It is interesting to note that GIBSON'S very much earlier data (GIBSON 1959) on very thin films of PbTe are in very good agreement with CARDONA'S work although at that time very little was known about the band structure of these materials so that no interpretation was possible and as a result GIBSON'S work received little attention.

The interpretation of GIBSON'S and CARDONA'S data shows conclusively that both the conduction and valence band extrema are at the point $L=(\pi/a)$ **[111]** on the BRILLIOUIN zone face. It was assumed by CARDONA and GREENAWAY (1964) and also by other authors that the three lead chalcogenide compounds all have similar band structures, and the temperature coefficient of the forbidden energy gaps which is positive in all three compounds, unlike in most materials provides strong support for this.

ZEMEL et al. (1965) have also made electrical and optical measurements on single crystal films of lead chalcogenide. From their optical data they calculated the refractive indices of the films in the 2.0 to 15.0 microns region. By comparing their film data with available data for bulk specimens they conclude that epitaxial films of PbTe, PbSe and PbS have properties very similar to those of bulk material of those compounds.

DIXON and RIEDL (1965) measured the infra red reflectivity of PbTe. From these measurements, and electrical data and using the classical free-carrier dispersion theory and the procedure described by SPITZER and FAN (1957) they obtained values for the susceptibility hole mass of PbTe over a wide temperature region (24—300°K).

The optical properties of semiconductors can easily be explained in terms of band theory. We make the usual assumption that the alloys we shall be considering have similar band structure to the compounds from which they are formed.

The first theoretical work on the band edge structure of the lead chalcogenide compounds was by DIMMOCK and WRIGHT (1964). In their model which assumes there are three bands forming the conduction band and three forming the valence band, they used the *kp* perturbation method developed by KANE (1956). An alternative approach is the pseudo potential method used by KLEINMAN and LIN (1964) and LIN and KLEINMAN (1966) and this will be compared with the extended APW method described by RABII (1968) in the following section.

2.2.1. *The development of the theory on energy bands in PbTe.* The augmented plane wave method contains the basic assumption that the crystal potential for a valence electron is periodic i.e. around each nucleus of the lattice there is a spherically symmetric potential of radius R_c which should be the same for all atoms if they are alike. Between these spherical equipotentials at R_c the potential is assumed to be constant. With these assumptions it is now possible to use the one electron SCHRÖDINGER equation.

To determine the eigenvalue energies, E, we consider the space within the spheres and the space outside the spheres separately and then apply the appropriate continuity conditions. Within a sphere, the wave function can be written as

$$\psi=\sum_{l=0}^{\infty}\sum_{m=-l}^{l} A_{lm} P_l^{|m|}(\cos\theta)\exp(im\Phi)\, U_{nl}(|\vec{r}-\vec{r}_n|) \tag{2.1}$$

where A_{lm}, are expansion coefficients, $|\vec{r}-\vec{r}_n|$, θ, Φ spherical coordinates, $P_l(m)$ LEGENDRE polynomials and U_{nl} are solutions of the radial wave equation:

$$-\frac{1}{r^2}\frac{\mathrm{d}}{\mathrm{d}r}\left(r^2\frac{\mathrm{d}U_{nl}}{\mathrm{d}r}\right)+\left[\frac{l(l+1)}{r^2}+U_n\right]U_{nl}=EU_{nl}. \tag{2.2}$$

Well outside the spheres in the region of constant potential we can assume the wave function to be a single plane wave e^{ikr}. It can now be shown that for ψ to be continuous, the solution inside the sphere must have the form (SLATER, 1937):

$$\begin{aligned}\psi_i=\exp(i\vec{k}_i\vec{r}_n)\sum_{i=0}^{\infty}\sum_{m=-l}^{l}(2l+1)i^l\frac{jl(k_iR_n)}{U_{nl}(R_n)}U_{nl}(|\vec{r}-\vec{r}_n|)\\ \times\frac{(l-|m|)!}{(l+|m|)!}P_l^{|m|}(\cos\theta)\,P_l^{|m|}(\cos\theta_i)\exp im(\Phi-\Phi_i)\end{aligned} \tag{2.3}$$

where θ_i and Φ_i define the direction of $\vec{k}_i$: $\vec{j}_1$ are spherical BESSEL functions and we have taken the origin of the coordinate system to be at $\vec{r}$. Such wave functions which contain both plane wave and *a* spherical potential solution character are called augmented plane wave functions, (APW), and it is convenient to write a general wave function as a linear combination of a particular set of APW's. Hence a particular problem is solved once the coefficients, v_i, in this linear expansion have been determined. Thus if ψ_k is an eigenfunction of

$$H\psi_k=E\psi_k \tag{2.4}$$

we write:

$$\psi_k(\vec{r})=\sum_l v_i\psi_i. \tag{2.5}$$

Since $u_{nl}=u_l(r_l, E)$ each APW is a function of both E and k. It can readily be shown that $\psi_k(\vec{r})$ of equation (2.5) will be a solution of (2.4) if the equations

$$\sum_j(H-E)_{ij}v_j=0 \tag{2.6}$$

for all i, where $(H-E)$ is the matrix whose elements are:

$$(H-E)_{ij}=\int\psi_i^*(H-E)\psi_j\,\mathrm{d}\tau \tag{2.7}$$

(2.6) holds if the determinant $(H-E)_{ij}=0$ and this condition can be used to determine the eigenvalues E, for a particular value of k in the first BRILLOUIN zone. Hence the first task is to choose a suitable set of APW's. To do this we make use of the symmetry of the particular lattice which has not so far been considered in the discussion. Symmetry requires that the wave vector k_i associated with ψ_i is drawn from the set $[\vec{k}+\vec{K}_i]$ where $\vec{K}_i$ is the infinite set of the reciprocal lattice vectors. However, it is clear that i must be finite so that approximations are introduced by which this infinite set is reduced to a finite set.

The APW method was used by CRONKLIN et al. (1965) to determine the band structure of PbTe. The HAMILTONian included relativistic terms and was written in the following form:

$$\varkappa=\frac{P^2}{2m}+V(\vec{r})+\frac{\hbar}{4m^2c^2}\vec{\sigma}[(\nabla V)\times\vec{P}]+\frac{\hbar^2}{8m^2c^2}(\nabla^2V)-\frac{P^4}{8m^3c^2}. \tag{2.8}$$

This form was obtained by reducing DIRAC's four component field equation to the two-component SCHRODINGER's equation (MESSIACH, 1962). The first two terms are the usual kinetic and potential-energy terms, and the third term is the spin-orbit interaction term which can split and mix degenerate levels. The other two relativistic terms are strongly dependent on the angular momentum character of the wave functions, which in turn depends on the particular point in k space, so these terms can change the relative spacing of the bands and their shape.

When the APW method is applied to a compound such as PbTe, one has to take into account the fact that the radii of the Pb and Te spheres will not be equal. CRONKLIN et al., (1965) determined these radii by assuming that the Pb and Te spheres touch without overlapping and that the spherically averaged potential from the Pb sphere evaluated at the surface of the Pb sphere is equal to that at the surface of the Te spheres evaluated using the spherical potential within the Te sphere. The one electron potential is taken to be the sum of a COULOMB potential and an exchange potential. The COULOMB potential arises from the nuclei and from the charge density of all electrons. The exchange potential is:

$$-6\,[3\rho(r)/8\pi]^{1/3} \tag{2.9}$$

where $\rho(r)$ is the charge density of all electrons. In this way the energy levels can be calculated at points in the BRILLOUIN zone using the APW method. The potentials were obtained from a HARTREE-FOCK-SLATER calculation using the computer programme developed by HERMAN and SKILLMAN 1963.

In Figure 2.1. the energy bands determined in this way are shown for the [111] direction near to the forbidden energy gap. These diagrams need to be slightly modified to obtain agreement with the optical data for PbTe reported by CARDONA and GREENAWAY (1964).

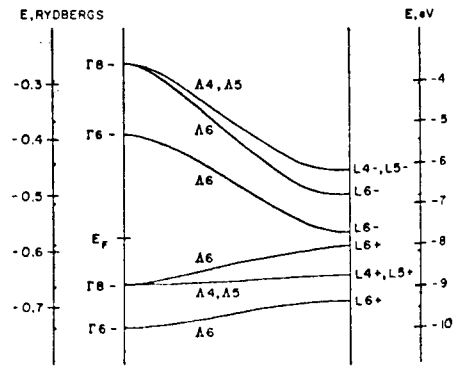

Figure 2.1. PbTe energy bands in the [111] direction near the forbidden gap.

A check of the accuracy of the APW calculation can be obtained by using the wave functions calculated by this method for calculating electrical properties of the materials, such as the deformation potential and in general good agreement is obtained between these two values and those determined experimentally. A check of this sort on the calculations on PbTe was reported by CONKLIN et al. The calculated wave functions can also be used to determine effective masses using the kP method. Using this method and CONKLIN's band structure PRATT and FERREIRA (1964) calculated the effective masses and obtained good agreement with their own experimental data.

DIMMOCK and WRIGHT (1964) have used an approach based on a nearly free-electron model and kP perturbation theory (KANE, 1956). They actually used a parameterized (kP perturbation) model of the conduction and valence band extrema, although they did take into account spin-orbit mixing of the double-group level of the same symmetry. The parameters they used involved both the relative spacings between the bands considered and the momentum matrix elements between

bands. The order of the bands and their relative spacings were adjusted to give reasonable agreement with the experimental data. The schematic energy level diagram for lead salts in a f.c.c. lattice is given in figure 2.2 for the L point including both crystal field and spinorbit splittings. One can see that all the bands at L are doubly degenerate. The splittings are known from group theory but of course this does not give the final order of the levels. The possible order of these six levels is $6! = 720$. However since the valence and conduction bands each consist of three bands and DIMMOCK and WRIGHT rejected arrangements in which the gap lies between two levels split only by spin-orbit interaction, the two spin-orbit split pairs must be on opposite sides of the gap. To be consistent with experimental data they assumed that lead salts are direct band gap semiconductors which have both valence and conduction band extrema in the [111] direction. They also assumed that both these bands were each made up of 3 bands. These assumptions reduce the number of arrangements to 144. Using further reasoning DIMMOCK and WRIGHT reduced the number of arrangements to 14 and using kP perturbation theory simplified their model for PbTe to the four bands (shown in figure 2.3.).

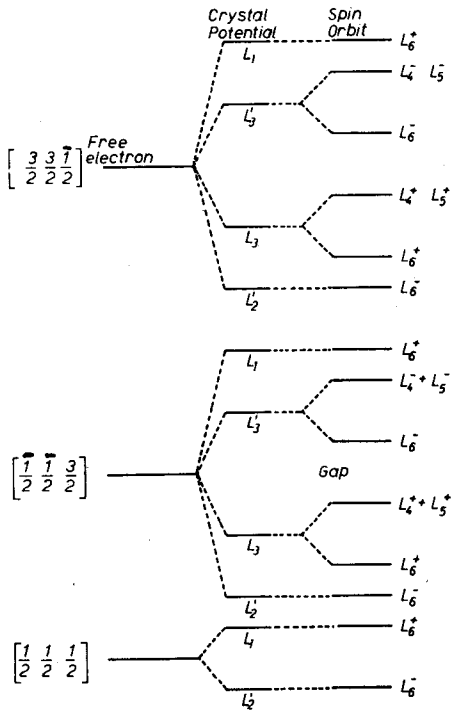

Figure 2.2. Schematic energy diagram for lead salts.

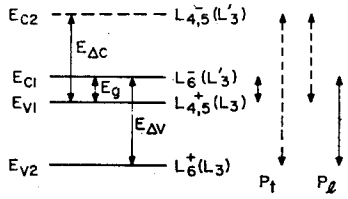

Figure 2.3. A schematic diagram of the energy band states at L point for GeTe and SnTe.

To simplify the calculation they reduced this still further into a two band model which gave good agreement with transport data for PbTe.

KLEINMAN and LIN (1964) and LIN and KLEINMAN (1966) have reported another theoretical study of the band structure of PbTe which involves four arbitrary constants which have to be derived from experimental data by a fitting procedure. In this new pseudopotential scheme of calculation, the crystal pseudopotential was taken to be a superposition of simple atomic pseudopotentials which were expressed as follows:

$$(2.10) \qquad V_{eff} = 0 \quad r < r_0, \qquad V_{eff} = (2Z/r)\,[1 - e^{-\beta(r-r_0)}] \quad r > r_0.$$

Using the FOURIER transformation of V_{eff} and SLATER's (1930) expressions for analytical atomic fuctions and four adjustable parameters they determined firstly numerical values of parameters which appears in the pseudopotentials.

In order to obtain the energy band structure of PbTe and the other two lead salts, KLEINMAN and LIN also used the well known experimental fact that the valence and conduction band extrema are at the L-point. The energy bands of PbTe they obtained which are given in figure 2.1. have been shown to be consistent with the experimental data of CARDONA and GREENAWAY. We note that the agreement between experimental and calculated data can only be tested to a limited extent because the position of the broad peaks of the reflectivity can not be measured very precisely. Furthermore the theoretical results for band separations have to be compared with $\varepsilon_2 E^2$ where ε_2 is the imaginary part of dielectric constant. This must be stressed because there are differences in the energy band diagrams calculated by KLEINMAN and LIN and those obtained by CONKLIN et al. although both authors can obtain very good agreement between their schemes and the same experimental data.

RABII (1968) repeated the APW calculations including further terms neglected by the previous authors and obtained values for the transverse factors in better agreement with experiment but in general his results confirmed the results of LIN and KLEINMAN.

Recently PARADA and PRATT (1969) showed theoretically that the states associated with Te vacancies lie well up in the conduction band.

2.3. SnTe compound

Tin telluride is the only compound in the Sn-Te system and has the NaCl structure. This compound always exhibits very high P-type conductivity as a result of Sn vacancies (BREBRICK, 1963) each of which gives rise to a double ionized acceptor level (HOUSTON et al, 1964).

A considerable amount of data has been published on SnTe both on bulk and film specimens. The absorption coefficient is very high and the only optical transmission measurements have been on films typically of the order of 1 micron thick. BYLANDER et al. (1965) have shown that a single crystal film of SnTe with a carrier concentration of 1×10^{20} cm^{-3} and a thickness of 1.4 micron had a sharp absorption edge in the infra-red region near 0.5 eV. They assumed that this was associated with the onset of direct transitions between a valence and a conduction band and also suggested that the true energy gap might be less than 0.5 eV because the high carrier concentration could produce a strong Burstein shift of the edge to an energy much larger than that measured. RIEDL et al. (1966) have devised a method for growing single crystal SnTe films on sodium chloride substrates and a procedure for varying the carrier concentration in these films from 4×10^{19} to 7×10^{20} cm^{-3}. They calculated the carrier concentration from the position of the wavelength of the reflectivity minima in the infrared region. The existence of a relationship between the reflectivity minima and the carrier concentrations has been previously established by the same authors (RIEDL et al. 1965). They also calculated the susceptibility effective mass ratios of free carriers at both room temperature and 80°K using the experimental reflectivity data of BIS (1964). and showed that it varies between 0.080 and 0.140. They calculated the room temperature dielectric constant to be 41 and 48 for two different specimens with hole concentrations of 4.8×10^{20} and 4.8×10^{19} cm^{-3} respectively. SCHOOLER et al. (1966) observed a strong BURSTEIN shift of the fundamental absorption edge using specimens with hole concentrations of 3.6×10^{19} to 1.4×10^{20} cm^{-3}, holes. For a specimen with a lower hole concen-

tration they estimated the band gap to be less than 0.3 eV. ESAKI (1966) and ESAKI and STILES (1966) have confirmed this estimate and have shown clearly that SnTe is a semiconductor and not a semimetal as many authors had thought. They evaporated a SnTe film about 4000 Å thick onto an oxidized evaporated strip of Al, to make a suitable tunnel junction. By analysing the tunnel current, using the FOWLER-NORDHEIM current-voltage relationship (1928) ESAKI showed the band gaps at room and liquid helium temperatures to be as low as 0.2 eV and 0.3 eV respectively.

CARDONA and GREENAWAY (1964) measured the transmission and reflectivity of thin epitaxial SnTe films evaporated onto a NaCl substrate. They did not observe the fundamental absorption edge but determined the positions of the second, third and fourth energy transitions from both transmission and reflectivity measurements, which provides very useful information on the band structure of this compound.

To explain the room temperature electrical and thermal measurements ROGERS (1968) proposed a two-valence band model in which the light mass band was non-parabolic but the heavy mass band was parabolic. He also obtained band parameters from his model using COHEN's dispersion law (1961) for energy surfaces with both rotation and reflection symmetry. ROGERS suggested that the heavy mass valence band in SnTe was similar to that in PbTe but that the energy separation between the valence band edges was much greater in SnTe, than in PbTe. This would result in an effective mass at the top of the valence band being much smaller in SnTe so that the carrier concentration and the room temperature HALL mobility should be greater in SnTe than in PbTe. To check this one would have to use SnTe specimens containing a much lower carrier concentration say about 10^{16}—10^{17} cm^{-3} but unfortunately so far as is known no specimens containing less than 10^{19} cm^{-3} have been produced to date.

Recently TSU et al. (1968) have determined a set of band parameters for SnTe from a consideration of all the available optical data and using the simple four band model proposed by DIMMOCK and WRIGHT (1964) for lead chalcogenide compounds. TSU et al. used the band scheme at the L point shown in figure 2.3. where the double headed arrows indicate the allowed kP coupling for transverse and longitudinal matrix elements denoted by P_t and P_l. respectively. They assumed that E_{Δ_c} was much larger than E_g or E_{Δ_v} so that the 4×4 secular determinant could be reduced to a 3×3 determinant describing the two valence bands and the principal conduction band only.

(2.11)
$$\begin{vmatrix} E_g + \frac{\hbar^2 k_l^2}{2m_0} - E' & \hbar k_t P_t/m_0 & \hbar k_l P_l/m_0 \\ \hbar k_t P_t/m_0 & \frac{\hbar^2 k_l^2}{2m_l(\nu_1)} - E' & 0 \\ \hbar k_l P_l/m_0 & 0 & E_{\Delta_v} \frac{\hbar^2 k_l^2}{2m_0} - \frac{\hbar^2 k_t^2}{2m_0}\left[\frac{m_0}{m_t(\nu_2)}\right] - E' \end{vmatrix} = 0$$

where $E' = E - \hbar k_t^2\, 2m_0$ and $m_l(\nu_1)$ and $m_t(\nu^2)$ are the longitudinal and transverse masses of the first and second valence bands, respectively. It is possible to make a further approximation. If

(2.12)
$$\hbar^2 k_{lF}^2 / 2m_l(c_1)\, E_{\Delta v} > 1$$

where k_{lF} is the longitudinal Fermi momentum and $m_l(c_1)$ the parabolic longitudinal mass of the first conduction band, the 3×3 determinant can be reduced to a 2×2 determinant. Tsu et al. also found that quantity on the left of 2.12. was in fact about 2 for SnTe but nevertheless used this parabolic approximation, because it appeared to be good enough for calculations of the FERMI energy and the susceptibility mass to within an error of a few percent in comparison with the 4×4 model.

Since SnTe is always P-type the solution of the 2×2 determinant for the valence band is adequate.

$$(2.13) \qquad E_{v_1}(\vec{k}) = \frac{1}{2} E_g + \frac{1}{4} \hbar^2 k_l^2 \left[\frac{1}{m_l(c_1)} - \frac{1}{m_l(v_1)} \right] + \frac{\hbar^2 k_t^2}{2 m_0} -$$

$$- \frac{1}{2} \left\{ \left[E_g + \frac{1}{2} \hbar^2 k_l \left(\frac{1}{m_l(c_1)} + \frac{1}{m_l(v_1)} \right) \right]^2 + 4 \hbar^2 k_t^2 P_t^2 / m_0 \right\}^{\frac{1}{2}}$$

where E_{v_1} is the value of the energy which is parabolic with respect to k_l for small k_t, but almost linear with respect to k_t for small k_l. The band parameters can be obtained from this expression using a computer fitting procedure. The best set of band parameters obtained by TSU et al. (1968) is given in Table 2.1 together with the band parameters for SnTe obtained using the third order determinantal solution for the energy dispersion relation marked with*. They used the experimental data

TABLE 2.1.

E_g (eV)	$E_{\Delta v}$ (eV)	$\frac{P_t}{m_0}$ (eV)	$\frac{P_l}{m_0}$ (eV)	$\frac{m_l(v_1)}{m_0}$	$\frac{m_l(c_1)}{m_0}$	$\frac{m_l(v_2)}{m_0}$	$\frac{m_t(v_2)}{m_0}$
0.2.	0.54	6.5	—	0.28	0.07	0.07	0.033
0.2*	0.54	6.5	2.92	0.28	—	—	0.03

from various authors obtained for SnTe, but we note that not all specimens were of the same quality.

The above table shows that the error introduced in the reduction of the 3×3 to the 2×2 determinant does not have much influence on the band parameters obtained.

The energy dispersion relation for SnTe is given in figure 2.4. The E_{c_2} bands are shown by broken lines because their position is not known accurately as the information on the value of $E_{\Delta c}$ is limited. TSU et all. believed that the second conduction band should also be located at the L point and that it would have a rather high energy so that it would never be occupied.

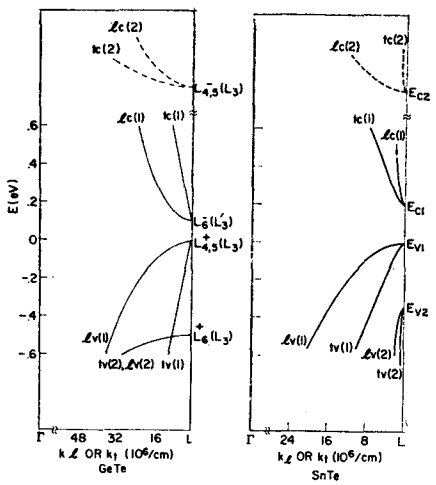

Figure 2.4. The band edge energy dispersion relation for GeTe and SnTe.

2.4. GeTe compound

GeTe has a face centred rhombohedral lattice at room temperature with the parameters $a=5.962$ Å and $\alpha=88°21'$ (SCHUBERT et al., (1953). When the temperature is increased to about 460 °C, the lattice transforms to a face centred cubic NaCl type structure with a lattice constant of $a=5.986$ Å. MC HUGH and TILLER (1960) reported that a congruently melting compound has an equilibrium composition of $Ge_{0.975}$ Te and a hole concentration of about $10^{20}\,cm^{-3}$. MAZELSKY and LUBELL (1962) also found the hole concentration of GeTe to be of the same order ($7\times10^{20}\,cm^{-3}$). Because of this stoichiometric deviation and hence the existence of Ge vacancies in the lattice, GeTe is always *P*-type. These values of carrier concentration together with the known deviation from stoichiometry are consistent with the proposition that each of the vacancies provides two positive holes. Measurements of the optical and electrical properties of single crystal GeTe in bulk and film specimens have been reported, by TSU et al. (1967). These specimens had rather high hole concentrations ($10^{21}\,cm^{-3}$) even though they contained less than 1% excess tellurium. By fitting the reflectivity data to theoretical expression for the free carrier dispersion relations they obtained values for the optical dielectric constant of about 37.5 and 35 at room, and liquid helium temperatures respectively. The carrier relaxation time obtained from the same fitting procedure was about $0.38\ 10^{-14}$ sec.

In further work, TSU et al. (1968) showed that a picture of the GeTe band structure could be deduced from optical and other data obtained from film specimens of GeTe. They assumed that GeTe had a similar band structure to that of the lead salts, treated GeTe as cubic and used a similar four band model to that of SnTe. For GeTe the reduction of the 4×4 kP determinant to a 2×2 determinant is better justified than in SnTe because the ratio:

$$\hbar^2 k_{lF}^2/2m_l(c_1)\,E_{\Delta_v}\approx 1.0. \tag{2.14}$$

This shows that the first longitudinal conduction and second longitudinal valence bands are practically parabolic. Using the same equations (2.11) and (2. 13) and their own data, TSU et al. (1968) obtained for the best set of band parameters:

$E_g\,(eV)$	$E_{\Delta v}\,(eV)$	$\frac{P_t^2}{m_0}\,(eV)$	$\frac{P_l^2}{m_0}\,(eV)$	$\frac{m_l(v_1)}{m_0}$	$\frac{m_l(c_1)}{m_0}$	$\frac{m_l(v_2)}{m_0}$	$\frac{m_t(v_2)}{m_0}$
0.1	0.60	6.8	0.34	0.85	0.425	2.8	2.8

They also proposed the band-edge energy dispersion relations for GeTe given in Figure 2.4. which can be seen to be very similar to those for SnTe.

The adsorption coefficients for an allowed direct transition between the valence and conduction band can be calculated as a function of the FERMI energy, using FAN's expression (1956).

$$\alpha=\frac{2\pi e^2 h P_t^2}{3ncm_0^2 h\nu 4\pi^3}\int \mathrm{d}\vec{k}\,\delta(h\nu-E_{c_1}+E_{v_1}) \tag{2.15}$$

where n is the reflective index and P_t a transverse matrix element which is assumed to be constant. By comparing their measured values for GeTe values calculated from this expression (see Fig. 2.5.), TSU et al. concluded that there may be a very strong BURSTEIN shift in GeTe and that the true energy gap could be between 0.1 and 0.2 eV. This is consistent with the room temperature energy gap for GeTe of 0.1 eV. obtained from tunnelling measurements also by Tsu et al. A similar value was also obtained by ESAKI (1966) who further showed that the rate of decrease of the energy gap for GeTe with increasing temperature was about 2×10^{-4} eV (deg °K)$^{-1}$.

CARDONA and GREENAWAY (1964) measured the reflectivity of GeTe film specimens in the far ultra violet region and determined the energies of the third to the sixth transitions, inclusively. Unfortunately however they did not observe either the absorption edge or the energy of the second transition.

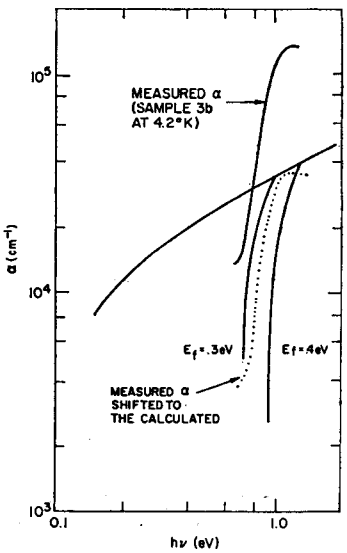

Figure 2.5. A measured absorption edge for GeTe compared to absorption calculated for three Fermi energies.

2.5. GeSe and SnSe compounds

As far as is known, only two papers have been published on the optical properties of GeSe and SnSe compounds both of which have the orthorhombic B29 structure. OKAZAKI (1958) and KANNEWURF (1960) obtained values for the lattice parameters of GeSe of $a = 4.40$: $b = 10.82$ and $c = 3.85$ Å. OKAZAKI (1960) also studied the electrical properties of polycrystalline GeSe and from the slope of the resistivity curves at high temperature estimated the energy gap to be about 1.0 eV. KANNEWURF and CASHMAN (1961) studied the room temperature absorption in extremely thin single crystal specimens of GeSe in the form of filaments. They grew their specimens by heating polycrystalline ingots in a quartz boat through which was passed a continuous flow of hydrogen gas. Their results indicated the existance of a forbidden direct transition corresponding to an energy gap of about 1.53 eV.

SnSe has an orthorhombic unit cell and is isomorphous with GeSe i.e. both have a distorted sodium chloride structure. DEMBOVSKII et al. (1963) showed that SnSe has a phase transition at 540°C which they assumed to be a second order transition. ALBERS et al. (1962) made single crystals of SnSe containing less than 2.5×10^{16} cm^{-3} impurities from polycrystalline materials which they first purified. Their measurements of optical transmission at room temperature and at 77°K indicated the presence of a transition between the valance and the conduction band with an energy of about 0.9 eV. At 77°K they also observed several other transitions between 0.2. and 0.9. eV and they suggested that one of them might be an absorption band due to interband transition of holes from the highest band to a lower lying valence band.

2.6. The other IV—VI compounds used in this work

The crystal structures, energy band gaps and certain other properties of the other relevant IV—VI semiconducting compounds are shown in Table 2.2. together with the main references.

TABLE 2.2.

Compound	Structure	Energy Gap	Majority carrier	Melting point
PbSe	B1	0.29[I]	N.P	1081[II. III]
SnS	B29	1.08[IV]	P	881[IV. V]
GeS	B29	1.8[VI]	—	674[V]

References. I. SCANLON (1959), II. SIMPSON (1964), III. MILLER and KOMAREK (1966), IV. ALBERS et al. (1962), V. ELLI (1963), VI. YABUMOTO 1958.

Quite a lot of work has been done on PbSe and it appears to be very similar to PbTe and PbS in all its properties including the energy band structure. ZEMEL et al. (1965) have shown that single crystal films of PbSe, have very similar properties to those of bulk material as is the case with other IV—VI compounds and the average value of the optical dielectric constant of PbSe obtained from their reflectivity data on 2 samples at room temperature was 23. Calculations of the band structure of PbSe by DIMMOCK and WRIGHT (1964): LIN and KLEINMAN (1966) and RABAII (1968) indicate that the structure is very similar to that of PbTe.

There is much less data available on GeS and SnS and there is still considerable uncertainty in the magnitudes of their energy gaps. The main reason is that they all have high carrier concentrations normally higher than 10^{20} or 10^{21} and so the measured gaps may well be displaced by BURSTEIN shifts. It is expected that tunnelling measurements will shortly provide information on this however.

2.7. IV—VI semiconductor alloys

A relatively small amount of data has been published on IV—VI alloys and information on their optical properties, which is the main concern of this thesis is particularly limited. The mutual solid solubility of IV—VI compounds has been examined for fourteen of the eighteen possible ternary systems and nine of the eighteen possible quaternary systems. These data are summarised in Table 2.3. It is seen that complete solid solubility occurs mainly when both compounds have the same lattice structure which is usually NaCl i.e. B1. These data were largely obtained using X-ray diffraction measurements. The optical work that has been done is mainly limited to the PbTe-SnTe and PbSe-SnSe alloys which appear to be possible detectors and emitters in the range between 8 and 14 microns or even beyond. There has also been a little work on transport properties. A review of all this work has recently appeared (STRAUSS 1968).

TABLE 2.3.

Compound		Solubility of A in B mol % A	Solubility B in A mol % B
A	B		
PbSe	PbTe	100[I]	100[I]
PbS	PbTe	3 to 100[III]	1 to 100[II]
SnTe	PbTe	100[III]	100[III]
SnSe	PbTe	60[IV], 61[V], 70[VI]	10[V], 20[IV]
GeSe	PbTe	35[VI]	/
GeTe	PbTe	20[VIII], 30[IX] 100[X]	8[X]
PbS	PbSe	100[XI]	100[XI]
SnSe	SbSe	43[XII]	25[XII]
GeSe	PbSe	8[XIII], 9[V]	20[XIII], V
SnS	PbSe	33[V]	40[V]
SnTe	PbSe	100[V]	100[V]
GeS	PbSe	8[V]	/
SnSe	PbS	15[V]	30[V]
GeSe	PbS	8[V]	10[V]
SnS	PbS	10[III], 100[VII]	55[III]
GeSe	SnTe	20[V], 40[V]	5[V]
SnSe	SnTe	20[VI], 22[XII]	28[XII], 75[IV]
GeTe	SnTe	100[XII], VIII	100[XII], VIII
GeTe	SnTe	20[XII]	20[XII]
SnS	SnSe	100[III]	100[III]
GeSe	SnSe	100[V]	100[V]
GeSe	SnS	100[XIV]	100[XIV]
GeSe	GeTe	5—100[XIII], 15[XV] 53[XVI], 63[V]	5[V], 8[XVI], 10[III]

References: I. YAMAMOTO (1956), II. DARROV et al. (1966), III. ALBERS et al. (1926), IV. NISHIYAMA and CKADA (1960), V. KREBS and LANGNER (1964), VI. NIKOLIĆ (1965), VII. MOROZOV and CHIHFA (1963), VIII. MAZELSKY and LUBELL (1962), IX. SHELIMOVA et al. (1964), X. WOOLLEY and NIKOLIĆ (1965), XI. SIMPSON (1964), XII. KREBS et al. (1961), XIII. SHELIMOVA et al. (1966), XIV. ELLI (1963), XV. ANTONOV and NASIROV (1966), XVI. MUIR and GASHMAN (1967).

2.7.1. *Optical properties of IV—VI alloys.* In this brief review of the optical properties, we have included mention of our own published data to be described later in this thesis. The first optical transmission measurements in the alloys were made by SCANLON (1959) on single crystals of PbTe—PbSe and PbSe—PbS alloys. He observed a linear decrease of the energy gaps where either PbTe or PbS was added to PbSe and observed both direct and indirect energy gaps in both alloys. Even at the present time his direct energy gaps for the compounds and the alloys are those most widely quoted.

ALBERS et al. (1962) also made transmission measurements of single crystal alloys of SnS-SnSe and found an almost linear change of the indirect energy gap in this system too. The carrier concentration in these specimens was rather low for an alloy-about 5×10^{17} cm^{-3}.

WOOLLEY and NIKOLIĆ (1965) reported room temperature transmission measurements for PbTe-GeTe and NIKOLIĆ (1966) for PbTe-GeSe alloys. In both systems the energy gap increases with increasing concentration of GeTe and GeSe respectively. Since pure GeTe is believed to have a very low room temperature energy gap (0.1eV-ESAKI, 1966) one might expect that the energy gap should decrease when GeTe is added to PbTe. However since this is not the case, we anticipate that the gap should reach a maximum and then fall and this appears to be what happens although the published work is incomplete.

NIKOLIĆ (1965) reported room and liquid nitrogen temperature transmission measurements for PbTe-SnTe alloys and observed a decrease in the energy gap with increasing tin content. These alloys also have a positive temperature coefficient of the energy gap which is similar to that in PbTe, but opposite to that in SnTe. BYLANDER (1966) also measured the transmission at room temperature through single crystal epitaxial films of PbTe-SnTe alloys and confirmed NIKOLIĆ'S observation of the decrease in E_g with alloying. Further confirmation was reported by DIMMOCK et al. (1966) who observed that spontaneous and coherent fluorescent emission could be excited by a GaAs laser from alloys containing 19 mol % and 17 mol % SnTe. The coherent emission of the two alloys was at 15 and 14.9 microns respectively again showing that the room temperature energy gap decreases when SnTe is added to PbTe. DIMMOCK et al. (1966) proposed a band structure inversion model for PbTe-SnTe alloys to explain these data which is illustrated in figure 2.6. This model accounts for the fact that linear extrapolation of the gap energy against SnTe content gives an energy gap value for pure SnTe of the correct magnitude but negative in sign. This suggests that the bands become inverted as shown.

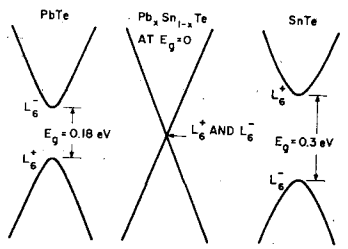

Figure 2.6. Schematic diagram of the velence and conduction bands for PbTe, PbTe—SnTe at Eg = 0, and SnTe.

It is interesting to note that WAGNER and WILLARDSON (1968, 1969) have shown that the CZOCHRALSKI technique can be used to grow single crystals of PbTe-SnTe alloys from stoichiometric and nonstoichiometric cation rich melts. Their crystals had free carrier concentrations of about 10^{19} cm^{-3} and mobilities between 500 and 9000 cm^2/*Vs*.

In analogy with the PbTe-SnTe system, STRAUSS (1967) also explained the decrease in the energy gap in the PbSe-SnSe system using an inversion model. However this model predicts a very small energy gap for pure SnSe (about 0.1 eV at room temperature) in marked contract with the measured room temperature value of 0.9 eV (ALBERS et al. 1962) quoted by STRAUSS in his review paper (1968). We note that here STRAUSS's single crystal film specimens which were on KCl substrates, were made from single alloy sources i.e. using the technique first introduced by BYLANDER (1966). Confirmation of the decrease of the energy gap of PbSe-SnSe alloys with SnSe content was obtained by BUTLER et al. (1966) from their measurements of the emission wavelengths of laser diodes and by NIKOLIĆ (1967) using optical transmission. NIKOLIĆ also observed a similar decrease of the room temperature energy gap in PbSe-SnTe and PbSe-SnSe alloys.

The first optical work on GeTe-GeSe alloys was published by MUIR and CASHMAN (1967, 1968) who made both electrical and optical measurements on

a single crystal specimen of 75 mol% GeSe, 25 mol% GeTe. They concluded that this alloy was a degenerate semiconductor with a large free carrier concentration (about 10^{20} holes cm^{-3}). Hence their measured value of the fundamental absorption edge of 0.82 eV is probably too large because of the BURSTEIN shift. Finally we note that work has been published on the crystallographic and optical properties of some of the lead germanium chalcogenide alloys (NIKOLIĆ, 1969).

3. DESCRIPTION OF SPECIMEN PREPARATION

3.1. Preparation of the IV—VI compounds

The compounds used for the work in this thesis are: PbTe, PbSe, SnSe, SnS, GeTe, GeSe and GeS. They were all prepared in the laboratory by a direct combination of a stoichiometric mixture of the constituent elements. The elements used to prepare the compounds were at least 99.999% pure and were obtained either from L. LIGHT and KOCH or from JOHNSON, MATTHEY. It was not considered necessary to purify the elements further.

If the elements used were supplied in the form of a single lump, the lump of each element in turn was placed in a mortar and reduced to smaller grains. The mortar was first properly cleaned with concentrated nitric acid and then washed several times with distilled water. The stoichiometric quantities of the constituent elements were weighed out, placed in a quartz tube which was evacuated to about 5×10^{-5} mm Hg and then sealed off. The quartz ampoule was suspended by an Kanthal wire in a vertical tube furnace maintained at a temperature at least 100°C higher than melting points of the compound and of the constituent elements. The ampoule was shaken at intervals to aid mixing. The temporature of the furnace was measured using a calibrated Pt — Pt/Rh thermocouple. The compounds were usually left in the furnace for two hours and then quenched either by immersing the ampoule in cold water or by removing it from the furnace and leaving it in air to cool down. The compounds were then set to anneal in furnaces usually at about 600—700°C.

X-ray powder photographs were then taken to check that each of the compounds had lattice parameters in reasonable agreement with those found in the literature. Occasionally X-ray photographs were taken of samples cut from different points along an ingot to demonstrate that it had a constant lattice parameter throughout its length.

Particular care had to be taken in the preparation of GeS and SnS since a very high pressure of sulphur gas is developed inside the ampoule at high temperatures. Thick quartz ampoules tubes were always used in this case (about 1.5 mm wall thickness in a diameter of 6 mm) and the total sulphur content was always kept below 1 gm. In later preparations the ampoule was lowered into the furnace in two stages: first it was heated for about 30 minutes in the cooler regions of the furnace and then it was lowered towards the centre. A still better procedure would be to raise the temperature of a totally cold furnace. In the earlier preparations before these procedures were adopted, two ampoules exploded causing damage to the furnaces.

The ingots of GeS and SnS were necessarily very small but the ingots of the other compounds each weighed between 15 and 40 grams. During the course of this work we had to prepare ingots of every compound at least five times.

3.2. Preparation of the alloy specimens

Alloy specimens weighing between two and six grams, were prepared by melting the required quantities of the respective compounds in evacuated quartz tubes usually at about 1150°C. The tubes were left at this temperature for two hours. The alloys were then annealed until X-ray photographs indicated that equilibrium had been obtained. Details of annealing times and temperatures are given in chapter 5. After annealing the ampoules were quenched in cold water or air.

In many cases the range of solid solution is incomplete and to obtain the largest range of concentration possible it is necessary to anneal the alloys at temperatures very close to the melting point. However if a specimen melts as a result of a fluctuation in the furnace temperature, it has to be discarded so that considerable care and patience have to be used in the annealing procedure.

Measurements of lattice parameters and optical transmission were only made using ingots containing a single phase i.e. those which gave sharp lines, in an x-ray photograph. Some of the specimens made for optical work contained a large quantity of pin holes and other broke during the polishing procedure, so that many of the specimens were prepared twice or three or four times before satisfactory specimens were produced. Usually measurements were made on two different specimens.

Normally a complete set of specimens of one alloy system, but of various compositions was made in one day, each of the specimens being made under nominally identical conditions. About 10—20 specimens of each system were made.

3.3. Preparation of bulk specimens for optical measurements

The specimens for optical measurements were cut from ingots prepared as described in 3.2. The ingots were mounted on fibre blocks with "Durofix" adhesive, and slices between 0.5. and 1.5. mm across were cut from them with a carborundum wheel 3 in. in diameter and 6×10^{-3} in. thick rotating at 4000 rpm. The slices were then removed from the block and attached with "Durofix" to the end of a steell cylindrical rod about 5 in. long. The rod was a clearance fit in a 1″ hole bored through a cylinder 4″ long and about $2^1/_2$″ in diameter. The end of the rod on which the specimen was stuck was made of phosphor bronze to reduce wear. The slices were first ground using the table of a tool post grinder on which the rod was mounted by means of a V clamp. The 4″ grinding wheel (universal grinding wheel c 220 kv) was rotated at 4000 rpm. Next the steel rod was put into the hole of the bar and the specimens were polished by holding the bar so that they were in contact with a rotating "microcloth" impregnated with either 6 micron, 3 micron or $^1/_4$ micron "Diamond compound". "Hyprez lubricant" was used during this polishing. No further polishing was carried out on specimens used only for transmission measurements, but for specimens used in reflectivity work a higher degree of polish was necessary so in this case a final polish using alpha alumina (particle size 1 or 0.3 micron) was given.

In many cases an electropolishing procedure was used finally to remove the damaged surface layers. For this procedure the specimen was potted in an epoxy resin, "Ceemar", together with a brass rod to which it was connected electrically with silver paint. With this arrangement, all the electrolytic current passed through the front face of the specimen. The electrolyte was usually a 5% solution of nitric acid in ethane diol although on occasions CP4 and CP6 and some other electrolytes

used by RIEDL (1962) for PbTe were also tried. The construction of the electropolishing machine was such that the specimen rotated about its own axes so producing a washing action.

After several minutes of electropolishing, crystallites of the specimen usually became clearly visible under the microscope showing that the surface layers had been removed and that the specimen surface was suitable for reflectivity measurements. The other surface which was usually parallel to the polished one was always left unpolished to avoid parasitic reflectances which can occur from back faces if they are also highly polished. An alternative is to use wedge shaped specimens (CARABATES 1917).

While the specimens used in reflectivity measurements could be thick i.e. up to 3 mm, the specimens used for transmission measurements had to be as thin as possible. So for transmission measurements, after a polish had been obtained on one specimen surface it was dissolved off the rod with acetone and turned over, and the unpolished surface was ground until the slice was approximately 100—200 microns thick. Finally it was polished to get a specimen which was as thin as possible while at the time did not contain any holes. Usually after polishing, the specimens were between 70 and 100 microns thick, although occasionally it was possible to make slices as thin as 30 microns. Such specimens were very difficult to handle. After the polishing the specimens were removed once more from the rod and washed carefully in pure acetone to remove all traces of "Durofix" and were then finally washed in alcohol. The specimen was next mounted with a single blob of Durofix across the narrow slit of the brass specimen holder used for room temperature measurements. At liquid nitrogen temperature, the arrangement was slightly different and the brass specimen holder to which the specimen was attached had two identical slits side by side so that both the incident and transmitted intensity could be measured readily by displacing the holder.

3.4. Preparation of film specimens

Several articles have been published on the techniques of preparing film specimens of semiconducting alloys. One, two or even more sources have been used in this work. For instance POTTER and KRETSCHMAR (1964) have described a so called four temperature method for making InSb-InAs specimens. In this three crucibles, each containing one of the 3 elements, were heated to the different temperatures necessary to obtain film specimens of the required InSb-InAs alloy. The glass substrate was heated to a fourth temperature to allow diffusion to take place within the film. In a second method the compounds rather than the elements are evaporated. BIS and ZEMEL (1966) have described their arrangement of two separate "ovens" containing either PbTe or PbSe. Both compounds, were evaporated at the same time into a heated NaCl substrate and single crystal alloys of various compositions could be obtained by varying the temperatures of the ovens.

The first films prepared from a single source i.e. from an alloy sample were made by BYLANDER (1966) who prepared epitaxial films of PbTe alloys. These films had the same lattice constant as the bulk source material to within the experimental error of two parts in 6000!

STRAUSS (1967) has also shown that single crystal films can be made using a single alloy source, in this case of PbSe-SnSe and this technique was mainly used in the present work although occasionally two separate sources have also been used.

Particular care was taken in preparing the bulk specimens used for evaporation. The same technique was used as before but the ampoules were evacuated for longer typically 3 hrs until a lower pressure, 1×10^{-5} mm or better, was attained. Also the ampoules were kept in the furnace for a longer time, typically 4 hrs, and were then allowed to cool in air. The evaporators used were made by Edwards: type numbers E12E3, 19A8/136 and 12E3; details of these will be described later. The temperatures of the source and substrate were in the ranges 600—800°C and 60—250°C respectively and the rate of deposition was usually about 500—700 Å/min. After deposition the films were allowed to cool down in a vacuum although many of them were kept at their deposition temperature to anneal for 1—1.5 hours. Usually two specimens were made at a time and about 200 evaporations have been carried out in the course of the work. Various substrates have been used, principally NaCl, KBr, mica and glass depending on the type of experiment for which the film was to be used in. Also at the beginning of the investigation formvar was used as a substrate for electron microscope studies. It was desirable that for both transmission and reflectivity measurements the films should be single crystals, so that for this work transparent single crystal substrates of NaCl or KBr were used. These substrates were pieces measuring about $1'' \times 0.5''$ which were freshly cleaved just before being put into the evaporator. The thickness of films used for transmission measurements in the ultraviolet-visible region and in the infra-red region were typically about 1000 Å and 1 micron, respectively. In some cases a weighed piece of microscope slide was put very close to the substrate and from its increase in weight a value for the thickness of the film was obtained. This method was checked by measuring the thickness of the film on the glass useing an interference technique with visible light (TOLANSKY, 1948). For thicker films where interference with visible light is not easily seen, the thickness was often obtained from interference effects apparent in the transmitted infra red beam.

The specimen evaporated onto the glass substrate was also occasionally used to determine the composition of the specimens by X-ray diffraction analysis. Unfortunately, however this technique can not be used to give information about the grain size of the film on the single crystal substrate since this is not in general the same as that on the glass. Hence attempts were made to determine this information from the specimen films themselves. The difficulty in this technique where used with a single crystal substrate is that the films are so thin that X-ray lines are also seen from the substrate. To identify these lines a second pattern was always obtained from the back of the substrate and in many cases, at compositions where the lines from the film were well away from any substrate lines, they could be identified and so the number of different grains determined. Other authors have also found it possible in many cases to determine the nature of similar films e.g. SCHOOLER and ZEMEL (1964): 3 micron films of PbS, and Bis and Zemel (1966): 0.5 micron films of PbTe-PbSe. In some cases however it was found in the present work that the lines from the film and the substrate were too close for clear identification to be made and a different procedure had to be adopted in which the film was transferred to an amorphous substrate. The substrates are of course water soluble so that the films were removed from their substrates by bringing them to the surface of a watch glass containing water. It was hoped that they would sink in one piece to a glass substrate resting at the bottom of the watch glass. Unfortunately the films invariably parted into small pieces which remained floating on the surface. It was possible to collect some of the pieces onto the slide but this was an unreliable technique; often there was not enough material to give good X-ray

lines or NaCl or KBr lines were still present and the film had to be rewashed at the risk of damaging it. We later arrived at a simple method for transferring a film from a NaCl substrate to a glass substrate in one piece. A thin layer of "Durofix"

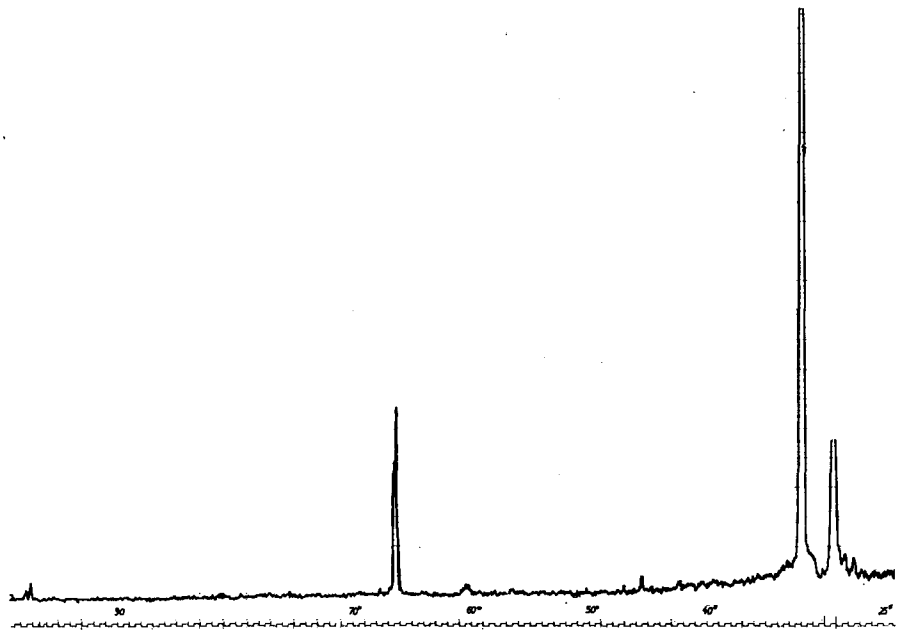

Figure 3.1. A Bragg diffractometer recording of 7o mol % GeTe and 30 mol % PbTe on NaCl substrate.

is spread onto a glass substrate and the front side of the film is stuck to it and left for about 30 minutes. The NaCl substrate is then cleaved to leave a in layer of NaCl stuck with the film to the glass and the whole arrangement is then immersed in water. The NaCl dissolves away leaving the film in one piece firmly stuck to a glass substrate. Very good X-ray diffraction patterns showing even the relatively weaker BRAGG diffraction lines were obtained with this arrangement. This was the case even with very thin films (under 0.4 micron) since the X-ray source could be run up to 35 kV and 24 mA giving very intense beams. Several diffractometer recordings for various alloys on NaCl and glass substrates are given in Figures 3.1. to 3.4.

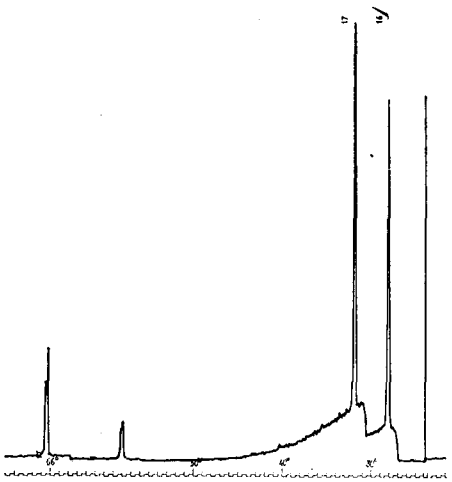

Figure 3.2. A Bragg diffractometer recording of 20 mol % GeTe and 80 mol % PbTe on NaCl substrate

It was often convenient to make specimens for electron microscope studies during the same evaporation in which the optical specimens were prepared. However the optical specimens were typically 1 micron thick while the electron microscope

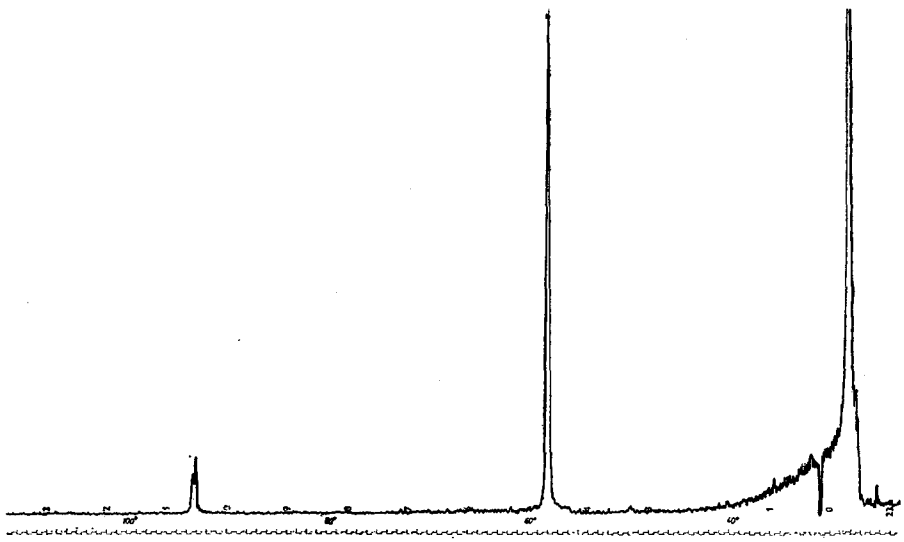

Figure 3.3. A Bragg diffractometer recording of a film of 20 mol % GeTe and 80 mol % PbTe on glass substrate.

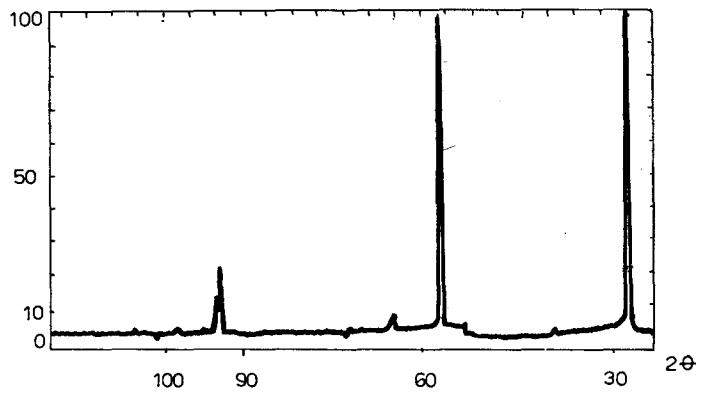

Figure 3.4. A Bragg diffractometer recording of a film of 5 mol % SnTe and 95 mol % PbTe on glass substrate.

specimens which had to be transparent to the electron beam were about 0.1 micron thick. Hence the substrates were exposed for different times using a specially designed shutter. Further details of the preparation of specimens used in electron diffraction work are given in chapters 4 and 5.

4. METHODS OF MEASUREMENT AND APPARATUS

4.1. Optical properties of solid semiconductors

The optical absorption coefficient, of a semiconductor provides valuable information on its band structure. The lowest (fundamental) absorption edge gives the minimum energy separation between the conduction and valence bands and also information about the nature of the transition. In Figure 4.1. the absorption coefficient is plotted against wave length for a typical semiconductor. In the ultraviolet region, (1), the absorption coefficient is very largely due to electronic polarization, (2), in the visible and near infra red region, to electron excitation from the valence to the conduction band, and at higher wave lengths, (3), the absorption is largely due to free carriers. Electronic polarization and free carrier absorption can both be treated successfully using classical theory but electron excitation is of course essentially a quantum mechanical process.

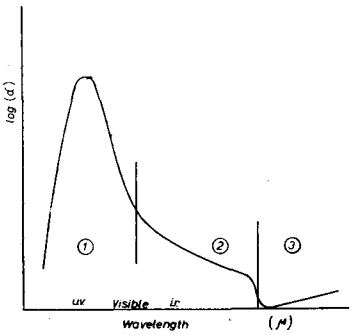

Figure 4.1. The variation of the absorption coefficient, α, with wavelength

The absorption coefficient rises very rapidly at and above the fundamental edge to values very often $\sim 10^4$ and $10^6\,cm^{-1}$. These can only conveniently be obtained from transmission measurements by using very thin specimens about 1000 Å thick or less which are usually prepared by vacuum evaporation. The optical constants can also be determined from reflectivity measurements using the KRAMERS-KRONIG dispersion relation. Since this involves an integral over the whole frequency range, measurements have to be carried out over as broad frequency region as possible. The advantage of reflectivity work is that measurements can be made on bulk specimens. In this way the influence of the large number of imperfections which can be present in thin films prepared by vacuum deposition techniques is avoided. A disadvantage is that the measurements are very dependent on the condition and previous treatment of the surface.

There are six possible contributions to optical absorption: (1) excitation of electrons from the valence band to a conduction band, (2) generation of lattice vibrations, (3) generation of excitons, (4) excitation of free carriers within a band, (5) excitation of free carriers from one band to another of the same type, (6) absorption by imperfections. The present work is mainly concerned with the first absorption process, usually called the "fundamental process". The minimum energy separation of the conduction and valence bands is called the energy gap.

The absorption coefficient α is defined by the wave equation

$$\nabla^2 E - \mu_0 \sigma \frac{\partial E}{\partial t} - \mu_0 \varepsilon \frac{\partial^2 E}{\partial t^2} = 0. \tag{4.1}$$

E is the electric field; μ_0 the permeability of free space; σ the electrical conductivity ε the dielectric constant of the medium.

From equation (4.1) one can easily obtain the following:

$$\alpha = \frac{2\omega k}{c} = \frac{4\pi k}{\lambda} \tag{4.2}$$

Using FERMI's Golden Rule it can be shown that for an electronic transition

$$\alpha = \frac{2\pi}{3 m^2 nch\nu} |\varkappa_{ij}|^2 n(\nu) \tag{4.3}$$

where $\varkappa_{ij}$ is the matrix element for the transition and $n(\nu)$ is the density of electron states corresponding to this frequency.

If the COULOMB interaction between the electron hole pair is neglected, α can now readily be calculated. This is a reasonable approximation because of the effects of screening by carriers and impurities and can be justified by the agreement obtained between this expression and experimental results on samples at high temperatures. Without the interaction the energy can be expressed by

$$E(k) = E_c + (\hbar^2/2 m_e) k^2 \tag{4.4}$$

near the bottom E_c of the conduction band and by

$$E(k) = E_v - (\hbar^2 m_h) k^2 \tag{4.5}$$

near the top E_v of the valence band, where m_e and m_h are the effective masses of electrons and holes in the conduction and valence bands respectively. Hence near the fundamental absorption edge the transition energy can be written

$$h\nu_{cvk} = E_g + \left(\frac{\hbar^2}{2 m_r}\right) k^2 \tag{4.6}$$

BARDEEN et al. (1956) has shown that for direct and indirect allowed transitions, α is proportional to $\left(\frac{h\nu - Eg}{h\nu}\right)^{\frac{1}{2}}$ and $\left(\frac{h\nu - Eg \pm Eph}{h\nu}\right)^2$ respectively and also for direct and indirect forbidden transitions α is proportional to $\left(\frac{h - Eg}{h\nu}\right)^{\frac{3}{2}}$ and $\left(\frac{h\nu - Eg \pm Eph}{h\nu}\right)^3$ respectively where Eph is the energy of the phonon absorbed (+) or emitted (—). Hence from the frequency dependence of α, one can in principle determine the nature of the transition.

We should now discuss briefly the meaning of the terms direct and indirect and allowed and forbidden transition. A direct transition is when an electron is excited from the valence band to the conduction band without any change in its wave vector k. An indirect transition involves the emission or absorption of a phonon, which assists the excitation of a valence electron with one value of k to a part of the conduction band where it will have a different wave vector $\vec{k}$. Indirect transitions in general have a lower transition probability than direct transitions.

To discuss the meaning of the terms allowed and forbidden transitions we must consider in detail the perturbing HAMILTONIAN causing the transition.

In a magnetic field described by a vector potential A, it is well known (e.g. LANDAU and LIFSHITZ — fields, 1958) that in the HAMILTONIAN describing an electron, $\vec{P}$ must be replaced by $\vec{P} + \frac{e\vec{A}}{c}$

$$\varkappa = \frac{1}{2m}\left(\vec{P} + \frac{e\vec{A}}{c}\right)^2 + V(\vec{r}) = \left[\frac{\vec{P}^2}{2m} + V(r)\right] + \left[\frac{e}{mc}\vec{P}\cdot\vec{A} + \frac{1}{2m}\cdot\frac{e^2}{c^2}\vec{A}^2\right] \tag{4.7}$$

since P and A commute in the gauge $\nabla\vec{A}=0$. For the fields present in normal light sources

$$\frac{1}{2m}\frac{e^2}{c^2}A^2 \ll \frac{e}{mc}\vec{P}\cdot\vec{A}$$

so that

$$\varkappa = \varkappa_0 + \varkappa' \tag{4.8}$$

where

$$\varkappa' \simeq \frac{e}{mc}\vec{P}\cdot\vec{A} \simeq \frac{e}{mc}A_0\vec{P}\cdot\vec{e}_k\, e^{i\vec{k}\cdot\vec{r}} \tag{4.9}$$

where $\vec{e}_k$ is a unit vector. Hence, using FERMI's Golden Rule the transition probability per unit time between states i and j is

$$W_{ij} = \frac{2\pi}{\hbar}|\varkappa_{ij}'|^2\,\delta(E_i - E_j) \tag{4.10}$$

The probability that a photon is absorbed can be readily calculated by expressing A_0 in terms of annihilation and creation operators whose matrix elements are known so that we obtain an expression for the absorption coefficient

$$\alpha \simeq \left|\frac{e}{mc}\int \psi_i^*\,\vec{P}\vec{e}_k\, e^{i\vec{k}\cdot\vec{r}}\psi_j\,\mathrm{d}\tau\right|^2 \tag{4.11}$$

Suppose for convenience $\vec{e}_k$ is the z direction so that $\vec{P}\cdot\vec{e}_k = p_z$, and since the optical wavelengths are usually much larger than the linear dimensions of the wave functions we replace $e^{i\vec{k}\cdot\vec{r}}$ by 1 then

$$\alpha \simeq \left|\int \psi_i^* P_z \psi_j\, d\tau\right|^2 \tag{4.12}$$

Now

$$i\hbar\dot{z} = z\varkappa - \varkappa z \tag{4.13}$$

so

$$\int \psi_i^* P_z \psi_j \mathrm{d}\tau = \frac{m}{i\hbar}\int \psi_i^*(z\varkappa - \varkappa z)\psi_j\,\mathrm{d}\tau + \frac{m}{i\hbar}(E_i - E_j)\int \psi_i^* z\,\psi_j\,\mathrm{d}\tau \tag{4.14}$$

and $\int \psi_i^* ez\,\psi_j\,\mathrm{d}\tau$ is the electric dipole moment of the electron in the direction of the field. Hence transitions of this sort are called Electric Dipole Transitions.

It is important to note that such transitions are not always possible. If we change the definition of the coordinates such that $x \to -x$, $y \to -y$, and $z \to -z$, then clearly physically nothing is changed and the matrix elements must be the same. However, if ψ_i^* and ψ_j have the same parity — either both odd or both even — then

$$\int \psi_i^* z\,\psi_j\,\mathrm{d}\tau \overset{x\to -x}{\to} -\int \psi_i^* z\,\psi_j\,\mathrm{d}\tau \tag{4.15}$$

and so must be zero. Hence we arrive at LAPORTE's rule: Electric Dipole transitions are forbidden between states of the same parity.

This does not mean, however, that $\alpha=0$. In obtaining an expression for α, we neglected *ikr* in comparison with 1. but if $\alpha_{E\cdot D}=0$, we must reconsider this term since now

$$\alpha \simeq \left| \int \psi_i^* (\vec{e_k} \cdot \vec{r})(\vec{k} \cdot \vec{r}) \psi_j \, d\tau \right|^2 \tag{4.16}$$

Physically the integral represents transitions due to magnetic dipole and electric quadrupole moments of the electron. Transitions due to this are called "Forbidden" and the resulting absorption is generally much weaker than that due to electric dipole transitions.

One final point which can modify the position of the apparent gap should now be mentioned. BRIGGS (1953) observed a strong dependence of the position of the absorption edge in InSb on the carrier concentration in the sample. This has been explained theoretically by BURSTEIN (1954) and the effect is now usually referred to as the BURSTEIN effect. An explanation of this can be obtained by considering the expression for the absorption coefficient of a degenerate semiconductor (FAN 1956). The effect of doping can also be seen by considering a diagram of the energy bands. For example the energy bands for InSb are given in Figure 4.2. (GOBELI and FAN, 1960). One can see that for an N- type specimen (Figure 4.2a) interband transitions begin at a photon energy of $h\nu_1$. This is a heavy mass band transition. The absorption reaches its full value at a photon energy of $h\nu_2$ which is equal to the onset energy for transitions from the light mass band V_2. These two steps in absorption can be seen when $h\nu_2 - h\nu_1 \gg kT$. For a P- type specimen of InSb (Figure 4.2b) the situation is opposite to this, The absorption edge is now due to transitions from the light mass band at an energy $h\nu_2$. However, if the FERMI level moves deeper into the valence bands, the energy $h\nu_{12}$ (the maximum photon energy at which transitions between V_2 and V_1 can occur) becomes comparable to the energy $h\nu_1$ (Figure 4.2.c) so that the absorption associated with the transition between V_1 and V_2 can be seen near to the absorption edge.

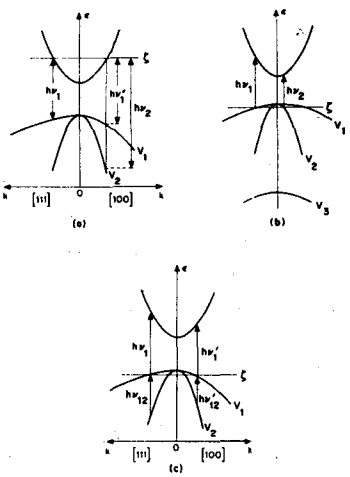

Figure 4.2. Schematic diagram of energy bands of InSb.

4.1.1. *Transmission and reflectivity of semiconductors.* Expressions for the transmission and reflectivity of semiconductors can be derived as in other transparent systems, either by applying the electromagnetic boundary conditions to the total incident, transmitted and reflected waves, or by summing the complex amplitudes of the individual waves arising from multiple reflection at the interfaces. We shall briefly consider the general approach in both methods.

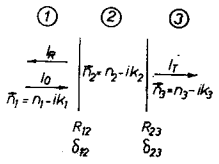

Figure 4.3

STRATTON (1941) has given rather complicated expressions for the transmission, T, and reflectivity, R, for the three arbitrary homogeneous media (Figure 4.3) separated by plane boundaries; R_{ij} and δ_{ij} represent the reflectivity and the phase angles of the boundary between media i and j respectively. If the extinction coefficient, k, is very small ($k<10^{-2}$) for media (1) and (3) and the specimens are thick

and self supporting (i.e. without substrate), then the final expressions for the average transmission and reflectivity become (MILLER, 1967)

$$T=\frac{(1-R_0)^2\exp(-\alpha d)}{1-R_0^2\exp(-2\alpha d)}, \tag{4.17}$$

$$R=R_0\left[1+\frac{(1-R_0)^2\exp(-2\alpha d)}{1-R_0^2\exp(-2\alpha d)}\right]=R[1+Te^{-\alpha d}]. \tag{4.19}$$

If internal reflection in the sample can be neglected as in strongly absorbing thick specimens

$$R_0^2\exp(-2\alpha d)\ll 1 \tag{4.19}$$

and

$$T=(1-R_0)\exp(-\alpha d) \tag{4.20}$$

and

$$R=R_0. \tag{4.21}$$

This shows that under these conditions the measured reflectivity is simply equal to the reflectivity at the first boundary.

The transmission can also be determined by measuring the transmissions of two identical samples differing only in thickness. Equation (4.17), can then be used to determine α. If the conditions are such that (4.20) can be used, the determination is trivial:

$$\alpha=\frac{1}{d_1-d_2}\ln\left(\frac{T_1}{T_2}\right) \tag{4.22}$$

where T_1 and T_2 are the transmissions of samples with thicknesses d_1 and d_2. But if (4.17) has to be used, α and R cannot be obtained analytically, and in this case graphical methods have often been employed (VAŠKO and MILER, 1961 or PRISHIVALKO, 1966).

In our work on bulk specimens the energy gap for each specimen was obtained by plotting a graph of $\log(I_0/I)$ against wave length where I_0 is the incident intensity and I the corresponding transmitted intensity.

An example of such a plot is given later in Figure 5.9. The optical density falls at the absorption edge to an approximately constant value which we refer to as $\log\left(\frac{I_0}{I}\right)_0$. (If this is not constant, $\log\left(\frac{I_0}{I}\right)_0$ is taken to be the minimum value of $\log\left(\frac{I_0}{I}\right)$. Since the edge is not infinitely sharp there remains the problem of how to define the wavelength of the edge. We have adopted the following procedure. First we assume equation (4.20) is valid although in fact the coefficient of reflection for our specimens is not usually known in this range.

Hence we can write

$$\log\left(\frac{I_0}{I}\right)_E=-\frac{\alpha d}{2\cdot 303} \tag{4.23}$$

and for convience write this in terms of the additional absorption above α_0, $(\alpha_E-\alpha_0)$.

Thus

$$\log\left(\frac{I_0}{I}\right)_E - \log\left(\frac{I_0}{I}\right) + \frac{(\alpha_E - \alpha_0)}{2{\cdot}303} d. \tag{4.24}$$

We now define the energy gap as ocurring when the additional absorption coefficient $(\alpha_E - \alpha_0)$ reaches some particular value which we somewhat arbitrarily take to be 300 cm^{-1} on the grounds that this gives the same value for the energy gap for pure *PbTe* as that of 0.32 eV given in the literature.

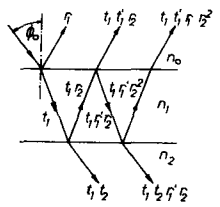

Figure 4.4

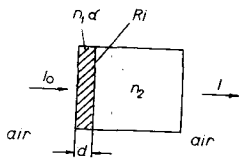

Figure 4.5

For a thin film on a substrate multiple reflection both within the film and the substrate is possible. Since the film is much more absorbing than the substrate, the most important multiple reflection process is that in which light is reflected at the back side of the substrate and then again at the substrate-film interface before being transmitted (Figure 4.5). If we neglect other multiple reflection processes, the overall transmission of the system can be expressed as

$$T = \frac{I}{I_0} = n_2 \frac{1 - R_w}{1 - R_w R_i} (T_a)^2 \tag{4.25}$$

where R_w is the energy reflection coefficient of the substrate-air interface; R_i is the total energy reflection coefficient at the substrate-film interface and T_a the expression for the transmitted amplitude through the film, given below (equation 4.27).

The second method of treating this problem is that of summing the complex amplitudes (HEAVENS, 1965) and is conveniently used for treating very thin samples. Clearly both methods must give the same results if the same assumptions are made. This method considers a beam of light of unit amplitude and wavelength incident on a homogeneous isotropic plane with refractive index n_1 and thickness d. The specimen is usually supported by a substrate whose index of refraction is n_2. The other medium is always air with index $n_0 = 1$ and the angle of incidence of monochromatic light is taken to be θ_0. The amplitudes of successive beams reflected back into the air are given in Figure 4.4. Since the change in phase of the beam in traversing the specimen is $\delta = \frac{2\pi}{\lambda} n_1 d_1 \cos\theta_1$ one can easily show that the reflected and transmitted amplitudes are

$$R_a = r_1 + \frac{t_1 t_1' r_2 e^{-2i\delta_1}}{1 + r_1 r_2 e^{-2i\delta_1}}, \tag{4.26}$$

$$T_a = \frac{t_1 t_2 e^{-i\delta_1}}{1 + r_1 r_2 e^{-2i\delta_1}}. \tag{4.27}$$

The reflected and transmitted energies, R and T, obtained from these are

$$R = \frac{r_1^2 + 2 r_1 r_2 \cos 2\delta_1 + r_2^2}{1 + 2 r_1 r_2 \cos 2\delta_1 + r_1^2 r_2^2}, \tag{4.28}$$

$$T = \frac{n_2}{n_0} \frac{t_1^2 t_2^2}{(1 + 2 r_1 r_2 \cos 2\delta_1 + r_1^2 r_2^2)}. \tag{4.29}$$

These expressions for reflection and transmission from film specimens are complicated because of interference phenomena and the influence of the film backing. By considering certain physical situations MOONEY (1945), HALL and FERGUSON (1955) and HEAVENS (1965), HOWSON (1964 and 1968) have reduced these expressions for T and R in various ways. The technique we have used to measure n_1 is to observe the position of the interference fringes. If the thickness of the film, d, is measured using an interferometer method, the refractive index n_1 can be obtained at all the wavelengths at which a fringe occurs from

$$m\lambda = 4 n_1 d \tag{4.30}$$

provided that the order, m, of the fringe is known. To find this we note that the wavelengths of two successive fringes (both maximum or both minimum intensity) are given by

$$\frac{m}{m+2} = \frac{\lambda_{m+2} \cdot n_{1\lambda m}}{\lambda_m \cdot n_{1\lambda m+2}} . \tag{4.31}$$

Approximate values of n_1 at these wavelengths can be obtained from measurements of reflectivity R. If we neglect absorption, $R = \frac{(1-n_1)^2}{(1+n_1)^2}$ and the values of n_1, only approximate because of this assumption, are nevertheless sufficiently accurate to give rough values of n from which, since it is known these are integral, can be correctly rounded to the nearest integer. Approximate values of thickness can also be obtained from (4.30) using these approximate values of n_1. We note that we have also made approximate refractive index measurements in the region of the plasma frequency from reflectivity data.

4.1.2. *Determination of optical constants.* A detailed review of the various methods used in the determination of optical constants has been given by HEAVENS (1955 and 1964). He describes the two principal techniques (a) intensity measurements using unpolarized light (usually at normal incidence) and (b) measurements using polarized light.

The first method is normally preferred because it is insensitive to polarization effects in the optical system and also, because irregulatities of the surface do not produce large errors in the results. In principle it is possible to obtain information on band structure from both reflectivity and transmission measurements made in this way but in practice only the first energy gap can be obtained from transmission measurements unless the specimen is very thin, i.e. a film, as the absorption at lower wavelengths is very high.

The optical dielectric constants $\varepsilon_1 + i\varepsilon_2$ can be evaluated from reflectivity data either by using the KRAMERS-KRONIG analysis first used by ŠIMON (1951) and improved by ROBINSON (1952) or by using the classical oscillator fitting procedure which has been discussed extensively by a number of authors. We shall describe first the KRAMERS-KRONIG analysis.

Using the FRESNEL equation the dispersion relation between θ and R can be expressed as:

$$\theta(\omega_0) = \frac{1}{\pi} \int_0^{\infty} \ln \left| \frac{\omega + \omega_0}{\omega - \omega_0} \right| \frac{\mathrm{d} \ln \sqrt{R(\omega)}}{\mathrm{d}\omega} \, d\omega \tag{4.32}$$

where the complex reflection amplitude $\sqrt{R}$ is given in the form $\sqrt{R}\,e^{i\theta}$, θ is the phase change on reflection and ω_0 is the plasma frequency. The integral covers the whole spectral region but if the contribution from frequencies far from ω_0 is small, particularly if R is nearly constant outside this range which is often the case (BOWLDEN and WILMSHURST, 1963), a close approximation to the integral can be obtained from detailed knowledge of the reflectivity in the spectral region around ω_0. Even if R is not constant at the limits of the range of observation it is still possible to obtain an approximate value for $\theta(\omega_0)$ by extrapolating $R(\omega)$ to infinite frequencies. Thus ANDERMANN et al. (1955) used an extrapolation procedure by making a classical oscillator fit to the data at the ends of the measured range. ROESSLER (1965) introduced a method which avoids the necessity of extrapolating the data and requires only experimental data in a limited spectral range. He divides the whole spectral range into three sections. The middle section, $b<\omega<e$, represents the region where the experimental reflectivity data are available. The equation for the phase change θ is then expressed in the form

$$\theta(\omega_0) = -\frac{1}{\pi}\int_0 f(R_1\,\omega_0)\,\mathrm{d}\,\omega - \frac{1}{\pi}\int_b^e f(R_1\,\omega_0)\,\mathrm{d}\,\omega - \frac{1}{\pi}\int_e^\infty f(R_1\,\omega_0)\,\mathrm{d}\,\omega, \tag{4.33}$$

where $f R_1(\omega_0) = \ln\sqrt{R}(\omega)\frac{1}{d\,\omega}\left(\ln\left|\frac{\omega+\omega_0}{\omega-\omega_0}\right|\right)$ and $\theta(\omega_0) = \gamma(\omega_0) + \Phi(\omega_0) + \beta(\omega_0)$ where $\gamma(\omega_0)$ and $\beta(\omega_0)$ are the contributions to $\theta(\omega_0)$ from the frequency ranges $\omega<b$ and $\omega>e$.

KRAMERS KRONIG analysis of this type can be used for both bulk and film specimens although there are complications arising from the substrate properties and multiple reflections when films are used. However as we have noted, it is possible with films to obtain detailed measurements of both transmission and reflection and indeed a similar analysis on transmission data only can be used to obtain the optical constants. For example NILSON (1968) used the expression for the phase change on transmission:

$$\theta(\nu_0) = \frac{2\nu_0}{\pi} P\int_0^\infty \frac{\ln T_f^{\frac{1}{2}}}{\nu^2-\nu_0^2}\,\mathrm{d}\,\nu - 2\pi\nu_0\,d \tag{4.34}$$

where T_f is the amplitude of the transmission inside the substrate. To obtain this measurements of transmission of the substrate alone as well as through the substrate and the film must be made. Once $\theta(\nu_0)$ is derived a similar analysis to ROESSLER's (1965) is used.

In practice, transmission measurements are usually more accurate than reflectivity measurements and are also less sensitive to surface properties but of course transmission measurements can not be made if the material is highly absorbing.

A classical oscillator fitting procedure can also be used to extract the optical constants from the measured reflectivity and transmission spectra. Good examples of this procedure occur in the work of SPITZER and KLEINMAN (1961) and DIXON and RIEDL (1965). Recently VERLEUR (1968) has devised an improved method of calculation which he calls an "automatic fitting procedure".

In our own work so far we have used a relatively simple expression for the dispersion law which is essentially the classical DRUDE law (e.g. TSU et al. 1968)

$$(n+ik)^2=\varepsilon_{opt}\left[1-\frac{\varepsilon_{opt}}{(\omega/\omega_p)^2+i\,(1/\omega_p\tau)^2\,\omega/\omega_p}\right]. \tag{4.35}$$

Equating real and imaginary parts we obtain:

$$n^2-k^2=\varepsilon_{opt}\left[1-\frac{1}{(\omega/\omega_p)^2+(1/\omega_p\tau)^2}\right], \tag{4.36}$$

$$2nk=\frac{\varepsilon_{opt}}{\omega\tau}\left[\frac{1}{(\omega/\omega_p)^2+(1/\omega_p\tau)^2}\right]. \tag{4.37}$$

Since the reflectivity can be expressed as a function of n and k

$$R=\frac{(n-1)^2+k^2}{(n+1)^2+k^2} \tag{4.38}$$

a computer fit to the experimental curve for $R(\omega)$ in the plasma region can be used to calculate the optical dielectric constants and the other parameters including the plasma frequency. The optical conductivity was also calculated from the parameters obtained during the fitting procedure.

$$\sigma_{opt}=\frac{\varepsilon_{opt}\,\tau\cdot 10^{-11}}{36\pi}. \tag{4.39}$$

The computer programme for this was written in Fortran with the help of M. SMILJANIĆ of the Institute of Physics of Belgrade and M. A. MCCONACHIE of the Cripps Computing Centre, Nottingham University.

4.2. Instruments used in the measurements of transmission and reflectivity

In general commercial chart recording spectrophotometers are less sensitive than monochromators with which measurements are recorded point by point. Hence both types of instruments may be used for thin specimens such as films from which fairly strong transmission signals are obtained but only monochromators can be used for the thicker bulk specimens. In all, 4 monochromators and 5 spectrophotometers have been used in this work.

The lowest measured energy gap in these alloys occurs in the infra-red but higher energy transitions occur at wavelengths which extend into the visible and ultraviolet. Unfortunately in transmission work these higher transitions could not be seen when the thicker bulk specimens were used although it was possible to see them with some film specimens.

4.2.1. *Monochromators.* The optical transmission measurements in the infra-red region were made either with a BARR and STROUD double monochromator V. L. 2 with KBr prisms or with a converted HALLE monochromator with a NaCl prism. The infra-red source used with both monochromators was a NERNST filament which consisted of a filament 3 cm long and about 1 mm in diameter made from a mixture of zirconium and yttrium oxides. The incident radiation was chopped at a frequency of 5 Hz and focussed onto an adjustable entrance slit by means of a combination of mirrors aluminised on their front surfaces. The detector was a HILGER and WATTS

Schwarz thermocouple (SMITH et al., 1957) arranged with both elements in series. The signal from this was fed via a quadruply screened matching transformer to a high gain amplifier. This was either a BARR and STROUD thermocouple amplifier with a maximum voltage gain of 5×10^7 and a bandwidth of 7% or a UNIPAN selective volt meter with a gain of 10^9 and a bandwidth of 5%. The noise level figure of the UNIPAN was better than that of the BARR and STROUD. The output of both amplifiers was read directly on a meter. Occasionally the signal from the detector was too big for the amplifier and had to be reduced using an external attenuator consisting of five T networks matched to the detector and the transformer.

The calibrations of the monochromators were checked in the region between 2.42 and 15 microns by observing the absorption spectrum for a thin polystyrene film both with the monochromators and with one of the calibrated spectrophotometers, PERKIN ELMER 457 or 337. Further checks were made using the absorption lines of water vapour at 1.901 and 2.673 microns and of carbon dioxide at 4.225 and at 14.90 microns. The resolution of the instruments was a function of wavelength, both being highest at about 2.5 microns. At this wavelength the bandwidths of the HALLE and the BARR and STROUD were about 20 and 300 Å. respectively.

In the visible region three types of monochromator were used. The Barr and Stroud was modified by replacing the prisms with a synthetic quartz prism and the other two instruments were the Specol and the SPM2 both made by Carl Zeiss, Jena. The range of all these instruments was about 6000 — 15,000 Å but their resolution varied considerably. For the Barr and Stroud and the Specol this was about 100 Å (at 8000 and 5.461 Å respectively) and for the SPM2 this was 6 Å at the 5,461 Å. The source used was a 36 watt car bulb and the detectors were usually photomultipliers although the Schwartz thermocouple was used at times with the Barr and Stroud.

The monochromators were calibrated using the lines from a high pressure mercury arc. This was satisfactory for the SPM2 but less so for the other instruments since their resolution was poorer and so the Barr and Stroud calibration was checked by measuring the absorption spectrum of didymium glass on both this machine and on a Perkin Elmer Spectrophotometer UV 137.

4.2.2. *Spectrophotometers.* Five spectrophotometers have been used in this work. A Unicam model SP 200 spectrophotometer equipped with sodium chloride optics was used for taking preliminary measurements of transmission in the region between 2 and 15 microns, and two Perkin Elmer grating spectrophotometers Models 337 and 457 have been used for more accurate measurements of transmission in the region from 2.5 to 25 and 40 microns respectively. Another Perkin Elmer spectrophotometer Model 137 equipped with quartz prisms has been used to measure the transmission of very thin homogeneous specimens in the visible and ultraviolet region but the Unicam SP 700 was found to be the best instrument for measuring transmission in this region of even thicker specimens with thicknesses from about 500 Å and 3000 Å. The samples had to be as thin as this because the materials had strong optical absorption in this spectral range.

4.2.3. *Methods of sample mounting for transmission and reflectivity measurements using monochromators.* This was similar for all of the instruments and is illustrated by describing the arrangement for the Barr and Stround. The bulk specimens were mounted over a slit cut in a brass disc. This was then fitted into a speci-

men holder in the exit beam and mounted on the accessory bar of the BARR and STROUD monochromator in such a way that when the specimen holder was rotated, the beam passed either through the slit covered by the specimen or through an identical uncovered slit. This is the so called "sample in sample out" method. At liquid nitrogen temperatures, a brass dewar vessel was used for transmission measurements. This was a modified version of the low temperature apparatus built by EVANS (1961) and included two KBr windows 1.5 inches in diameter and $^1/_4$" thick. The specimen was mounted across one of two identical slits (10 × 1 mm) of a specimen holder which was in close contact with the inner wall of the liquid nitrogen dewar. The dewar was moved so that the light passed either through the slit covered by the specimen or through the uncovered slit.

Measurements were made at other temperatures by filling the dewar with other liquids, e.g. solid CO_2 together with $CCl_4/CHCl_3$ was used to give a temperature of about 202 °K and water, heated electrically, to give a temperature of about 100 °C. The temperature was measured in each case with a copper constantan thermocouple.

The reflectivity measurements were made by comparing the intensity of the light reflected from the surface of the specimen with that reflected from a standard mirror. The standard mirror had the front surface aluminized and then covered with a protective coating of SiO. The "sample in sample out" method was again used.

For measurements of transmission through film specimens, three wide slits (4 mm × 11.5 mm) were mounted on the specimen holder. One was left uncovered, another covered with the film and substrate and the third with a substrate of similar thickness only. Hence the absorption due to the substrate and to the film could be separated. If a double beam spectrophotometer was used, a similar substrate was placed in the second beam.

4.3. X-ray measurements

During the course of this work several *X*-ray techniques were employed. Thus bulk specimens which were all polycrystalline were analysed by taking *X*-ray powder photographs and the crystal properties and composition of the film specimens were determined using *X*-ray diffractometers.

4.3.1. *X-ray powder photography.* The technique was used mostly to determine whether two compounds were in single or two phase solution or to determine the composition of alloy specimens for which the variation of lattice parameter with composition was known. However, it was also used to investigate several alloy systems, whose variation of lattice parameter with composition or range of solid solution was unknown. In all some 500 *X*-ray photographs were taken. The line used was CuKα with a Ni filter.

The camera used was mainly the Unicam 9 cm which has the van Arkel method of film mounting. The positions of the powder pattern lines and so the angles Φ were measured with a travelling microscope. The values of θ were plotted against values of an absorption correction function (HENRY at al., 1959) and the resulting straight line was then extrapolated to $f(\theta)=0$ corresponding to a BRAGG reflection of 90°. From this the true lattice parameter was obtained. The accuracy of a parameter determined in this way was about $\pm$ 0.002 Å.

The powdered specimens were stuck with Durofix on to a fine glass fiber so that the average diameter of the specimens was usually about 1/2 mm. Since glass and durofix are amorphous, no lines appear from these materials although it seems likely that the blurred smudge at low angles of θ could be due to scattering from them. Most of this work was carried out using a Solus Schall type 49917 X-ray machine containing a Philips tube.

4.3.2. *X-ray diffractometer analysis.* The measurements made on the film specimens with an *X*-ray diffractometer were used to determine whether the film was single crystal or polycrystalline and also to calculate the lattice constant so that it could be compared with the bulk value of the same composition. The equipment used was a Philips PW 1011 *X*-ray unit, a Philips goniometer PW 1050/25 and a Noreclo PU 1010 diffractometer. In general the CuKα line was again used although at the beginning when difficulties were experienced in obtaining good recordings from very thin films made on NaCl substrates, cobalt and iron targets were also tried.

The technique can of course also be used for bulk specimens and some checks were made on the lattice constants of some bulk specimens used.

4.4. Electron microscopy

Two electron microsopes have been used in this work, one a JEM7 of Japanese make at the Institute of Nuclear Energy in Belgrade and the other an AEI EM6 at Nottingham University. Both microscopes were used for obtaining information on the crystal structure of very thin film specimens as described in chapters 3.4. and 5.3.1.

For our purposes it is sufficient to consider the motion of electrons as similar to that of light. Detailed discussions of the special properties of electron microscopes are well covered in the literature (COSSLETT 1951; PINSKER 1953; STRILAND, 1966).

In this present work with the electron microscope the specimens were about 300—700 Å thick.

Typically an electron beam is about 10 to 20 μ in diameter although areas down to 0.2 μ^2 can be observed using a special "selected area" technique. Using this, the characteristic spots of single crystal material can be obtained from individual crystallites within polycrystalline material. However if the crystallite size were very small, the beam would cover a number of randomly orientated crystallites and a complicated spot pattern would be observed. At even smaller sizes — in practice if the beam size is greater in area by a factor of 10^3 than the crystallite size — the spots merge completely into rings whose diameters are determined by the separations of the possible crystal planes. Hence the pattern gives information on the grain size.

Some of the electron energy is always absorbed by the specimen resulting in a rise of temperature. This is particularly noticeable in very thin films since the mechanism of heat transfer from the film is rather inefficient and care must be taken to avoid recrystallisation or even melting of the film. Both effects have been observed in very thin films. (< 500 Å) in the present work.

4.5. Evaporation process

4.5.1. *Vapour deposition.* Vapour deposition processes can be either physical or chemical. Chemical deposition is the dissociation of a vapour species from a multicomponent system on to a substrate. Physical deposition, which is the technique used in the present work, is very often called simply evaporation and is a condensation process from a supersaturated vapour phase.

In this latter process materials are evaporated in a vacuum and then condensed on to a surface with a lower temperature than that of the source of evaporation. The advantages of working with a vacuum rather than with a modest pressure are that the materials being evaporated have lower boiling points, much fewer impurities are introduced into the film and well defined films of different shapes can be produced by putting a mask between the source of evaporation and the substrate.

The techniques of producing thin films have been reviewed by DUSHMAN (1949), HOLLAND (1960) and recently by POWELL et al. (1966).

As we have noted earlier, a compound film can be either produced from a single source or from multiple sources. If a single source is used in which the compounds are stoichiometric, films can be fairly readily obtained with many materials e.g. the alkali halides, the lead chalcogenide compounds and the selenides and tellurides of Group II with the exception of zinc sulfide. In all of these (except ZnS), decomposition does not normally occur during evaporation. However many other compounds do decompose at or below the temperatures needed for evaporation and then flash or multisource evaporation techniques must be used.

If homogeneous films are to be obtained the components must be evenly distributed on arrival at the substrate because the diffusion coefficients are usually not high enough to achieve homogeneity by self diffusion. It is also necessary to have a very good vacuum and very clean crucibles for the sources in order to obtain films free from large concentrations of impurities. Because of all these difficulties the multisource method is usually only used to prepare alloys and compounds which can not conveniently be produced by the other methods.

5. RESULTS

The experimental part of this investigation can be roughly divided into the production of and measurements on:

(a) bulk specimens, and

(b) film specimens of IV—VI semiconductor alloy specimens. The results for (a) are described in Section 5.1. and Section 5.2. and for (b) in Section 5.3.

Most of the experimental work on the bulk specimens has already been published (NIKOLIĆ, 1964. 1965. 1967, and 1969) the exception being that on PbTe-SnS and PbSe-SnS alloys.

5.1. Bulk specimens of lead — tin chalcogenide alloys

The mutual solid solubility of the ternary systems: PbTe-SnTe and PbSe-SnSe has been previously investigated by ABRIKOSOV et al. (1953): NISHIYAMA and OKADA (1960) and KREBS et al. (1961) and that of the quaternary systems: PbTe-SnSe, PbSe-SnTe and PbSe-SnS by KREBS and LANGNER (1964). This work has been repeated and is discussed here together with work on the PbTe-SnS system.

Specimens of all these alloys were prepared as described in Chapter 3.2 .After the specimens had been annealed and then quenched in cold water, *X*-ray photographs were taken to examine whether the specimens were in single phase equilibrium.

The work on alloys that had already been investigated was done partly to check the composition of the present specimens and also to discover whether a prolonged annealing treatment could extend the mutual solid solubility of the compounds. The details of this work will be given later in this chapter and discussed in the discussion section.

Before the present work was started no actual data had been reported on these alloys, other than measurements of structure. The present work has now been published (NIKOLIĆ, 1964, 1965, 1967 and 1969) and work on PbSe-SnSe alloys was published by STRAUSS (1967) at about the same time as our own. Also there have now been two other detailed studies of the PbTe-SnTe system (BYLANDER (1966) and DIMMOCK et al. (1966)), the special interest here being that, as we also found, the energy gap decreases with alloying.

5.1.1. *PbTe-SnTe Alloys.* Specimens of these alloys containing between 0 and 100 mol% SnTe were annealed at 700 °C for 21 days. *X*-ray photographs then showed that they were all in single phase equilibrium. All samples containing more than 15 mol % SnTe were found to be P-type, but below this concentration the samples were either N or P-type. Since it was found impossible to obtain optical transmission spectra on any of the P-type specimens we also have shown electrical measurements only on the N-type (15 mol% SnTe) specimens. In Figure 5.1. the optical density log I_0/I (I_0 and I are the intensities of the incident light and transmitted light respectively) of some PbTe-SnTe and PbTe-SnSe alloys is shown at room temperature. The energy gaps were calculated as described in the previous chapter, using a value of 300 cm^{-1} for α_E—α_0. The energy-gap values as a function of composition and temperature are plotted in Figure 5.2 and 5.3 respectively. One can see that

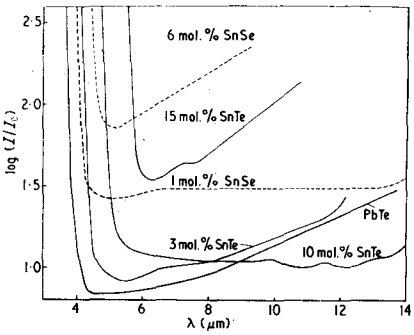

Figure 5.1 Optical density of PbTe—SnTe and PbTe—SnSe alloy samples of different composition.

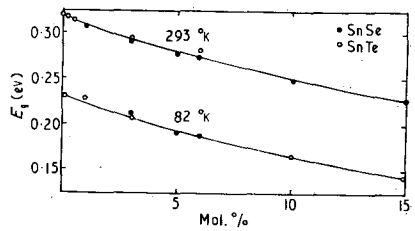

Figure 5.2 The variation of the energy gap with composition for PbTe—SnTe and PbTe-SnSe alloys.

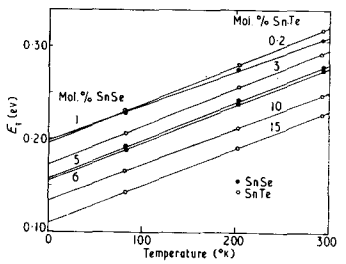

Figure 5.3 The varation of the energy gap with temperature of some PbTe-SnTe and PbTe-SnSe alloys.

the optical energy gaps for PbTe-SnTe alloys change nearly linearly with composition which may be an indication that the band forms are the same over the range of measurements.

The decrease in E_g at room temperature with concentration of SnTe in PbTe is given by:

$$E_g = 0.32 - 0.7\ X [e \cdot V]$$

where X is the molar fraction of SnTe in PbTe.

For each alloy measured, E_g was found to increase with temperature between liquid nitrogen and room temperatures and the temperature coefficient of the gap was between 0.4 and 0.420 meV deg K^{-1}.

5.1.2. *PbTe-SnSe Alloys.* Specimens containing up to 35 mol% SnSe were annealed at 700 °C for twenty-one days and were then all in single phase equilibrium. The optical density of two typical PbTe-SnSe alloys (denoted by broken curves) is shown in Figure 5.1 together with those for the PbTe-SnTe samples. The optical energy gaps E_g at 293 and 82 °K of specimens containing up to 6 mol % SnSe are plotted against composition in Figure 5.2. together with the results for the PbTe-SnTe alloys. The data for the two systems clearly lie close to the same curves showing their similarity. A positive temperature coefficient of between 0.4 and 0.42 meV deg K^{-1} was found which is also very similar to that of the PbTe-SnTe system. This was obtained from measurements of the variation of the energy gap with temperature made on several samples (Figure 5.3.).

5.1.3. *PbSe-SnTe Alloys.* Since the PbSe-SnTe alloys containing more than 70 mol % SnTe partly melted at 700 °C the annealing temperature was reduced to 630 °C. After annealing for fourteen days all the specimens were in single phase equilibrium. Although the lead selenide used in these experiments was P-type, the specimens containing up to 3 mol % SnTe were found to be N-type, although at high concentrations they did indeed become P-type.

It was shown by X-ray analysis that complete solid solution existed throughout the whole composition range and that the variation of the lattice parameter had a small positive deviation from the "VEGARD" line. The variation of the lattice constant a_0 with composition is shown in Figure 5.4.

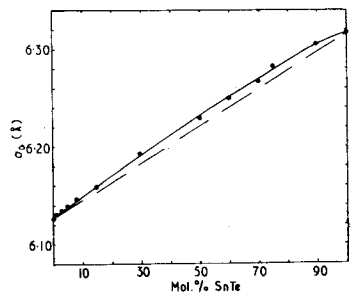

Figure 5.4 The variation of the lattice parameter with composition for the PbSe—SnTe system

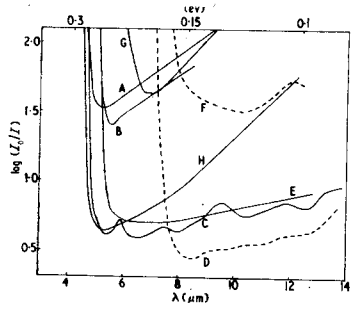

Figure 5.5 Optical density of the PbSe—SeTe and PbSe – SnSe alloy samples of different composition

Curve	A	B	C	D	E	F	G	H
Composition	1, 3 mol.% SnSe		1, 1, 3, 6, 6, mol% SnTe PbSe					

In Figure 5.5. the optical density of some samples of PbSe-SnTe of different thicknesses is shown, together with some measurements on PbSe-SnSe specimens.

The data at room temperature are shown with full curves and at liquid nitrogen temperature with broken curves. Sample *C* and partly also sample *D* exhibit transmission interference fringes. The free carrier absorption of the specimens is rather strong and measurements were not possible at concentrations greater than 6 mol % SnSe. The carrier absorption has to be taken into account in interpreting the absorption curves. The energy gaps at 82 °K and room temperature are plotted against composition in Figure 5.6.

A striking initial decrease in the energy gap occurs at both room and liquid nitrogen temperatures as the SnTe concentration is increased. At nitrogen temperatures this only continues up to 3% SnTe where it reaches a minimum and at higher concentrations it increases.

It may be significant to note that the specimens become P-type at about the concentration at which the slope changes sign.

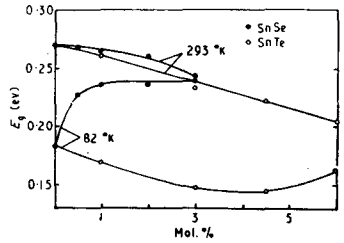

Figure 5.6 The variation of the energy gap with composition for PbSe—SnTe and PbSe—SnSe alloys

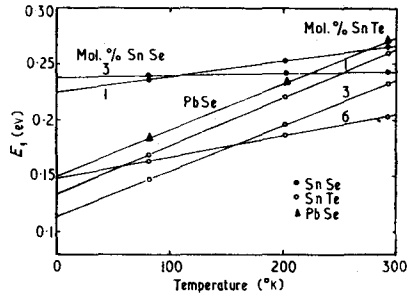

Figure 5.7 The variation of the energy gap with temperature for some PbSe—SnTe PbSe—SnSe alloys.

In Figure 5.7. the optical energy gaps, E_g, of several typical PbSe-SnTe specimens containing up to 6 mol % SnTe are plotted against temperature, together with two PbSe-SnSe specimens. It is apparent that E_g varies linearly with temperature in the region between 82 °K and 293 °K with a positive temperature coefficient between 0.180 and 0.4 meV deg K^{-1}.

5.1.4. *PbSe-SnSe Alloys.* Alloys in the composition range 0—40 mol% SnSe were annealed for fourteen days at 600.°C and single phase specimens were produced. All the specimens were P-type, except for that containing 3 mol% SnSe which was N-type.

Absorption curves for two of these alloys (A and *B* curves) are shown in Figure 5.5. The variation in the energy gap E_g with composition is plotted in Figure 5.6. and with temperature in Figure 5.7. together with the results of the PbSe-SnTe system. In these alloys E_g at room temperature decreases monotonically with increasing SnSe content but at 82 °K, E_g unexpectedly increases as the percentage of SnSe is raised.

These alloys also have positive temperature coefficients of E_g but the values are much smaller — between 0.016 and 0.14 meV deg K^{-1} — than those of the other alloys measured.

5.1.5. *PbTe-SnS Alloys.* Specimens of PbTe-SnS alloys containing up to 50 mol % SnS were prepared in the way described in Chapter 3. After having been annealed for fourteen days at 700 °C only the specimens containing up to 15 mol % SnS were in single phase equilibrium with a simple NaCl structure. It seemed possible that the range of solid solution might extend beyond the range observed. However, attempts to anneal the rest of the specimens at higher temperatures were unsuccessful as in all cases the specimens melted due to temperature fluctuations in the furnace. The values of the lattice parameters, a_0, are plotted against composition in Figure 5.8. The variation is nearly linear and can be represented by the following equation:

$$a_0 = 6.459 - 0.59\ X\ (\text{Å})$$

where X is the mole fraction of SnS.

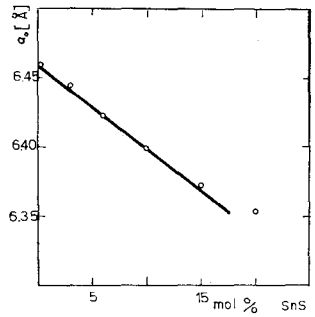

Figure 5.8. The variation of the lattice parameter with composition for the PbTe—SnS system.

In Figure 5.9. the optical density of the specimens containing 3 mol % SnS is shown at room and liquid nitrogen temperatures. From the form of the curve it can be seen that there is no apparent contribution to the absorption by free carriers. The energy gaps at room and liquid nitrogen temperatures were determined

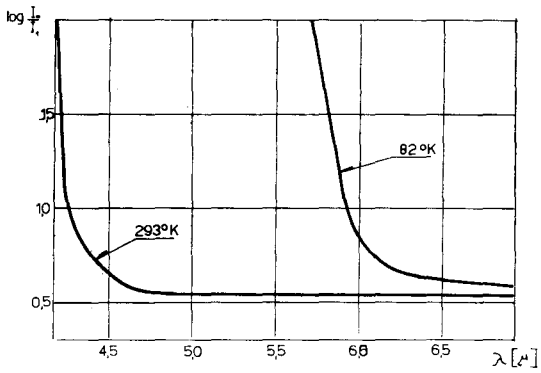

Figure 5.9. Optical density of PbTe—SnS alloy sample at room and liquid nitrogen temperatures

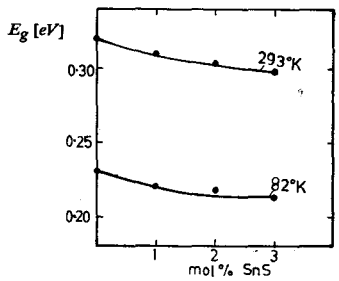

Figure 5.10. The variation of the energy gap with composition for PbTe—SnS alloys.

for several alloys containing between 0 and 3 mol % SnS and the values are plotted as a function of composition in Figure 5.10. Optical transmission measurements were not possible for specimens containing more than 3 mol % SnS although several attempts were made using specimens about 40 μm thick.

5.1.6. *PbSe-SnS Alloys.* The specimens preparation was similar to that described earlier. After fourteen days annealing at 700 °C the specimens containing up to 30 mol % SnS were in single phase equilibrium with the NaCl structure but at higher concentrations the specimens contained two phases.

The values of the lattice constant, a_0, obtained for these specimens are shown in Figure 5.11. The decrease in lattice parameter with SnS content is given by the equation:

$$a_0 = 6.127 - 0.385\ X\ [\text{Å}]$$

where X is the mole fraction of SnS.

No detectable transmission could be observed through any of the specimens of the PbSe-SnS alloys that were investigated.

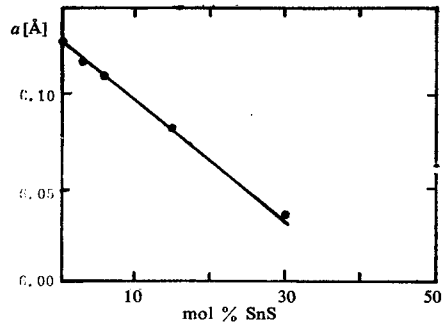

Figure 5.11. The variation of the lattice parameter with composition for the PbSe—SnS system.

5.2. Lead-germanium Chalcogenide Alloys

It is only recently that any appreciable work has been done on the pseudobinary alloy systems derived from lead and germanium chalcogenide compounds. In the present investigation, PbTe-GeTe and PbSe-GeSe alloys have been studied, as well as the quaternary alloys: PbTe-GeSe, PbTe-GeSe, PbTe-GeS, PbSe-GeTe, PbSe-GeS.

Since none of the germanium chalcogenides has the NaCl structure it is perhaps to be expected that their solubility in lead chalcogenide compounds would be rather limited. In fact our work has shown this is not the case and this will be discussed later.

So far as is known, the only reported optical work which has been published is by WOOLLEY and NIKOLIĆ (1965) and NIKOLIĆ (1969). A possible reason for the little work that has been done on this system is that the optical data on the germanium chalcogenide compounds are not in agreement and values of 1 eV and 0.1. eV have been reported for the energy gap of GeTe at room temperature by HEIT et al. (1964) and STILES et al. (1966) respectively.

5.2.1. *PbTe-GeTe Alloys.* Lead-germanium tellurium alloys were prepared in the usual way and then annealed at 600 °C for between two and six weeks before quenching in air. The variation of the room temperature values of the rhombohedral lattice parameters a_0 and angle α as a function of composition has been given by WOOLLEY and NIKOLIĆ (1965) who also reported measurements of the room temperature optical energy gaps for GeTe concentrations up to 40 mol %, In the present work we have observed that there is a rapid decrease in the room temperature energy gap between 40 and 42.4 mol % GeTe (Figure 5.12)

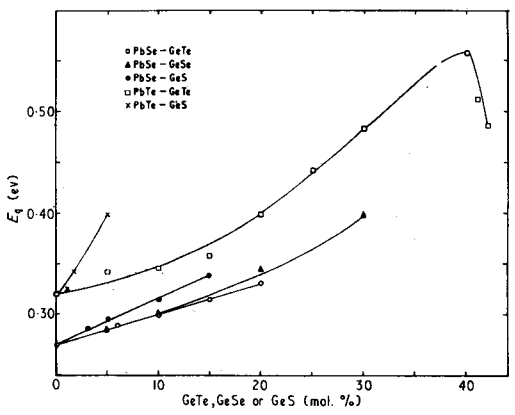

Figure 5.12. The variation of the energy gap with composition for the PbTe—GeTe, PbTe—GeS, PbSe—GeTe, PbSe—GeSe and PbSe—GeS alloys.

but it was not found possible to measure the energy gap at higher concentrations even using specimens of thickness down to about 40 μm. It was not easy to obtain optical specimens of sufficient quality, particularly at the higher concentrations, because some of the ingots contained small holes. Indeed in some cases it was nearly impossible to obtain a wafer specimen which did not contain any pin holes. However, it was always found possible to reduce the amount of light transmitted through the holes by suitable alignment of the specimen in the infra-red beam. Typical data showing the variation in the optical energy gap with temperature are plotted in Figure 5.13. together with the results from other systems.

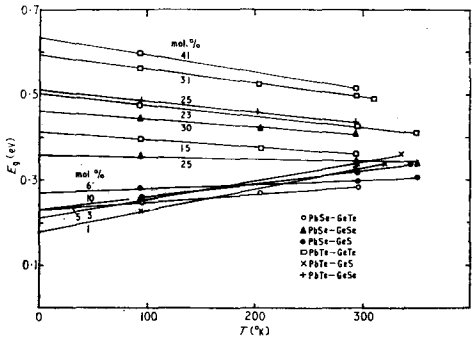

Figure 5.13. The variation of the energy gap with temperature for some PbTe—GeTe, PbTe—GeSe, PbTe—GeS, PbSe—GeTe, PbSe—GeSe and PbSe—GeS alloys.

For these alloys a negative temperature coefficient of about — 0.19 meV deg K^{-1} exists.

5.2.2. *PbTe-GeSe Alloys.* The specimens were prepared as described: the annealing was at 600 °C for twenty-one days. The *X*-ray photographs then taken showed that specimens containing up to 35 mol % GeSe were in single phase equilibrium and possessed the simple NaCl structure, but that all the other specimens had either two phases or the rhombic structure of GeSe. The variation of lattice parameters with composition is shown in Figure 5.14. The cubic lattice parameter decreases with GeSe content as:

$$a_0 = 6.459 - 0.745\,X\ [\text{Å}]$$

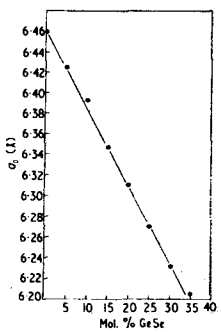

Figure 5.14. Variation of the lattice parameter with composition for PbTe—GeSe

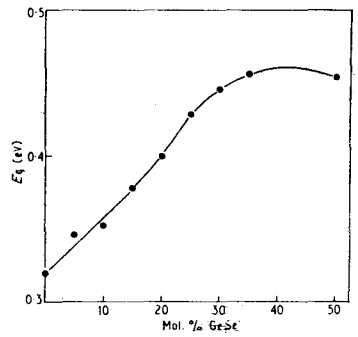

Figure 5.15. Variation of the room temperature optical energy gap with composition for PbTe—GeSe.

The energy gaps at room temperatures for various alloys throughout the composition range were determined and the values are shown as a function of composition in Figure 5.15. The variation in the optical energy gap with temperature is plotted in Figure 5.13 together with those of the other lead germanium chalco-

genide alloys. For these alloys the energy gap temperature coefficient, β, is negative with an average value of about —0.19 meV deg K^{-1} i.e. very similar to the values for PbTe-GeTe and PbSe-GeSe alloys.

5.2.3. *PbTe-GeS Alloys.* Specimens containing up to 30 mol % GeS were prepared and annealed at 630 °C for two weeks; their lattice constants, a_0, are plotted against composition in Figure 5.16. The specimens containing less than 5 mol % GeS were in single phase equilibrium and had the NaCl structure. The discontinuity in the curve shows the limit of solid solubility to be about 5.7 mol % GeS. a_0 in the range of solid solubility is given by the equation:

$$a_0 = 6.459 - 0.84\ X\ [\text{Å}]$$

where X is the mole function of GeS.

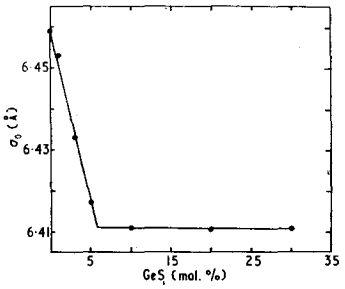

Figure 5.16. The variation of the lattice parameter with composition for the PbTe—GeS system.

The optical energy gaps of three alloys throughout the composition range were determined at about 90, 200, 300 and 350 °K. The room temperatures values are shown as a function of composition in Figure 5.12. and as a function of temperature in Figure 5.13., together with values for the other lead-germanium chalcogenide alloys. It is interesting to note that the energy gap temperature coefficient is positive for these PbTe-GeS alloys as it is for the lead-tin chalcogenide alloys (β=0.53 meV deg K^{-1}).

5.2.4. *PbSe-GeTe Alloys.* The alloy specimens were annealed at 705 °C for two weeks and then quenched in cold water. The values of the lattice parameters a_0, (NaCl structure) are plotted against composition in Figure 5.17. In the range of solid solubility a_0 is given by:

$$a_0 = 6.127 + 0.23\ X\ [\text{Å}]$$

where X is the mole fraction of GeTe. From the discontinuity in this plot the limit of solid solubility for these alloys can be seen to be about 16.5 mol % GeTe.

The variation of the optical energy gap E_g with composition and temperature is shown in Figure 5.12 and 5.13 respectively. In these alloys β is also positive but less than 0.2 meV deg K^{-1}.

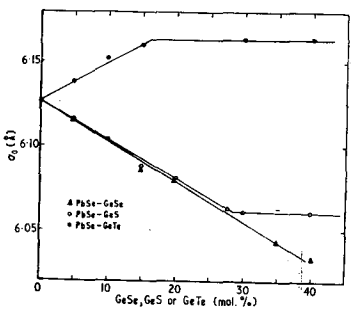

Figure 5.17. The variation of the lattice parameter with composition for the PbSe—GeS, PbSe—GeTe and PbSe—GeSe alloys.

5.2.5. *PbSe-GeSe Alloys.* Specimens containing up to 60 mol % GeSe were prepared and after annealing at 640 °C for three weeks it was found that those containing up to 40 mol % GeSe were in single phase equilibrium and had the NaCl structure. Values of the lattice parameters a_0 are plotted against composition in Figure 5.17. The variation can be expressed by the equation: $a_0 = 6.127 - 0.285\ X$ [Å] where X is the molar concentration of GeSe. The variation of the optical energy

gap with composition and temperature is shown in Figure 5.12 and 5.13 respectively. The energy gap temperature coefficient β is negative and has a value of about 0.15 meV deg K^{-1}. It is interesting to note that in earlier work by SHELIMOVA et al. (1966) and KREBS et al. (1964), the limit of solid solubility of GeSe in PbSe was reported to be at only 8 and 9 mol % of GeSe respectively. The reason for this discrepancy is very probably because their annealing temperatures were lower than the 630 °C used in the present investigation.

5.2.6. *PbSe-GeS Alloys.* Specimens containing up to 45 mol % GeS were prepared and after they had been annealed at 705 °C for two weeks, those containing up to 28 mol % GeS were found to be in single phase equilibrium. The values obtained for the lattice constant a_0 are plotted against composition in Figure 5.17. The linear variation in a_0 is given by the equation: $a_0=6.127-0.23\,X$ [Å] where X is the molar fraction of GeS.

The variations in the energy gap, E_g, with composition and with temperature are plotted in Figures 5.12 and 5.13 respectively, together with the results of the other lead germanium chalcogenide alloys. We note that the limit of solubility of 28% of GeS in PbSe found in this work is very much greater than that of 8% reported by KREBS and LANGNER (1964). Again their annealing temperatures were lower than those used here.

5.3. Film specimens of lead-tin-germanium chalcogenide alloys

The production of polycrystalline and single crystal films of these alloys on various substrates has been described in chapter 3.4 Two preliminary investigations were made to determine the most suitable substrate materials.

5.3.1. *The effect of the substrate on the structure of films of PbTe-GeTe Alloy.* The crystal structure of these films was examined by both *R*-ray and electron diffraction. At the beginning of this work, electron diffraction was used most since this appeared to be more suitable than *X*-ray diffraction for films as thin as about 1000 Å. but once a technique has been developed for transferring a film from a NaCl or a KBr substrate to an amorphous substrate, *X*-ray diffraction was used more frequently.

For electron diffraction work, very thin specimens 300—800 Å thick were prepared on substrates of sodium chloride, glass or microscope copper grids coated with formvar. Glass was found to be a poor substrate material because it usually resulted in amorphous specimens. Films evaporated onto formvar substrates were normally found to be polycrystalline although occasionally these too were amorphous. The formvar net clearly had a strong influence on the growth of the semiconductor films since after the formvar has been washed away in a chloroform bath the pattern of the formvar net on the film could still be seen. An example of this is seen in figure 5.18 which shows a photomicrograph of an evaporated film obtained from an alloy containing 90 mol% GeTe and 10 mol% PbTe. The pattern of the hexagonal formvar net can clearly be seen. It was shown that the pattern closely

followed the form of the net by distorting the net slightly in one direction. In figure 5.18 also some round spots are visible which do not always follow the geometric pattern of the formvar net. These spots can be seen more clearly in figure 5.19 which represent PbTe-GeTe alloys containing 20 mol% GeTe .When the net was

Figure 5.18

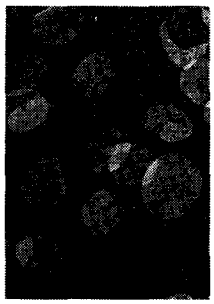

Figure 5.19

Figure 5.20

stretched as before, the round spots became ellipsoids as shown in figure 5.20 for the 90 mol% GeTe alloy. From the magnification the diameters of those spots were calculated to be between 3.600 and 5,800 Å.

From photographs at a higher magnification it appears that spots are holes with diameters of about 4000 Å. This is shown in figures 5.21 and 5.22 showing

Figure 5.21

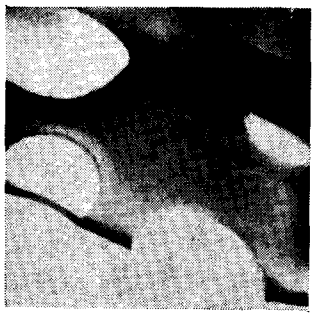

Figure 5.22

Figure 5.23

photomicrographs again of a 90 mol% GeTe alloy at magnifications of 55,000 and 60,000 respectively.

An interesting pattern was observed on one sample made from an alloy containing 90 mol% GeTe and 10 mol% PbTe and using a copper grid with formvar as a substrate as before but in this case the film was made considerably thicker than before (figures 5.23 at magnifications of 16,000). The almost hexagonal network pattern appears so similar to that in the thinner films that it seems probable that it is also due to the formvar network. An electron diffraction pattern was taken

for the same surface. The result, the ring pattern shown in figure 5.24 shows that the grain size was very much smaller than the size of the electron beam (~4000 Å) and so smaller than the hexagons (~4,000 Å). When the electron beam was moved across the surface the same ring pattern was obtained, indicating that the whole surface was of small crystal size. Hence we conclude that the hexagons are due to the formvar network.

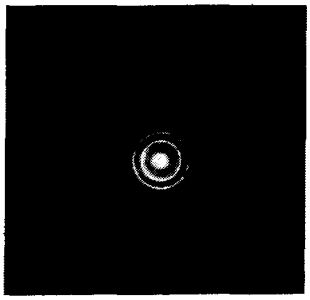

Figure 5.24

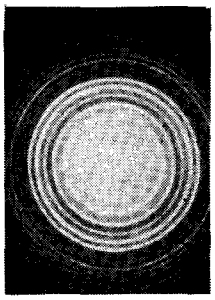

Figure 5.25

Similarly the ring pattern shown in figure 5.25. obtained for the surface from which figures 5.21 and 5.22 were obtained indicates that this material was also polycrystalline with small grain size and the structure in these cannot be the result of dislocations. The rings observed for the surfaces of figures 5.18 had an amorphous pattern showing that in this case the formvar was having an even bigger influence. In figure 5.19 a photomicrograph is shown of a film that has been folded over. An electron diffraction pattern of this film was again of rings characteristic of polycrystalline material with grain size $\approx$4000 Å i. e., very much smaller than the linear dimensions of the »holes« observed in the photomicrograph. We conclude that the »holes« cannot be grains nor could they be dislocation patterns since these would not extend across grain boundaries, and are in fact physical holes in the fibres. A similar conclusion based on grain size rules out grains and dislocation patterns as being responsible for the hexagonal structure of 5.23 etc.

When single crystal NaCl was used as a substrate the electron diffraction patterns obtained were either characteristic of polycrystalline material of large grain size or occasionally showed single-crystal behaviour. In this case it is assumed that the films grew by enlargement of islands around nuclei which form preferentially at crystallographic defects on the substrate surface. We attempted to take the electron as the photomicrographs and for convenience approximately the same magnification was used throughout.

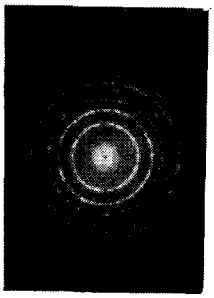

Figure 5.26

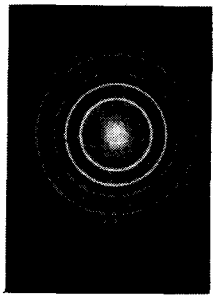

Figure 5.27

An example is shown in figure 5.26. of a diffraction pattern taken with a narrow electron beam: one can almost see individual diffraction spots. The number of individual resolved spots could actually be counted to provide an estimate of the number of crystals contributing to the observed pattern.

Figure 5.27 shows the ring pattern obtained from a thin film of PbTe-GeTe alloy containing 10 mol% GeTe, which again indicates a polycrystalline material of

small grain size. The picture of the surface from which the rings were obained is given in figure 5.28 where one can see that there were many small crystals in the field.

For specimens of large grain size (i. e. comparable to the beam size) the pattern approaches that of a single crystal. Figure 5.29: is of a surface of 90 mol% GeTe, 10 mol% PbTe on a NaCl substrate which clearly contains quite large size grains. From the scale it is clear that the grains could be comparable in size to the electron beam. For such surfaces, the electron diffraction patterns approach those of a single crystal

Figure 5.28

Figure 5.29

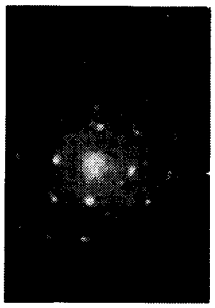

Figure 5.30

and contain a small number of spots. The diffraction pattern for this surface is shown in figure 5.30. A typical single crystal spot pattern obtained from a thicker specimen of the same material is shown in figure 5.31. The arrangement of the spots would appear to be consistent with the distorted NaCl lattice of this material. A further example of a single crystal pattern is shown in figure 5.32 for a specimen containing 43 mol% GeTe and 57 mol% PbTe.

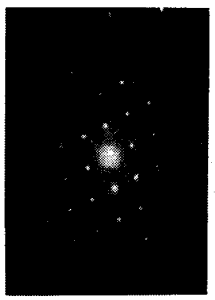

Figure 5.31

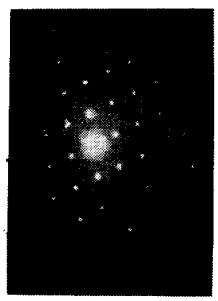

Figure 5.32

We have found from, investigations of this sort that thin (~500 Å) specimens obtained on heated NaCl substrates were occasionally single crystals but usually polycrystalline but about half of the thicker specimens (~1000 Å) were single crystals. Hence their lattice constant and so composition could be obtained from the size of the diffraction rings but we have found the error in the lattice constant obtained in this way to be quite large (i. e. ~2%).

5.3.2. *The effect of the substrate on the optical properties of films of PbTe-GeTe alloys.* The production of polycrystalline and single crystal film of IV-VI compounds and their alloys on various substrates NaCl, KBr, glass and mica has already been described in Chapter 3.4. The sodium chloride and potassium bromide substrates were carefully polished just before the evaporation although whenever it was possible both substrates were obtained by cleaving a single crystal rod. The glass used was microscope slide 0.20 mm thick. The homogenity of the films was usually confirmed by measuring the transmission and reflectivity of different areas of the films on both their front and back surfaces.

In figures 5.33 — 5 typical transmission spectra are shown. The specimen in 5.33 was a pure PbTe film evaporated on to a heated substrate of NaCl, in 5.34 a film of 20 mol% GeTe and 80 mol% PbTe alloy on heated NaCl and in 5.35 a thicker film of a GeTe -PbTe alloy on heated KBr.

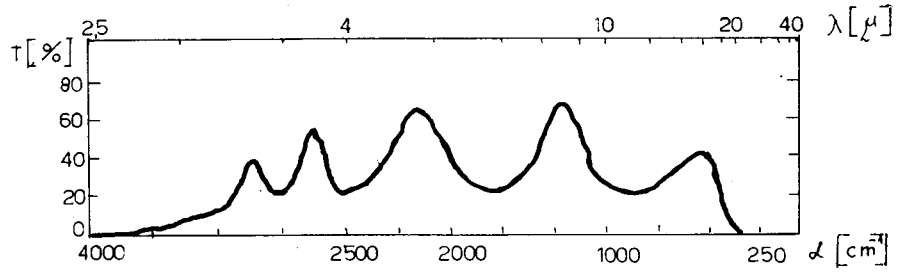

Figure 5.33

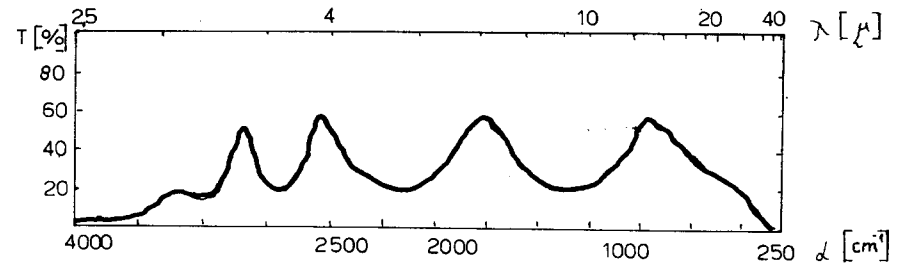

Figure 5.34

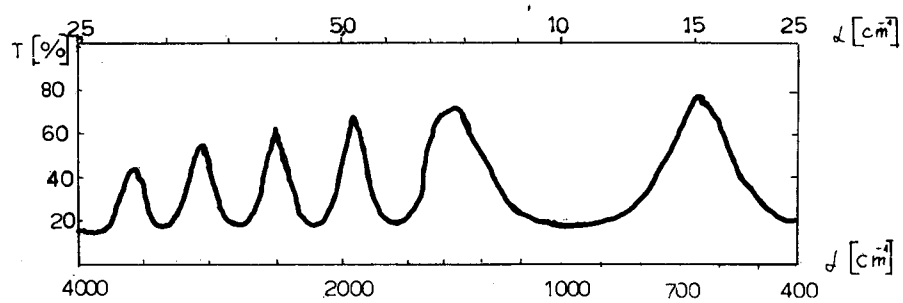

Figure 5.35

The clearly defined and uniform interference fringes in these figures show that films produced in this way are uniform in their composition and thickness. The film thickness was usually determined from the analysis of these interference fringes as previously described and reasonable agreement was usually obtained with the values obtained by measuring the weights of the substrates before and after evaporation of the films.

A typical differential spectrum for a GeTe film evaporated onto a glass substrate measured with a similar glass plate in the second beam is given on Figure 5.36. The oscillations in the transmission are due to interference in the substrate. The amplitude of these is small so that the results are not too seriously affected. The main disadvantages of this substrate is that it is only transparent up to about 5 microns.

It would appear that a mica substrate can have a sizeable effect on the transmission spectrum. An example of such a spectrum for a film on a mica substrate is shown in Figure 5.37.

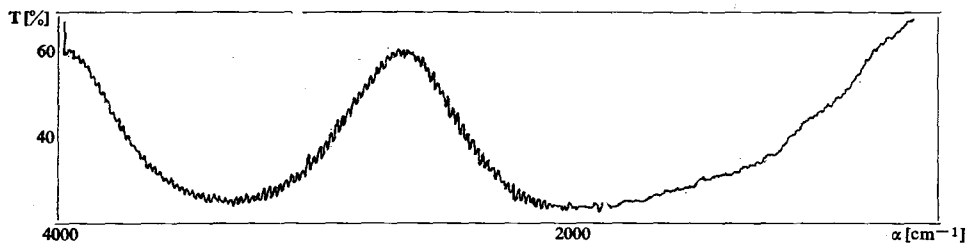

Figure 5.36

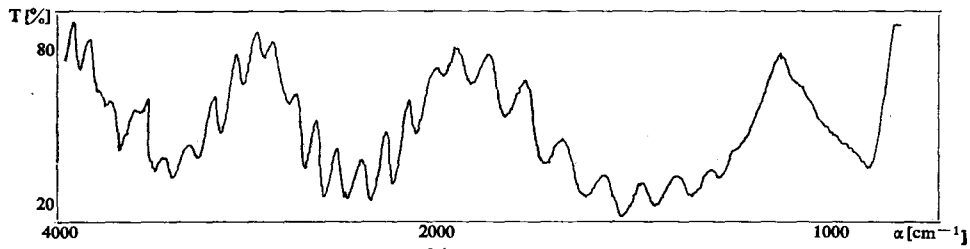

Figure 5.37

In nearly all cases the optical measurements were made on films freshly taken from the evaporator but a check was made to see whether exposure of the films to the atmosphere had any effect on their optical properties. In Figure 5.38 and 5.39

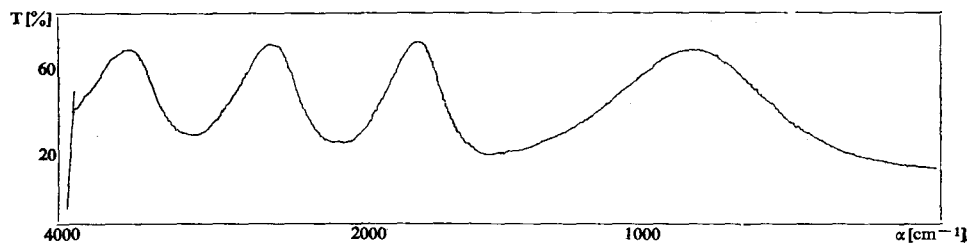

Figure 5.38

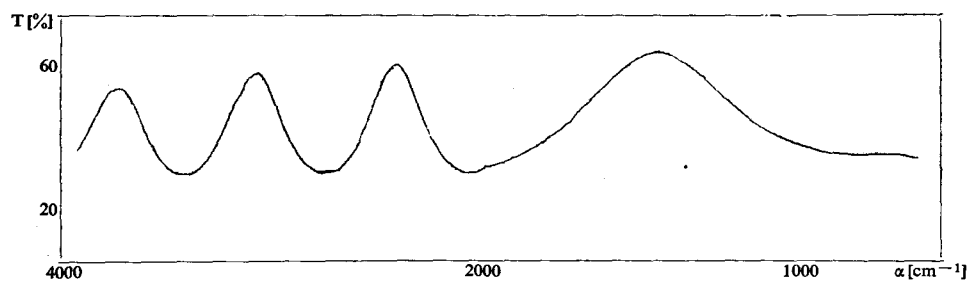

Figure 5.39

the transmission spectra taken under identical conditions are shown for the same specimen 90 mol% GeTe 10 mol% PbTe immediately after the evaporation and after 22 days respectively. The only difference between these spectra is that the maxim are slightly sharper for the specimen measured immediately after evaporation. However, in other checks we have noted that, the position of maxima were displaced after the films had been exposed to air for a long time: an example of this behaviour is seen in Figures 5.40 and 5.41 showing spectra for a film containing 10 mol% GeTe.

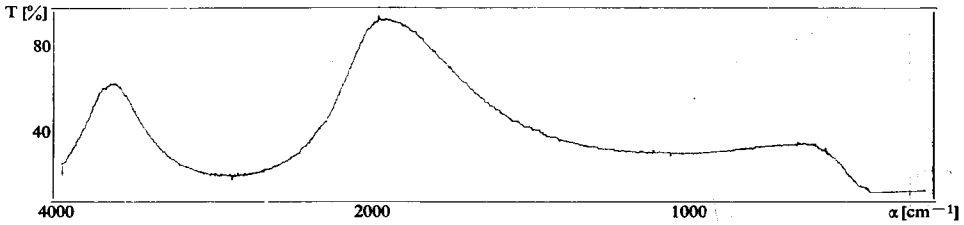

Figure 5.40

The spectrum shown in Figure 5.40 was taken immediately, and that in Figure 5.41 was taken after 5 months exposure to air. It is seen that after exposure the maxima are displaced to higher wavelengths. However on the whole one could say that the films were very stable.

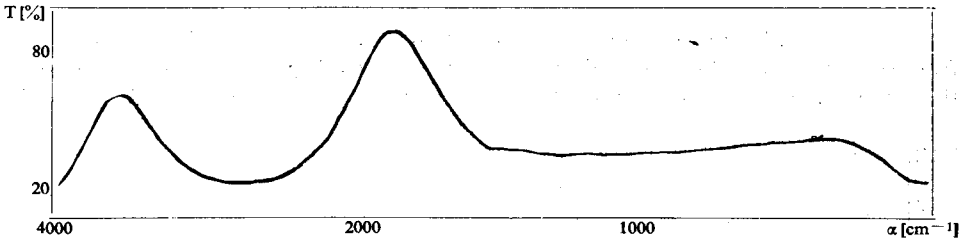

Figure 5.41

To summarize, we have found from these two preliminary investigations, that heated NaCl and KBr substrates are the most suitable for an investigation of the optical properties of these alloys.

5.3.3. *Optical properties of PbTe-GeTe film specimens.* All the film specimens of PbTe-GeTe alloys were evaporated on to heated KBr and NaCl substrates using a single source or occasionally two sources. Single crystal or polycrystalline specimens were obtained. In Table 5.1. details of the evaporation conditions are given for some specimens such as substrate temperature, the material used as substrate, the crystal structure of the specimen as obtained by X-ray diffractometer methods, the thickness of specimen d and the time of annealing.

Transmission and reflectivity measurements were made and several typical transmission spectra, obtained with Perkin-Elmer spectrophotometers, are presented in chapter 5.3.2. In addition similar transmission measurements have been carried

out using an SP 700 Unicam spectrophotometer for the visible and ultra violet regions, (Figure 5.42).

Further transmission data were obtained in the same wavelength region using Barr and Stroud and Specol monochromators. The optical density of several samples of different composition, obtained using these monochromators are given in figures 5.43 and 5.44 respectively. From these data we tried to estimate the energies of the higher order transitions for some of the specimens and this will be discussed in Chapter 6.1.

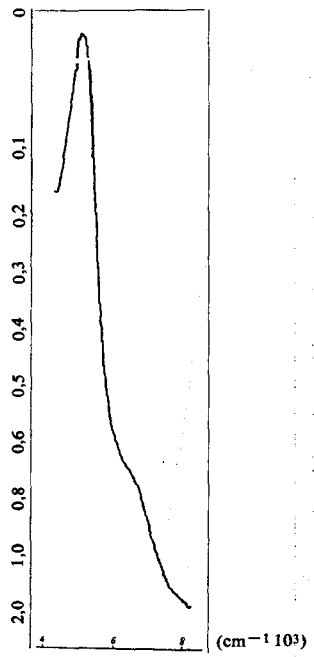

Figure 5.42 Transmission versus 1/10 λ for a 20 mol % GeTe, 80 mol % PbTe specimen.

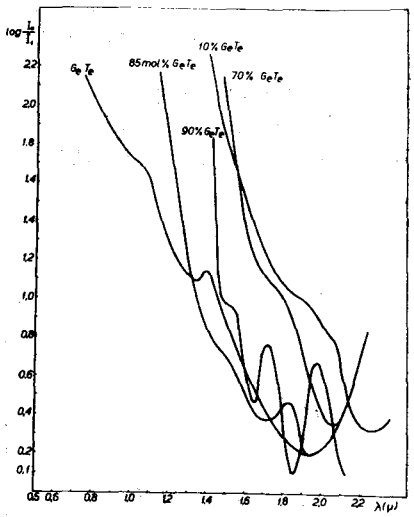

Figure 5.43 Optical density of PbTe-GeTe alloy samples of different composition in the infra red region.

The reflectivity of the alloys close to normal incidence and at room temperature was also measured in the range 0.5 to 18 microns using these monochromators.

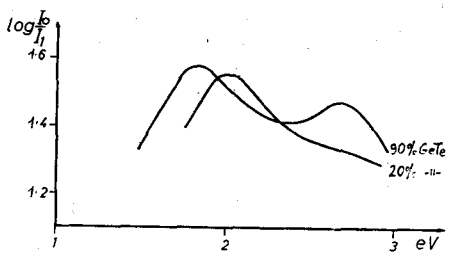

Figure 5.44 Optical density of PbTe—GeTe alloy samples of different composition in ultra violet region.

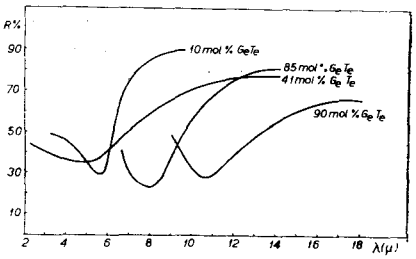

Figure 5.45 Measured reflectivity of PbTe—GeTe film specimens.

Experimental reflectivity data from several typical specimens are given in Figure 5.45. These results were used to calculate the optical dielectric constants, ε_{opt},

plasma wavelengths, λ_P, and relaxation times, τ, of the carriers using the classical free carrier dispersion relations given in chapter 4.1.2. and a least square method for fitting. The results obtained are listed in Table 5.1. together with the measuring conditions, thickness, the crystallographic properties of the specimen, and the results for σ_{opt}. The thickness of the films were determined where possible by the methods given in 4.1.1.

5..3.4. *Optical properties of PbTe-SnTe film specimens.* All specimens of PbTe-SnTe alloys were prepared by evaporation using single source techniques. The composition of the samples produced were checked by an X-ray diffractometer recording method and polycrystalline structure was usually confirmed. The lattice constant was found to be in agreement with the corresponding bulk alloys.

Two typical transmission spectra for these alloys are given in figures 5.46 and 5.47 for specimens with 10 and 20 mol% SnTe, respectively, and transmission and reflectivity spectra for a single crystal film sample of pure SnTe are given in figures 5.48 and 5.49 respectively.

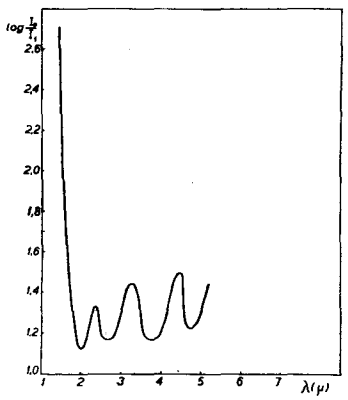

Figure 5.46 Optical density of a 10 mol % SnTe, 90 mol % PbTe film specimen.

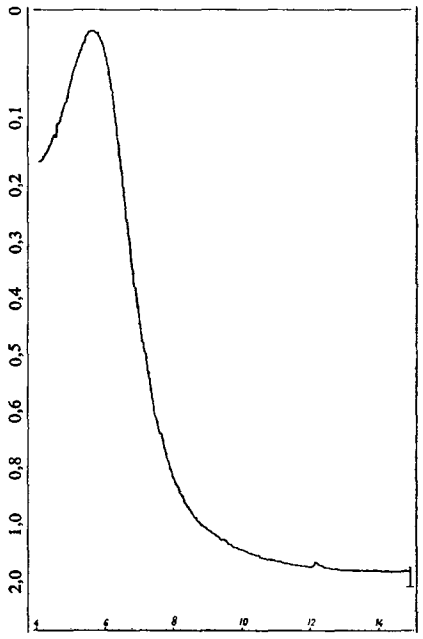

Figure 5.47 Transmissions versus $1/10^3\,\lambda$ for a 20 mol % SnTe, 80 mol % PbTe film specimen.

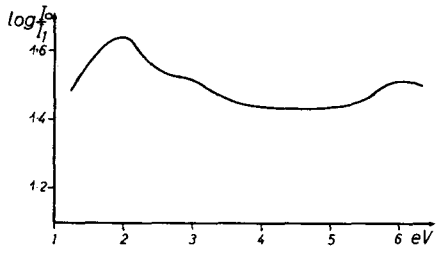

Figure 5.48 Optical density for a SnTe specimen.

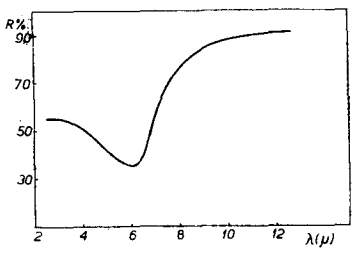

Figure 5.49 Measured reflectivity of a SnTe film specimen.

Reflectivity data for some of these specimens were also used to calculate optical dielectric constants using the fitting procedure, mentioned earlier and these results are given in Table 5.2 together with general information about the evaporation conditions, substrate, thickness of the film specimen and its crystal properties.

5.3.5. *Optical properties of PbTe-SnSe film alloys.* The specimens of PbTe-SnSe alloys were prepared by evaporation from a single source on to a heated NaCl or for some of the reflectivity work, on to a glass substrate. Using X-ray diffractometer recording we found that some of the specimens on NaCl were single crystal. A transmission spectrum obtained with a Perkin Elmer spectrophotometer is given in figure 5.50 for a typical specimen containing 3 mol% SnSe. The optical densities for the same specimen and for a 1 mol% sample are given in figure 5.51.

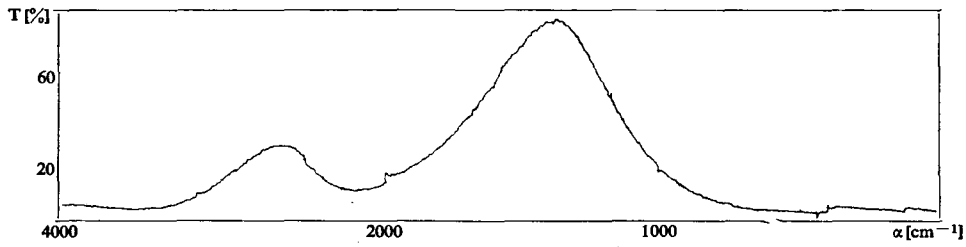

Figure 5.50 Transmission versus wavelength for a 3 mol % SnSe, 97 mol % PbTe specimen.

The optical densities of film and bulk specimens of SnSe are given in figure 5.52. The position of at least one higher energy transition can be roughly estimated from the film data.

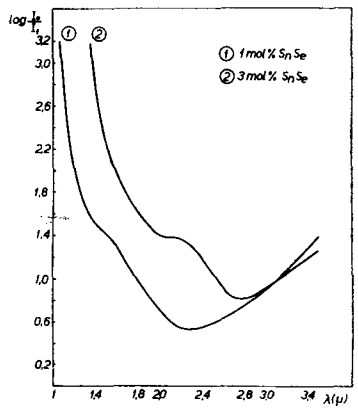

Figure 5.51 Optical density of two PbTe—SnSe film specimens.

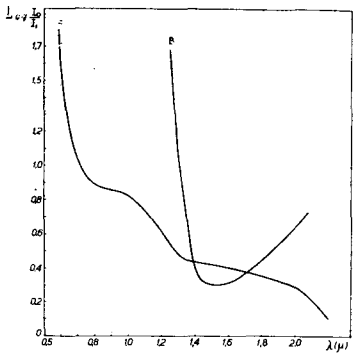

Figure 5.52 Optical density of a film specimen (F) and a bulk specimen (B) of SnSe compound.

Experimental reflectivity spectra are given in figure 5.53 for a specimen containing 3 mol% SnSe. The experimental detail and the results obtained by a fitting procedure for the reflectivity data are given in Table 5.2.

5.3.6. *Optical properties of GeSe film specimens.* Germanium selenide was evaporated from a single source on to a heated KBr substrate. The transmission spectra of the specimens were measured in the region 0.25 to 25 microns. A spectrum from 2.5 to 25 microns for a typical specimen is shown in figure 5.54. from 0.25 to 2.5 microns for a second specimen in figure 5.55.

The reflectivity data in the infra red region were fitted to those computed from the free carrier dispersion relation and from this the optical dielectric constant and optical conductivity were obtained. These results are given in Table 5.2.

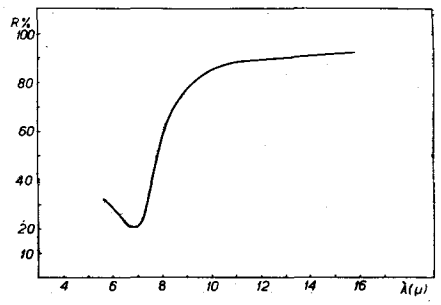

Figure 5.53 Measured reflectivity of a 3 mol % SnSe, 97 mol % PbTe film specimen.

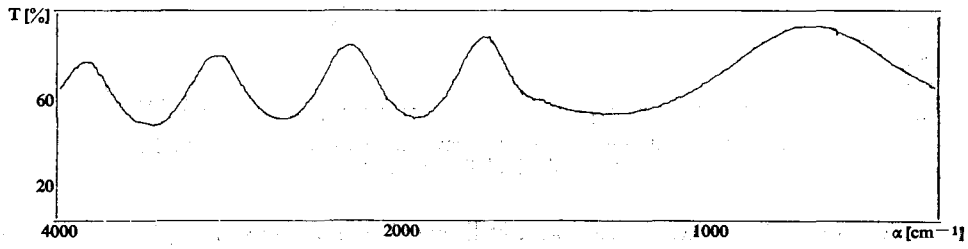

Figure 5.54 Transmission spectra for a GeSe film specimen of thickness 0.9μ in the infra red region.

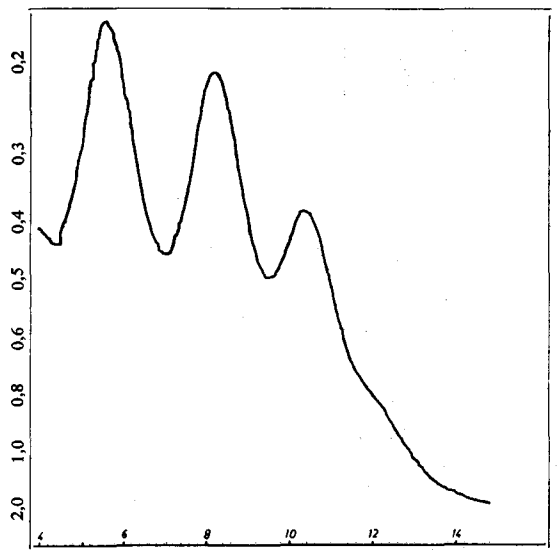

Figure 5.55 Transmission versus $1/10^3$ λ for a GeSe film specimen of thickness about 1000 Å.

TABLE 5.1

№	Composition	Substrate and Temperature	Time of Annealing (m)	ε_{opt}	L_p (μ)	$\tau \cdot 10^{14}$ (s)	σ_{opt} $(\Omega\ cm)^{-1}$	d (μ)
18	20% GeTe 80% PbTe	Mica; 90° C	30	42.6	3.67	15.8	2464	0.7
102	GeTe	Glass; 75° C	30	30.4	7.12	6.55	1220	0.8
111	85% GeTe 15% PbTe	KBr; 130° C	60	24.14	8.5	4.85	655	1.2
132*	43% GeTe 57% PbTe	NaCl; 120° C	60	17.7	4.8	2.51	693	0.7
194*	70% GeTe 30% PbTe	NaCl; 130° C	60	33.4	12.0	2.55	204	1.08
196*	90% GeTe 10% PbTe	KBr; 130° C	60	31.5	12.05	3.89	387	1.1
203*	20% GeTe 80% PbTe	NaCl; 140° C	25	36	3.75	2.37	2264	0.85
220*	41% GeTe 59% PbTe	NaCl; 92° C	110	32,09	4.26	0,87	400	1.3

TABLE 5.2

№	Composition	Substrate and Temperature	Time of Annealing (m)	ε_{opt}	L_p (μ)	$\tau \cdot 10^{14}$ (s)	σ_{opt} $(\Omega\ cm)^{-1}$	d (μ)
114	GeSe	KBr; 120° C	60	17,4	12.25	1.07	625	0.7
124*	3% SnSe 97% PbTe	NaCl; 120° C	600	30.5	7.28	6.92	1548	0.77
214	50% SnTe 50% PbTe	NaCl; 120° C	90	312	7.48	7.01	13640	0.8
225	5% SnTe 95% PbTe	KBr; 130° C	23	54.2	4.47	1.12	1060	0.9
228	SnTe	NaCl; 140° C	30	54	6.5	4.42	2230	0.6

6. DISCUSSION OF RESULTS

Before discussing the data described in this thesis it is perhaps appropriate to explain why measurements have been made on both bulk and film specimens of the same materials.

When this study of IV—VI alloys was started we had no intention of making film specimens, but later we realized that film specimens could give important information especially on the optical constants. Hence film specimens of three IV—VI alloy systems were made following a study to determine the best of several techniques of evaporation. Thus the work can be divided into two main parts namely bulk measurements and film measurements.

The bulk specimens were always polycrystalline and were used to obtain the variation of the fundamental absorption edge as a function of both composition

* Single crysta

and temperature. In addition, crystallographic measurements were made in an attempt to extend the solid solution range previously measured for various IV—VI compounds and in some cases to find for the first time the limit of solubility for such systems as PbTe-SnS, PbTe-GeSe etc. However considerable difficulty was found when trying to make reflectivity measurements necessary for a derivation of the optical constants using bulk specimens. The accuracy was often very poor because of the great difficulty in obtaining a mirror finish on a polycrystalline specimen and it was primarily for this reason that film specimens were made. There is of course a fundamental problem in obtaining these optical constants which applies to all specimens in that accurate measurements of reflectivity are needed over a wide range of frequency and in our case this was limited by the equipment available.

The transmision and reflectivity of film specimens are always higher than those of bulk specimens and since both can be measured for the same film specimen the optical constants (index of refraction, n, and the absorption coefficient, α), can be derived at a given energy. One important difficulty in work with film specimens is the presence of interference phenomena which can reduce the accuracy with which the optical constants are determined. However the location of the interference fringes is a function of the film thickness, so that for the best determination of the optical constants one should use the data from one thick and one rather thin film (about 10,000 Å to 30,000 Å and 300 Å thick) where the regions of inaccuracy are different. Much attention has been paid to the problem of producing IV—VI compound and alloy films, using techniques with one and two sources. Since both methods are rather new in the literature it was thought that it would be useful to describe the experience obtained in chosing suitable substrates (mentioned in chapter 5.3.1.) for both transmission measurements and electron and X-ray diffraction analysis, and also to describe the effect of substrate on the film structure. We have tried to find the most suitable evaporation conditions for obtaining single crystal film specimens. We note again that specimens were obtained with a very wide range of crystallographic properties beginning with amorphous specimens evaporated onto formvar and occasionally glass substrates, very good polycrystalline mirror like specimens and finally the acquisition of single crystal specimens on either KBr or NaCl monocrystalline heated substrates with almost 50% reproducibility.

The optical investigation on the film specimens (mainly single crystal) of PbTe-GeTe, PbTe-SnTe and PbTe-SnSe is at present incomplete and our work has been more concerned with establishing the fact that the production of good quality alloy films is possible for these materials. It is hoped to make more extensive optical measurements on these and films of other alloys at a later stage as part of a major project. However the optical measurements on the PbTe-GeTe films do provide some information regarding the fundamental energy gap of pure GeTe which is at present the subject of some disagreement.

6.1. Lead-Germanium Chalcogenide Alloys

It has been shown in the present work that there is an almost linear dicrease in lattice constant with increasing concentration of GeSe and GeS in lead telluride (Figure 5.14 and 5.16 respectively), with the exception of the alloys of lead selenide with germanium telluride for which the lattice constant increases (Figure 5.17). It has been shown also that solid solution of PbSe-GeSe and PbSe-GeS alloys extends further than previously thought. Thus KREBS et al. (1964) reported the limit of

solid solubility of GeSe and GeS in PbSe to be at only 8 mol % but they annealed their specimens at temperatures of only 480 °C and 470 °C respectively. In the present work, solubility was found to extend to about 40 mol % and 27 mol % respectively after the alloys had been annealed at 630 °C and 705 °C respectively.

It seems likely that the progressive decrease in lattice constant described above is merely a consequence of the smaller interatomic distances of germanium chalcogenide. The anomalous case of the PbSe-GeTe alloys in which there is a progressive increase in lattice constant despite the smaller lattice constant of GeTe could be a consequence of the much lower ionicity of the GeTe atoms.

It is very noticeable that in all of the alloys studied the energy gaps increase with germanium chalcogenide content (Figure 5.12 and 5.15). Similar increases are found in materials in which the gaps are known to involve an *s*-like conduction-band state, as in zinc blende type semiconductors where the energy gaps increase when an atom is substituted by the other atom of smaller atomic weight so that this may be some evidence for *s*-like conduction states in the present alloys. It is also interesting to note that the rate of increase of the energy gap is larger when PbTe or PbSe is alloyed with GeSe or GeS than with GeTe. We believe this is due to the fact that selenium and sulphur are more electronegative than tellurium and so produce a larger increase in the ionicity of the average bond and so a larger increase in the energy gap.

With the exception of the PbTe-GeS alloys, the energy gap temperature coefficient β of the germanium chalcogenide alloys (Figure 5.13) is either negative ($\beta = -1.9 \times 10^{-4}$ eV deg C^{-1} for PbTe-GeTe, PbTe-GeSe and PbSe-GeSe) or positive but less than 2×10^{-4} eV deg C^{-1} (PbSe-GeS and PbSe-GeTe). This suggests that β is more affected by the electron-phonon interaction than by expansion of the lattice; this expansion causes a positive increase in the gap for PbS and PbSe of about 2×10^{-4} eV deg C^{-1} (PAUL et al. 1962).

In earlier work it was shown (WOOLLEY and NIKOLIĆ, 1965) that the optical energy gap for PbTe-GeTe alloys increases at a nearly constant rate up to 40 mol % GeTe but the present work shows that at higher concentrations there is a rapid decrease (Figure 5.12).

Unfortunately an explanation of this change of optical energy gap for PbTe--GeTe alloys is complicated by the disagreement in the published results for the fundamental energy gap of GeTe compound. The first measurements indicated that the fundamental energy gap should be about 1 eV e.g. WOOLLEY and NIKOLIĆ (1965), MUIR and CASHMAN (1967), TSU et al. (1967) although HEIN et al. (1964) suggested it was between 0.5 and 1 eV. However, STILES et al. (1966) showed by tunelling measurements that the gap was about 0.1 eV at room temperature and about 0.2 eV at 4.2 °K, and SYSOEVA et al. (1965) obtained 0.2 eV from thermal conductivity measurements. It is possible as suggested for example by TSU et al. (1968) that the values obtained at ~1.0 eV could be due to a very large BURSTEIN shift of the 0.1 eV value due to the very high carrier concentration in GeTe of about 10^{20} cm^{-3}. This would not affect the tunnelling measurements but would affect the others. However we suggest that it is also possible that the energy gap of ~1 eV could correspond to the second minimum band separation, E_1. We have obtained

a value close to this by extrapolation from the experimental results of CARDONA and GREENAWAY (1964). In figure 6.1 the first, E_0, second E_1, and third ,E_2, minimum band separations are plotted for the five IV—VI compounds as a function of effective atomic charge q. These have been calculated in each case using the empirical formula given by SUCHET (1961)

$$q = n\left[1 - \left(\frac{z}{r'} - \frac{z'}{r}\right) C\right] \tag{6.1}$$

where n, the ionic charge number, equals two, z and z' are the atomic numbers, r and r' the cation and anion diameters for the elements respectively and c is a constant which we calculate to be $c = 1.19 \times 10^{-2}\,(\text{Å})^{-1}$. The values for the first minimum band separation for GeTe were taken from SYSOEVA et al. (1965). By extrapolating the curve for E_1 (Figure 6.1) as shown, a value for the second minimum band separation for GeTe of about 0.85 is obtained.

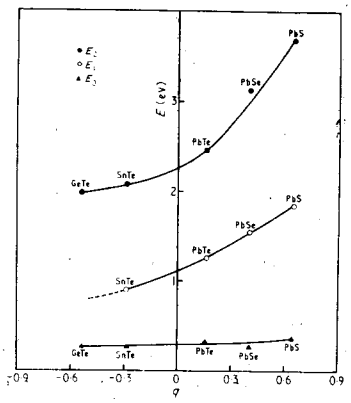

Figure 6.1. The variation of the first, E_0, second, E_1, and third E_2, minimum band separations for some IV—VI compounds as a function of effective atomic charge q.

CARDONA and GREENAWAY (1964) concluded that the band structures of GeTe are probably rather similar to those of PbTe, PbSe etc. in view of the 'striking' similarity of their reflection spectra although they did point out that the *d*-bands of GeTe and SnTe were much deeper than those of the others. It is interesting to see what information is provided on this point by the present work on PbTe-GeTe alloys. We assume first that the band structures of PbTe and GeTe are indeed very similar, and consider in turn what we should expect for GeTe gaps of 1.0 eV and 0.1 eV; the gap for PbTe is 0.32 eV. For a gap of 1.0 eV, we should expect a steady increase in gap as GeTe is added. This is found up to 40 mol% GeTe and indeed if this increase is extrapolated to pure GeTe, a gap value of ~1.0 eV is obtained. However with a gap of ~0.1 eV, which we believe is in fact the true value, a steady *decrease* would be expected. In this case, the increase found must surely imply that there are important differences in the band structures of PbTe and GeTe, such that the gaps are from different points in the BRILLOUIN zone in each case.

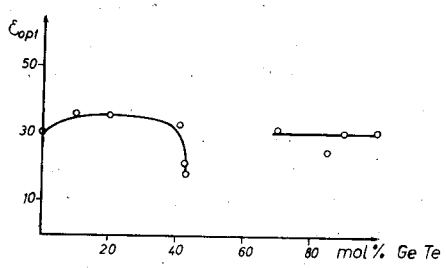

Figure 6.2. Optical dielectric constant versus composition for PbTe—GeTe alloys.

A possible model for the band structure of GeTe is shown in Figure 6.3 a and b together with the structure for PbTe 6.3 c (see also figure 2.1) which is quite well known. We see that in PbTe, the first transition is at the L point and the second at the Σ and we are postulating that the reverse is true in GeTe. We take the value of TSU et al. (1968) of 0.6 eV for the second transition in GeTe i.e. in our model the separation at the L point. On adding GeTe to PbTe, we would expect the separation at the L point to increase and at the Σ point to decrease. Clearly the rate of increase at the L point should be quite small since the two separations do not differ

greatly (0.32 and 0.6 eV) but the rate of decrease at the Σ point is very fast since the values there differ greatly (1.26 and 0.1 eV). Hence when the two separations become equal, the steady increase should be replaced by a rapid drop. We presume this is what is being observed above 40% GeTe. However the drop is so rapid that it is possible that it may drop to — 0.1 eV i.e. that there is band inversion as in

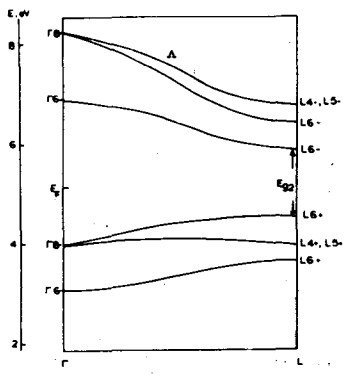

Figure 6.3. a

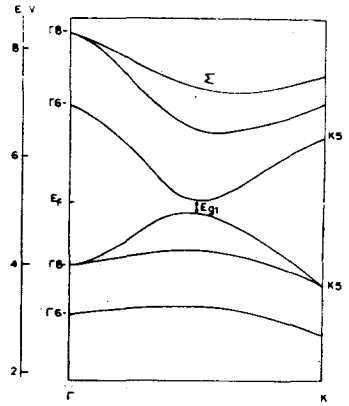

Figure 6.3. b

PbTe-SnTe etc. This is consistent with further information we have obatined from transmission measurements on very thin specimens of PbTe-GeTe alloys. Using figure 5.44 one can roughly calculate two energy transitions for pure GeTe of about 0.68 eV and 0.97 eV. When PbTe is added to pure GeTe both transitions apparently move towards lower energies i.e. adding PbTe to GeTe produces a *decrease* in the energy gap. This decrease i.e. an *increase* in the gap as the GeTe rich alloys become even richer in GeTe, could only simply join on to the *decrease* found about 40% GeTe if the bands become inverted at some concentration between 40% and 90%.

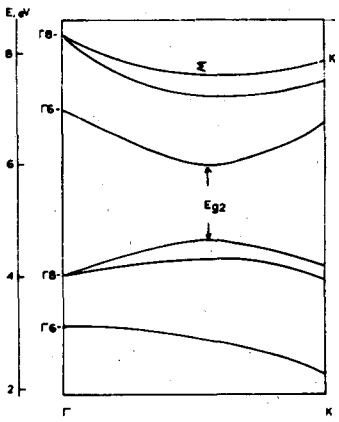

Figure 6.3. c

We quote here the transition values for two alloys 41% GeTe: 0.60 eV and 0.80 eV: 20% GeTe: 0.53 eV and 0.77 eV. Further transitions were observed in very thin specimens containing 90 mol% GeTe and 20 mol% GeTe (Figure 5.45). For the specimen with 90 mol% GeTe, two transitions were observed at about 1.8 eV and 2.6 eV but for 20 mol% GeTe only one transition could be obtained at 2.0. We note that CARDONA and GREENAWAY (1964) observed the third energy transition for GeTe to be at 1.98 eV and for PbTe to be at 2.2 eV and the fourth transition for GeTe to be at 3.2 eV. We assume therefore that the transitions observed in our specimens (Figure 5.45) were also the third and fourth. If this is true it means that these higher transitions have a tendency to decrease in energy when either PbTe is added to GeTe or vice versa. This is qualitatively consistent with our assumption that the band structures for pure PbTe and GeTe are different.

Several attempts have been made to prepare very thin alloys at compositions between 40 and 90% GeTe to examine these higher order transitions but the quality of these was not sufficient for the optical instruments available and this work is to be continued at a later stage.

Another fact which has bearing on these differences in band structure is the difference in sign of the energy gap temperature coefficient, β, for lead telluride and all the lead-tin chalcogenide alloys (+ve) and that for GeTe (ESAKI 1966) and for all the PbTe-GeTe alloys even that containing 2% GeTe (—ve). This demonstrates that even a very small percentage of GeTe apparently produces a modification of the band structure. Clearly it would be interesting to extend this work to smaller concentrations of GeTe.

We now discuss briefly how our data compares with the band structure model for GeTe of TSU et al. (1968). In their model, both the first and second transitions at 0.1 and 0.6 eV respectively are from two valence bands both at the L point. This model would thus predict a *decrease* in the first transition when GeTe is added to PbTe so we conclude it is incorrect. We note finally that the band parameters TSU et al. calculate from their susceptibility mass data versus carrier concentration are equally consistent with our model as with theirs.

We suggest that it would be very worthwhile investigating a number of these alloy systems very carefully at and near to the 50—50 mixture. The band inversion that apparently occurs could lead to very small band gaps and these in some materials would still be very small at a 50—50 concentration where the possibility of an ordered structure i.e. a compound exists. Such materials could be of considerable technical importance. Further measurements on PbTe-GeTe alloys have been made in the region of the plasma frequency, ω_p.

The reflectivities for several typical samples are given in figure 5.46 and these were used to compute the optical dielectric constant, the relaxation time and the optical conductivity. These data are given in Table 5.1. The optical dielectric constant is also shown as a function of composition in figure 6.2. It is interesting that there is also a rapid decrease in the dielectric constant at compositions greater than 40 mol % GeTe. This indicates a sudden decrease in the ionicity of the alloys at this composition which could also be consistent with a sudden change in band structure.

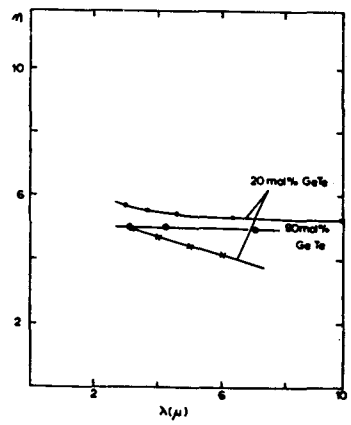

Figure 6.4.

The values at $\frac{N}{m_s}$, the ratio of the carrier concentration to the susceptibility mass calculated using the formula

$$m = \frac{4\pi Ne^2}{\varepsilon_{opt}\,\omega_p} \tag{6.2}$$

are given in table 6.1. Also given in this table are the values of the optical conductivity for the specimens and values of the D. C. conductivity of the specimens.

Finally a comparison is shown in Figure 6.4 between the values of the index of refraction obtained from the experimental interference fringes using the method described in chapter 4.1.3, with the values computed from the experimental reflectivity data at the plasma frequency minimum. For one 20 mol% GeTe, 80 mol%

PbTe specimen one can see that the interference fringe data give an almost constant, n, whereas the reflectivity data give values of n which decrease with increasing wavelength. This lack of agreement has previously been observed in many other systems. The values of n extrapolated to zero wavelength obtained from both these

TABLE 6.1.

Composition	GeTe	90% GeTe 10% PbTe	70% GeTe 30% PbTe	41% GeTe 59% PbTe	20% GeTe 80% PbTe	10% GeTe 90% PbTe
$N/m_s \times 10^{66}\,cm^{-3}\,g^{-1}$	0.65	0.35	0.28	1.6	2.7	0.78
$\sigma_{opt}\,(\Omega\,cm)^{-1}$	1.220	387	204	400	2264	1420
$\sigma_{DC}\,(\Omega\,cm)^{-1}$	5570	3120	1620	236	84	157

results together with a value for a 90 mol% GeTe 10 mol% PbTe alloy obtained from data for n from the interference fringe method are all in reasonable agreement with the value calculated from the optical dielectric constant, ε_{opt}, given in figure 6.2.

6.2. Lead-Tin Chalcogenide Alloys

We have shown for the first time that as in the lead-germanium chalcogenide alloys there is a linear decrease in lattice constant with increasing concentration of SnS in PbTe (Figure 5.8.). We have also confirmed a similar decrease in adding SnSe to PbTe (NIKOLIĆ, 1965); this was first demonstrated by KREBS et al. (1964). We also showed in that paper but have not given the data again here that solid solution in these PbTe-SnSe alloys extends a little further than was found by Krebs et al. They annealed their specimens at 520 °C compared with the annealing temperature in the present work of 700 °C.

Here we shall discuss the work we have carried out mainly with a view to investigate how the optical energy gap varies with concentration and temperature. It was observed that the decrease in the gap on alloying PbTe with SnSe is no greater than in alloying with SnTe i.e. the effect of replacing a tellurium atom by the more electronegative selenium seems to have little effect on the gap in contrast to what was found in the lead germanium chalcogenides.

When PbSe is alloyed with SnTe, a decrease in the energy gap at both room and liquid nitrogen temperatures (Figures 5.6 and 5.7) was observed up to concentrations of ~3% SnTe. At liquid nitrogen temperature there is apparently a minimum at around 4% SnTe and at about this concentration, the specimens also become P-type. Furthermore from CARDONA and GREENAWAY's reflectivity data (1964) for PbTe it is clear that when lead is substituted for by either Sn or Ge, the energies of all the measured reflectivity peaks decrease also. There are then two possible effects that could arise when SnTe is added to PbSe both of which should produce a decrease in transition energies i.e. the effect of replacing Pb by Sn, and the effect of replacing Se by the less electronegative Te. The effect of adding Sn atoms to a PbTe or PbSe compound should be greater than that of adding Se atoms, as we can see from the relative sizes of the changes in the energy gaps for PbTe-SnSe, PbSe-SnSe and PbTe-SnSalloys (Figure 5.2, 5.6 and 5.10).

From their data CARDONA and GREENAWAY concluded that the smallest direct energy gap E_g which corresponds to transitions between the $L_6^+ - (L_4^-, L_5^-)$ states

for PbTe does not exist in either SnTe or GeTe, implying that overlapping of the first valence and conduction bands occurs in these materials. Some evidence for this overlapping for SnTe came earlier from the work of DAMON et al. (1963) who measured the magnetic field dependence of the Seebeck coefficient for SuTe. It is interesting to note that if we extrapolate the variation of the room temperature energy gap with composition for the PbTe-SnTe and PbSe-SnTe alloys given in Figures 5.2 and 5.6, values for pure SnTe of about — 0.3 eV are obtained in both cases (NIKOLIĆ, 1965, 1967). This value, which is now believed to correspond to inverted bands although was earlier assumed to be due merely to overlapping agrees well with that deduced by DIMMOCK et al. (1966) from a consideration of data from various sources although in view of the distance of the extrapolation, this good qualitative agreement is partly fortuitous.

A relatively large positive temperature coefficient associated with the optical energy gaps was found for lead tin chalcogenide alloys. Values between 0.4 and 0.415 meV deg K^{-1} were obtained for PbTe-SnTe and PbTe-SnSe (Figure 5.3), between 0.18 and 0.4 meV deg K^{-1} for PbSe-SnTe and between 0.016 and 0.14 meV deg K^{-1} for SnSe alloys (Figure 5.7).

Using the following thermodynamic equation it is possible to give a qualitative explanation for the existence of a relatively large difference in the positive temperature coefficient of the optical gaps of the alloys we are considering (CARDONA and GREENAWAY, 1964)

$$\beta = \left(\frac{\partial E}{\partial T}\right)_P = \left(\frac{\partial E}{\partial T}\right)_V + \frac{1}{V}\left(\frac{\partial V}{\partial T}\right)_P V \left(\frac{\partial P}{\partial V}\right)_T \left(\frac{\partial E}{\partial P}\right)_T . \tag{6.3}$$

The first term is due to electron-phonon interaction and the second due to thermal expansion. Knowing that for both PbTe and PbSe, β is about 0.4 meV deg K^{-1} and that

$$\frac{1}{V}\left(\frac{\partial V}{\partial T}\right)_P V \left(\frac{\partial P}{\partial V}\right)_T \left(\frac{\partial E}{\partial P}\right)_T \sim 0 \cdot 2\ meV\ \mathrm{deg}\, K^{-1}. \tag{6.4}$$

(PAUL et al. 1962) it is clear that for the two alloy systems PbTe-SnTe, PbTe-SnSe the electron-phonon interaction must have a positive value and this is true for PbSe-SnTe also. A positive electron-phonon interaction could imply that the band extrema which produce this transition are not the absolute extrema of the bands and that the bands draw closer together with increasing temperature.

Our film transmission data for PbTe-SnTe alloys given in figures 5.47 and 5.48 do not show a transmission similar to that found in PbTe-GeTe alloys — see figure 5.44. Furthermore the temperature dependence of the energy gap is very similar in both PbTe and PbTe-SnTe alloys, and this might suggest that PbTe and SnTe have similar band structures. Confirmation of this point could come from the observation of higher energy transitions for PbTe-SnTe alloys. Unfortunately although we have made several attempts, we have not been able to observe these higher transitions for the alloys in transmission data, although we did observe the third, fourth and even fifth transition (at about 2 eV, 3 eV and 6 eV respectively) in pure SnTe (Figure 5.49). The transmission peaks were not as sharp as those obtained by CARDONA and GREENAWAY (1964) who found transitions at 0.97 eV, 1.96 eV and 3.06 eV from transmission data and at 6.1 eV from reflectivity data but they are in reasonable agreement.

From our reflectivity data on pure SnTe (Figure 5.50) and on several PbTe-SnTe alloys we computed such parameters as ε_{opt}, τ, σ_{opt} etc., which are given in table 5.2 together with results for other materials. It is interesting to note that the optical

dielectric constants have a tendency to increase rather fast with increasing SnTe content in these alloys. For an alloy with 50 mol% SnTe and 50 mol% PbTe the dielectric constant is as high as 312. This might be the result of an extremely high ionicity produced by making a compound of 50% SnTe and 50% PbTe, i.e. an ordered structure.

For the sample of SnTe used to obtain the reflectivity spectra, given in figure 5.50, the position of the reflectivity minimum at the plasma frequency could be used to obtain the approximate value of hole concentration. Using SCHOOLAR's data (1966) we could see that our specimen had a rather high hole concentration, (higher than 10^{20} cm^{-3}). This high carrier concentration could be the main reason why we could not produce specimens of PbTe-SnTe alloys containing more than 50 mol% SnTe good enough to obtain reliable reflectivity data.

We next discuss the optical work we have made on PbTe-SnSe alloys. Examples of some of the transmission and optical density data which were obtained are given in figures 5.51 and 5.52 respectively. We note that there is some similarity with the data on the PbTe-GeTe alloys — see figure 5.44. The optical density for a pure SnSe film specimen given in figure 5.53 (F) shows also an energy transition at about 1.4 eV besides the fundamental one which appears at about 0.9 eV.

The existence of the fundamental energy gap for SnSe at about 0.9 eV is confirmed by the bulk data also given in Figure 5.67, and earlier data on bulk single crystal specimens by ALBERS et al. (1962). All these values, however, disagree completely with the value of 0.1 eV obtained by linearly extrapolating data for PbSe-SnSe alloys — STRAUSS (1967). This may be because this extrapolation procedure can only be expected to be valid if the band structures of the two compounds are similar so this may be evidence that the structures are in fact rather different.

As far as we know no information has been published on the band structure of SnSe so it is very difficult to say if alloying with this compound can change the lead telluride band structure. However we can see that even alloys with 1 and 3 mol% SnSe show transmissions at about 0.8 eV and 0.6 eV respectively which do not appear in pure PbTe or in alloys of PbTe and SnTe. We note that SnSe ha an sorthorhombic lattice structure like GeSe and SnS but of course unlike PbTe, SnTe, etc.

The reflectivity spectrum for the 3 mol% SnSe specimen shown in Figure 5.55 and the optical constants computed from it are rather similar to those of PbTe, SeTe and their alloys.

6.3. GeSe film specimens

The transmission data for GeSe given in Figure 5.55 and 5.56 have been used to obtain information on this compound of which very little is known. We obtained a value for the fundamental energy gap of about 1.6 eV which is in reasonable agreement with the earlier value of 1.53 eV obtained by KANNEWURT and CASHMAN (1961). From the reflectivity minimum at the plasma frequency, values for the optical dielectric constant and the optical conductivity were obtained at about 17 and 625 $(\Omega\,cm)^{-1}$, respectively. ε_{opt} is thus sufficiently large to indicate that the material is ionic. We have also calculated values of 21.3 and 1710 for the dielectric constant and conductivity respectively of a single crystal alloy of 75 mol% GeSe and 25% GeTe (sample No. 5101) from the published reflectivity data of MUIR and CASHMAN (1968). This value of the dielectric constant can be seen to be broadly consistent with our values for pure GeSe and GeTe (see Table 5.2).

7. CONCLUSIONS

In the work presented in this thesis we have shown that the fundamental energy gap decreases with alloying from that of the lead compound for all the lead-tin chalcogenide alloys studied. A marked decrease from that of PbTe was also observed in the energy gap for PbTe-GeTe alloys but only for concentrations above 40 mol% GeTe. This decrease in the energy gap makes all the materials studied promising potential detectors or emitters in the part of the infra-red region between 4 and 15 μm and probably beyond. For these purposes it will probably be particularly convenient to have single crystals and it is of interest to note therefore that we have successfully produced single crystal films of PbTe-GeTe and that other single crystal films have also been produced in particular PbTe-SnTe (BYLANDER, 1966) and PbSe-SnSe (STRAUSS, 1967). In view of this we might hope that some of these alloys will be of practical use in the near future.

It is to be hoped that experiments on high quality single crystal specimens could provide enough data to yield detailed information on the band structure of alloys. Very little theoretical work has been done on these with the exception of Ge-Si alloys and we feel a useful first step would be to calculate the structure of an ordered alloy. In particular we would suggest alloys with 50 mol% GeTe and 50 mol% PbTe or 50 mol% SnTe and 50 mol% PbTe because it seems likely that there is a good chance of obtaining ordered specimens of these which should closely resemble compounds. Furthermore, the energy band structures of the IV—VI compounds are well known.

ACKNOWLEDGEMENTS. The author would like to express his sincere gratitude to Professor E. R. ANDREW for his great interest and encouragement and for allowing the use of the facilities of the Physics Department and to Professor K. W. H. STEVENS for his helpful advice on several occasions.

I would like especially to thank Dr. L. J. CHALLIS for his very helpful supervision and discussions and also for his great help with language problems during the writing of this thesis.

I would like also to thank:

Professor R. MARKOVIĆ from Belgrade University for his encouragement and advice during this work.

Professors A. MILOJEVIĆ and D. TJAPKIN, from Belgrade University for encouragement and for the facilities of the Institute of Physics — Belgrade University, where a part of this work was carried out.

The technical staff of the Departments of both Nottingham and Belgrade Universities who were concerned with the development and servicing of apparatus and the processing of photographic work.

The author's colleagues provided much valuable assistance.

My thanks are also due to Mr. M. A. MCCONACHIE and Mr. SMILJANIĆ for help with computing programmes and to Mrs. E. M. FROST, Miss D. M. PRITCHARD and Mrs. J. W. MELLOR who also helped greatly by typing a difficult manuscript in a short time.

APPENDIX A.

The Determination of Optical Constants from Reflectivity Data by a Computer Fitting Procedure

We assume that at some frequency f_i, n_i and k_i are given approximately by equations 4.50, 4.51 in terms of the unknown parameters P_1, P_2 and P_3. ($P_1=\varepsilon_{opt}$, $P_2=\lambda_p$, the plasma wavelenth and $P_3=1/\omega_p\tau$ where τ is the carrier relaxation time and ω_p the plasma frequency). Hence analytical functions F_i (f_i, P_1, P_2, P_3) can be derived using 4.52 so that F_i is the reflectivity calculated from these parameters in the approximation that 4.50, .51 are a good representation of n and k. The fitting procedure consists of adjusting the parameters P_1, P_2, P_3 until $F_i \sim R_i$ where R_i is the measured reflectivity. Typically some 30 values of R_i were measured i.e. $i=1\rightarrow 30$. This procedure was carried out by modifying standard computer subroutines for least mean square analyses.

10. REFERENCES

ALBERS, W., HAAS, C., OBER, H., SCHODDER G. R. and WASSCHER, J. D., 1962, J. Phys. chem., Solids, **23**, 215—20.

ANDERMANN, G., CARON, A., and DOWS, D. A., 1965, J. Opt. Soc. Am., **55**, 1210—16.

ANTONOV, V. B., and NASIROV, Y. N., 1966, Jzv. Akad. Nauk. Azerb. SSR, 77—81.

BARDEEN, J., BLATT, F. J., HALL, L. H., 1956 Photoconductivity Conf., Wiley, London.

BAUER, E., 1964, Pergamon Press, Ed. Francomba M. H. and Saton, H.

BIS, R. F., 1964, Solid St. Com. **2**, 161—2.

BIS, R. F., and ZEMEL, J.N., 1966, J. Appl. Phys., **37**, 228—30.

BRAUNSTEIN, R., MOORE, A., and HERMAN, F., 1958, Phys. Rev. **109**, 695—710.

BREBRICK, R.F., 1963, J. Phys. Chem. Solids, **24**, 27—36.

BRIGGS, H. G., and FLETCHER, R. C. 1953, Phys. Rev., **87**, 1130—31.

BOWLDEN, H. J., and WILMSHURST, J. K., 1963, J. Opt. Soc. Am., **53**, 1073—78.

BURSTEIN, E., 1954, Phys. Rev., **93**, 632—3.

BUTLER, J. F., and CALAWA, 1966, Physics of Quantum Ectr., Mc Graw, H., N. Y.

BYLANDER, E. G., DIXON, J. R., RIEDL, H. R., and SCHOOLAR, R. B., 1965, Phys. Rev., **138**, A864—65.

BYLANDER, E. G., 1966, Mat. Sci. Eng., **1**, 190—94.

CARABATES, C., 1967, Le Journal de Physique, **28**, 825—31.

CARDONA, M., and GREENAWAY, D. L., 1964, Phys. Rev., **133**, A 1685—97.

COHEN, M. H., 1961, Phys. Rev., **121**, 387—95.

COSSLETT, V. E., *Practical Electron Microscopy*, 1951, Netherlands, Lond.

CRONKLIN, J. B., JOHNSON, L. E., and PRATT, G. W., 1965, Phys. Rev., **137**, A 1282—94.

DARROV, M. S., WHITE, W. B., and ROY, R., 1966, Trans. TMS-AIME, **236**, 654—8.

DIMMOCK, J. O., and WRIGHT, G. B., 1964, Phys. Rev., 135, A 821—30.

DIMMOCK, J. O., MELUGUILIS, I., and STRAUSS, A. J., 1966, Phys. Rev. Letts., **16**, 1193—96

DIXON, J. R., and RIEDL, H. R., 1965, Phys. Rev., **138**, A 873—881.

DIXON, J. R., and RIEDL, H. R., 1962, ‚Semiconductors' Conf. Exeter.

DUSHMAN, S., 1949, *Scient. Found. of Vacuum Technique*, J. Wiley, N. Y.

DAMON, D. H., et al., 1963, J. Appl. Phys., **34**, 3083—5

DEMBOVSKII S. A., et al. 1963, Zh. Neorg. Khim. **8**, 1025—6.

ELLI, M., 1963, Atti, Accad. Nazl. Lincei, **35**, 538—47.

ESAKI, L., 1966, Physics of Semicond. Confer., Kyoto, 589—97.

ESAKI, L., STILES, P. J., 1966, Phys. Rev. Letters, **16**, 1108—1111.

EVANS, J. A., 1961, Ph. D. Thesis, Nottingham University.
FAN, H. Y., 1956, Prog. Phis., **19**, 107—155.
FAN, H. Y., 1951, Phys. Rev., **82**, 900—905
FOWLER, R. H., and NORDHEIM, L., 1928, Proc. Roy. Soc. Lond., *A* **119**, 173—81.
GIBSON, A. F., 1950, Proc. Phys. Soc., B **63**, 756—67.
GIBSON, F. F., 1952, Proc. Phys. Soc., B **65**, 378—88.
GLICKSMAN, M., 1956, Phys. Rev., **102**, 1496—501.
GOBELI, G. W., and FAN, H. Y., 1960, Phys. Rev., **119**, 613—20.
GUNTHER, K. G., 1959, Compound Semicond. VI, 311—25, N. Y. Reinhold.
GUNTHER, K. G., 1966, The Use of Thin Films, Ed. Anderson, J. C., Acad. Press. Lond.
HALL, J. F., and FERGUSON, W. F. C., 1955, J. Opt. Soc. Am., **45**, 714—18.
HARRIS, L., and SIEGEL, B. M., 1948, J. Appl. Phys., **19**, 739—41.
HEAVENS, O. S., 1955, Optical Properties of Thin Solid Films, London.
HEAVENS O. S., 1964, in ‚Physics of Thin Films', Vol. 2., Hass, G., Ed., Acad. Press, N.Y.
HENRY, N. F. M., LIPSON, H., WOOSTER, W. A., 1951, Macmillan, London.
HERMAN, F., GLICKSMAN, M., and PARMENTER, R. H., 1957, Progress in Semicond., **2**, 3—33, Ed. A. F. Gibson, London, Heywood.
HERMAN, F., 1954, Phys. Rev., **93**, 1214—25.
HERMAN, F., and SKILLMAN, S., 1960, Semicond. Conf. Prague, 20—8.
HIRTH, J. P., and POUND, G. M., 1963, Condensation and Evaporation., Pergamon Press, N. Y.
HOLLAND, L., 1960, Vacuum dep. of thin Film, Champan and Hall. London.
HOUSTON, B. B., ALGAIER, R. S., BABISKIN, J., and SIEBENMANN, 1964, Bull. Am., Phys. Soc., **9**, 601.
HOWSON, R. D., 1964, Le. J. De. Physique **25**, 212—217.
HOWSON, R. D., 1968, Brit. J. Appl. Phys., **1**, 15—23.
IOFFE, A. F., and REGEL, A. R., Progress in Semicon., 1960, **4**, 237—291, London, Heywood.
JOHNSON, E. R. and CHRISTIAN, S. M., 1954, Phys. Rev., **95**, 560—1.
KANE, E. O., 1956, Phys. Chem. Solids, **1**, 82—99.
KANNEWURF, C. R., and CASHMAN, R. J., 1961, J. Phys. Chem. Solids, **22**, 293—98.
KLEINMAN, L., and LIN, P. J., 1964, Proc. Inter. Conf. of Semicond., Paris, 63—68.
KREBS, H., GRÜN, K., KALLEN, D., 1961, Z. Anorg, Allgem. Chem., **312**, 307—13.
KREBS, H., and LANGNER, D., 1964, Z. Anorg. Allgem. Chem., **334**, 37—49.
LANDAU, L. D., and LIFSHITZ, E. M., 1958, Quantum Mechanics, Pergamon Press, Oxford.
LIN, P. J., and KLEINMAN, L., 1966, Phys. Rev., **142**, 478—489.
MAYER, H., 1955, Physik, dun Schichten, Wiss. Verlag., Stuttgart, 75.
MAZELSKY, R., LUBELL, M. S., and KRAMER, W. E., 1962, J. Chem. Phys., **37**, 45—7.
MC HUGH, J. P., and TILLER, W. A., 1960, Trans. TMS-AIME, **218**, 187—88.
MESSIACH, A., 1962, Quantum Mechanics, North Holland, Smsterdam.
MILER, M., 1967, Infrared Physics, (GB), **7**, 135—44.
MILLER, E., and KOMARCK, K. L., 1966, Trans TMS-AIME, **236**, 832—40
MOONEY, R. L., 1945, J. Opt. Soc. Am., **45**, 714—18.
MOROZOV, I. S., and CHIHFA, L., 1963, Russ. J. Inorg, Chem., **8**, 878—80.
MOSS, T. S., 1959, Optical Properties of Semicond., Butterworth's Sci, Pub. Lond.
MUIR, J. A., CASHMAN, R. J., 1967, J. Phys. Chem. Solids, **28**, 1009—16.
MUIR, J. A., CASHMAN, R. J., 1968, Phys. Rev., **169**, 602—04.
NILSON, P. O , 1968, Applied Optics, **7**, 435—42.
NIKOLIĆ, P M., 1964, Proc. 9th Conf. ETAN, Bled, Yugoslavia.
NIKOLIĆ, P. M., 1965, Brit. J. Appl. Phys., **16**, 1075—79.
NIKOLIĆ, P. M., 1967, Brit. J. Appl. Phys., **18**, 897—903.
NIKOLIĆ, P. M., 1969, Brit. J. Appl. Phys., S 2, V **2**, 383—88.
NISHIYAMA, A., and OKADA, T., 1960, Mem. Fac. Sci., Kyusyu Univ. **3**, 3—7.

OKAZAKI, A., 1958, J. Phys. Soc. J., **13**, 1151—55.
OKAZAKI, A., and ASANADE, S., J. Phys. Soc. J., **15**, 989—97.
PARADA, N. J., and PRATT, G. W., 1969, Phys. Rev. Lett., **22**, 180—82.
PARMENTER, R. H., 1955, Phys. Rev., **97**, 587—98.
PARMENTER, R. H., 1956, Phys. Rev., 104, 22—32.
PASHLEY, D. W., 1963, Metallurgy of Ad. El. Mat., Ed., Brock, G. R., Inters. Pub. N. Y.
PHILLIPS, J. C., 1962, Phys. Rev., **125**, 1931—6.
PRATT, G. W., et al. 1964, Proc. Conf. Semicond., Paris.
PINSKER, Z. G., 1953, Electron Diffraction, Trans. Spink, J. A., and Feigl, E., Lond.
POTTER, R. F., and KRETSCHMAR, G. G., 1964, Infrared Phys., **4**, 37—65.
POWELL, C. F., 1966, Vapor Deposition, Wiley, N. Y.
PRISHIVALKO, A. P., 1966, Optika Spektrosk., **21**, 124—6.
RABII, S., 1968, Phys. Rev., **167**, 801—08.
RIEDL, H. R., SCHOOLAR, R. B., and HOUSTON, B., 1966, Solid St. Com., **4**, 399—402.
RIEDL, H. R., and DIXON, 1962, Semicond. Confer. Exeter, 179—85.
RIEDL, H. R., DIXON, J. R., and SCHOOLAR, R. B., 1965, Solid St. Com., 3, 323—25.
ROBINSON, T. S., 1952, Proc. Phys. Soc., Lond., B **65**, 910—11.
ROGERS, L. M., 1968, B. J. Appl. Phys., **1**, 845—52.
ROESSLER, D. M., 1965, Brit. J. Appl. Phys, **16**, 1119—23, 1359—66.
SCANLON, W. W., 1959, Solid State Physics, Ed. Seitz, F., and Turnball, D., **9**, 83—139.
SCHOOLER, R. B., RIEDL, H. R., and DIXON, J. R., 1966, Solid St. Com., **4**, 423—4.
SCHOOLER, R. B., and ZEMEL, J. N., 1964, J. Appl. Phys., 35, 1148—51.
SCHOOLER, R. B., DIXON, J. R., 1965, Phys. Rev., **137**, A 667—70.
SCHUBERT, K., and FRICKE, H., 1953, Zs. f. Metallkunde, **44**, 457.
SHELIMOVA, L. Y., ABRIKOSOV, N. K., ZHDANOVA, V. V., and SIZOV, V. V., 1966, Izv. Akad. Nank SSSR, Neorg. Mat., **2**, 2103—09.
SCHELIMOVA, L. Y., ABRIKOSOV, N. K., and BESSOUOV, V. I., 1964, Izv. Akad. Nauk. SSSrR, 180—83.
ŠIMON, I., 1951, J. Opt. Soc. Am., **41**, 336—45.
SIMPSON, D. R., 1964, Econ. Geol., **59**, 150—53.
SLATER, J. C., 1937, Phys. Rev., **51**, 846—51.
SLATER, J. C., 1949, Phys. Rev., **76**, 1592—1601.
SMITH, D. O., COHEN, M. S., and WEISS, G. P., 1960, J. Appl. Phys., **31**, 1755—62.
SMITH, D. O., 1961, J. Appl. Phys. Suppl., **32** (3), 705—805.
SMITH, R. A, JONES, F. F., and CHASMAR, R. P., 1968, Detection I. R. R. Oxford.
SPITZER, W. G., and FAN, H. Y., 1957, Phys. Rev., **106**, 882—90.
SPITZER, W. G., and KLEINMAN, L., 1961, Phys. Rev., **121**, 1324—35.
STIRLAND, D. J., 1966, The Use of Thin Films. Ed, Anderson, J. C., Acad. Press, Lond.
STÖHR, H., and KLEMM, W., 1939, Z. Anorg. Chem., **241**, 305.
STRATTON, J. A., 1941, Electromagnetic Theory, Inter Ser In Physics, N. Y.
STRAUSS, A. J., 1967, Phys. Rev., **157**, 608—611.
STRAUSS, A. J., 1968, Trans. Met. Soc. A. I. M. E., **242**, 355—65.
TAUC, J., and ABRAHAM, A., 1961, J. Phys. Chem. Solids, **20**, 190—92.
TOLANSKY, S., 1948, Multiple-beam Interferometry, Clarendon Press, Oxford.
TSU, R., HOWARD, W. E. and ESAKI, 1967, Solid St. Com., **5**, 167—71.
TSU, R., HOWARD, W. E., and ESAKI, L., 1968, Phys. Rev., **172**, 779—88.
VAŠKO, A., and MILLER, M., 1961, Czech. J. Phys., **11** B, 283—5.
VERLEUR, H. W., 1968, J. Opt. Soc. Am., **58**, 1356—64.
VERLEUR, H. W., BARKER A. S., and BERGLUND, C. N., 1968, Phys. Rev., **172**, 788—98.
WAGNER, J. W., and WILLARDSON, R. K., 1969, Trans. TMS-AIME, 245, 461—4.
WAGNER, J. W., and WILLARDSON, R. K., 1968, Trans, TMS-AIME, 242, 366—71.

WEISS, P., and SMITH, D. O., 1961, J. Appl. Phys. Suppl., **32**, (3), 85 S—86 S'.
WOOLLEY, J. C., EVANS, J. A., and GILLETT, C. M., 1959, Proc. Phys. Soc., **74**, 244—48.
WOOLLEY, J. C., GILLETT, C. M., and EVANS, J. A., 1961, Proc. Phys. Soc., **77**, 700—704.
WOOLLEY, J. C., 1962, Compound Semiconductors I, Ed. Willardson R. K., and Goering H. L.
WOOLLEY, J C., Progress in Solid State Chemistry, 1964, **1**, 275—315, Pergamon Press, Oxford.
WOOLLEY, J. C., WARNER, J., 1964, Can. J. Appl. Phys., **42**, 1879—85.
WOOLLEY, J. C., and NIKOLIĆ, P. M., 1965, J. Electrochem. Soc., **112**, 82—84.
YABUMOTO, T., 1958, J. Phys. Soc. J., **13**, 559—62.
YAMAMOTO, S., 1956, Sci. Rept., Tohoku Univ., **40**, 11—16.
ZEXEL, J. N., TENSEN, J. D., and SCHOOLAR, R. B., 1965, Phys. Rev., **140**, A 330—342.

CONTENTS